Validation of Human Body Model Lumbar Spine Performance for Use in New Seating Positions

Dustin Draper

München 2022

Aus dem Institut für Rechtsmedizin der
Ludwig-Maximilians Universität München

Vorstand: Prof. Dr. med. Matthias Graw

Validation of Human Body Model Lumbar Spine Performance for Use in New Seating Positions

Dissertation
zum Erwerb des Doktorgrades der Humanbiologie
an der Medizinischen Fakultät der
Ludwig-Maximilians-Universität zu München

vorgelegt von
Dustin Draper
aus
Ventura, USA

2022

Mit Genehmigung der Medizinischen Fakultät
der Universität München

Berichterstatter:	Prof. Dr. Steffen Peldschus
Mitberichterstatter:	PD Dr. Matthias Woiczinski Prof. Dr. Hans Herlein
Mitbetreuung durch die promovierte Mitarbeiterin:	Dr.Therese Fuchs
Dekan:	Prof. Dr. med. Thomas Gudermann
Tag der mündlichen Prüfung:	03.06.2022

Eidesstattliche Versicherung

Draper, Dustin

Ich erkläre hiermit an Eides statt, dass ich die vorliegende Dissertation mit dem Titel:

Validation of Human Body Model Lumbar SpinePerformance for Use in New Seating Positions

selbständig verfasst, mich aüser der angegebenen keiner weiteren Hilfsmittel bedient und alle Erkenntnisse, die aus dem Schrifttum ganz oder annhernd bernommen sind, als solche kenntlich gemacht und nach ihrer Herkunft unter Bezeichnung der Fundstelle einzeln nachgewiesen habe.
Ich erkläre des Weiteren, dass die hier vorgelegte Dissertation nicht in gleicher oder in hnlicher Form bei einer anderen Stelle zur Erlangung eines akademischen Grades eingereicht wurde.

München, June 4, 2022

Dustin Draper

Unterschrift Doktorand

Contents

List of Figures

List of Tables

Zusammenfassung

Mit dem Aufkommen neuer Sitzpositionen in Kraftfahrzeugen mit zunehmender Zahl an automatisierten Fahrfunktionen werden neue Werkzeuge und Methoden geschaffen, welche in der Entwicklung von passiven Sicherheitsmaßnahmen für diese neuen Konfigurationen helfen sollen. Ein solches Werkzeug sind Modelle des menschlichen Körpers auf Basis der Finite-Elemente-Methode, kurz Menschmodelle genannt. Sie haben gegenüber traditionellen anthropomorphen Testgeräten, auch als Crashtest-Dummys bezeichnet, den Vorteil, dass sie nicht auf eine bestimmte Belastungsart beschränkt sind. Während für einen Frontalaufprall, einen Seitenaufprall und einen Heckaufprall jeweils ein anderer Dummy verwendet werden muss, kann ein Menschmodell für alle drei Belastungsarten eingesetzt werden. Darüber hinaus haben Menschmodelle das Potenzial, dort genutzt zu werden, wo kein physischer Dummy eingesetzt werden kann. Ein solches Belastungsszenario ist in potenziellen Unfällen in zurückgelehnten Sitzpositionen zu finden. Hier können mit Menschmodellen verschiedene Konzepte und Konfigurationen untersucht werden. Eine Herausforderung für Dummys und Menschmodelle liegt darin, dass sie validiert sein müssen, um zuverlässige Prädiktionen zu erlauben. Für den Fall der Nutzung von Menschmodellen zur Untersuchung der Belastungen der Lumbalwirbelsäule in zurückgelehnten Sitzpositionen wird ein hierarchischer Validierungsprozess vorgeschlagen. Die erste Validierungsebene umfasst dabei die Zwischenwirbelscheiben, die zweite umfasst das Bewegungssegment. Die gesamte Lumbalwirbelsäule stellt das dritte Validierungsniveau dar und das Ganzkörpermodell das vierte. Das Ziel dieser Vorgehensweise ist es, mit Modellen geringerer Komplexität zu beginnen, auf diesen aufzubauen, um die zusammengesetzten Modelle zu analysieren und das aus den einfacheren Modellen erlangte Verständnis zu nutzen, um die Unsicherheiten in den größeren Modellen zu eliminieren.

In Kapitel 3 wird die durchgeführte Validierung unter Nutzung der Daten von Newell et al. [84] beschrieben. Es wurde untersucht, wie sich die Zwischenwirbelscheiben von fünf Menschmodellen unter Kompression verhalten. Die genutzten Experimente umfassten das axiale Komprimieren der

Zwischenwirbelscheiben in einer Universalprüfmaschine bei einer Kompressionsrate von 1/s. Die fünf untersuchten Modelle waren THUMS v3 TUC (THUMS v3), THUMS v4.01 (THUMS v4), THUMS v5.02 (THUMS v5), GHBMC v4.5-D (GHBM) und ViVa 2016 (ViVa). Eine weit verbreitete Methode zum Vergleich von Antwortkurven beim Vorliegen von Ergebniskorridoren, die Correlation Analyse (CORA), welche dimensionslose Bewertungszahlen liefert, wurde genutzt. Das Modell mit dem besten CORA-Ergebnis war THUMSv3 mit einem Wert von 0,74, gefolgt vom Modell THUMSv5 mit einem CORA-Wert von 0,68. Der hohe Wert für das Modell THUMSv3 ergibt sich, da seine Antwortkurve die mittlere experimentelle Antwortkurve kreuzt, während jene von THUMSv5 mit einem gleichmäßigen Abstand der experimentellen Kurve folgt. Deshalb wurde THUMSv5 als Modell mit dem besten Zwischenwirbelscheibenverhalten eingeordnet. Dies ist gültig unter den Belastungsbedingungen der Experimente. Zum Ausschluss generell ungeeigneter Modellantworten in diesem Lastfall wurden die experimentellen Ergebnisse im Interquartilsabstand mit den Modellergebnissen verglichen. Da sich in allen Fällen zumindest eine teilweise Überdeckung ergab, wurde kein Modell als Ausreißer bzw. als generell ungeeignet für die weiteren Untersuchungen bewertet.

In Kapitel 4 wird die Untersuchung von Bewegungssegmenten als nächsthöherer Komplexitätsstufe beschrieben. Die Bewegungssegmente bestehen aus einer Zwischenwirbelscheibe, den beiden angrenzenden Wirbeln, sowie dem Ligamentum longitudinale anterius, dem Ligamentum longitudinale posterius, dem Ligamentum interspinale, dem Ligamentum supraspinale den Ligamenta flava, und den Ligamenta intertransversaria. Für diese Untersuchung wurden die Ergebnisse der Experimente von Christou [25] als Grundlage verwendet. Jene Experimente wurden mit Hilfe eines Fallturms durchgeführt, um einen Beschleunigungspuls auf das Bewegungssegment aufzuprägen und an einem Aufnehmer unterhalb der Probe die übertragene Kraft aufzuzeichnen. Die Simulationsergebnisse wurden nicht mit der CORA-Methode bewertet wegen der zu geringen Zahl vorliegender experimenteller Ergebnisse für das Erstellen von Kurvenkorridoren. Stattdessen wurden die Maximalkräfte zwischen Simulation und Experiment verglichen. THUMSv3 wies die größte Übereinstimmung mit den experimentellen Werten auf. Alle anderen Modelle zeigten eine konservative Abschätzung dessen, was in den Experimenten beobachtet wurde. Über die numerische Deaktivierung des Kontakts zwischen den Wirbeln wurde die Situation mit entfernten Facettengelenken simuliert. Dabei überträgt nur die Zwischenwirbelscheibe Kräfte und Ergebnisse ähnlich zu denen in Kapitel 3 wurden berechnet. Der Unterschied in den Simulationen mit und ohne Facettengelenkkontakt stellt die Bedeutung der Gelenke in der untersuchten Bewegungssegmentbelastung heraus. Der groben Vernetzung der Modelle wird

hier die Bewegungsunterdrückung und künstliche Gelenksteifigkeitserhöhung zugeschrieben. Die Verwendung eines Fallturms in den Experimenten führte zu zusätzlichen Unsicherheiten in der numerischen Modellierung der Versuche. Experimente mit Universalprüfmaschinen erlauben im Vergleich deutlich höhere Konfidenz für die Modellvalidierung, weil sie einfacher beschrieben werden können und zu einem Grad, den Simulationen erfordern, dokumentiert werden können.

Für Kapitel 5 wurden Experimente an der gesamten Lumbalwirbelsäule von Demetropoulos [33] und Stemper et al. [109] als Basis für die Simulation von quasistatischer und dynamischer Kompression sowie quasistatischer Flexion genutzt. In Belastungen der Zwischenwirbelscheiben und Bewegungssegmente ist die Orientierung der Proben relativ zur Orientierung des Versuchsaufbaus von Bedeutung. Bei Belastungen der gesamten Lumbalwirbelsäule kommt die Orientierung der Wirbelkörper in den einzelnen Proben hinzu, welche als Wirbelsäulenhaltung bezeichnet werden. Hierzu wurde eine eindeutige Beschreibung zum Vergleich mit Simulationsmodellen vorgeschlagen. Für die Untersuchung der Lumbalwirbelsäulenbelastung wurden vier verschiedene Haltungen der THUMSv5-Wirbelsäule betrachtet: Die Haltung, in der das Modell ausgeliefert wird, die aus einer Positionierung des Modells in zurückgeneigter Sitzlehne extrahierte Haltung sowie aus dieser Haltung abgeleitet eine stärkere Extension und eine stärkere Flexion. Für die quasistatische axiale Kompression liegen die Ergebnisse aller Modelle mit Ausnahme THUMSv4 im experimentellen Ergebniskorridor, was sich mit den Erkenntnissen zu den Zwischenwirbelscheiben deckt. Für die quasistatische Flexion wurde für alle Modelle eine zu steife Antwort beobachtet. Dass die Validierung unter Biegung weitere Aufmerksamkeit benötigt deckt sich mit den Erkenntnissen zur Bewegungssegmentvalidierung. Für die dynamischen Fallturmtests aus Stemper et al. [109] wird das kinematische Verhalten, beschrieben durch die Winkeländerungen der Zwischenwirbelscheiben, am besten durch das Modell THUMSv5 abgebildet. Dies wird mehr der initialen Modellgeometrie als anderen Parametern zugeschrieben, was die Antworten der in der Haltung variierten Varianten dieses Modells unterstützen. Die an einem Aufnehmer unter der Probe gemessene Kraft wird von den Modellen generell überschätzt, was großteils einer Oszillation zugeordnet wird, welche in den Experimenten zwar auch vorhanden ist, in der Simulation aber sehr stark ausgeprägt ist.

Die in Kapitel 6 beschriebene Validierung nutzte die Freiwilligen-Schlittenversuche von Mühlbauer [77] als Basis. In jenen Versuchen wurde ein Freiwilliger in einer aufrechten Sitzposition sowie unter verschiedenen Rückenlehnenwinkeln untersucht. Für diese Niedriggeschwindigkeitspulse musste eine deutlich längere Simulationszeit berücksichtigt werden. Zusätzlich musste

die Erdbeschleunigung abgebildet werden, da sie Lasten in der Größenordnung der Belastungen durch die Schlittenpulse verursachte. Die globale Kinematik der Menschmodellsimulationen unterschied sich von den Beobachtungen in den Freiwilligenversuchen. Diese Unterschiede können durch die Abbildung der Gurtvorspannungen sowie limitierter Validierung der Weichgewebe für Anwendungen der Menschmodelle im Niedriggeschwindigkeitsbereich verursacht werden.
Für Kapitel 7 wurde die zurückgeneigte Sitzposition bei hohen Geschwindigkeiten betrachtet mit Fokus darauf, wie verschiedene Anfangshaltungen die Maximalkräfte und die Kinematik der Lumbalwirbelsäule beeinflussen [35]. Unterschiede in der Haltung verursachten Unterschiede in den Kräften und der Kinematik der Lumbalwirbelsäule, während die Auswirkung auf die externe Kinematik des gesamten Körpers minimal blieb. Da es bislang keine breit akzeptierten Grenzwerte für die Belastung der Lumbalwirbelsäule von Fahrzeuginsassen gibt, werden weitere Untersuchungen benötigt zur Entwicklung eines Kriteriums, welches den gleichen Schutz der Insassen wie in bereits existierenden Lastfällen erlaubt. Ein solches Kriterium muss sitzkonfigurationsunabhängig sein, da viele zukünftige Farzeuginnenraumszenarien nicht nur sehr verschieden voneinander, sondern auch potenziell modular aufgebaut sein werden, so dass herkömmlich definierte Sitzpositionsbewertungen in den neuen Lastfällen reevaluiert werden müssen.
Vor dem Hintergrund des beobachteten Einflusses der Wirbelsäulenhaltung und -anatomie auf das Verhalten in zurückgeneigter Sitzposition wird erwartet, dass Menschmodelle eine bedeutende Rolle dabei spielen werden, Verletzungsrisiken in derartigen Insassenlastfällen zu verstehen. Um Menschmodell-basierte Risikobewertung vollständig zu erlauben, werden weitere experimentelle Daten benötigt, insbesondere auf der Ebene der gesamten Lumbalwirbelsäule und auf der Ebene des gesamten Körpers.

Abstract

With the advent of new seating positions for vehicles with more and more autonomous driving functions, new tools and methods are being developed to aid in the development of passive safety features in these new configurations. One such tool are the Human Body Models (HBMs), which improve on the traditional Athropomorphic Testing Devices (ATDs), also known as crash test dummies, in that the HBM are not confined to certain loading scenarios. Whereas a different dummy must be used for a front crash, a side crash, and a rear crash, a single HBM can be used for all three. Additionally HBMs have the potential to be used where currently no physical ATD can be utilized. One such loading scenario is in potential impacts involving reclined seating positions, where HBMs can be used to evaluate a range of concepts and configurations. The challenge with using both ATDs and HBMs is that they must be validated in order to provide reliable predictions. For the case of using HBMs to investigate loading of the lumbar spine in reclined seating scenarios, a hierarchical validation process is proposed. The first level of validation will be performed on the intervertebral discs, the second level will be applied to a single functional spinal unit, the third level will be the complete lumbar spine, and the fourth level the full-scale HBM. The aim of this approach is to start with models which have lower complexity and build upon those models until the full models with increased complexity can be analyzed, with the goal being that the understanding derived from the simple models will remove uncertainty in the larger models.

In Chapter 3 a validation was done using experimental data from Newell et al. [84] to evaluate five Human Body Models for how well their respective intervertebral discs (IVDs) performed in compression. These experiments involved compressing IVDs axially using a material testing machine at a rate of $1s^{-1}$. The five models investigated were the THUMS v3 TUC (THUMS v3), THUMS v4.01 (THUMS v4), THUMS v5.02 (THUMS v5), the GHBMC v4.5-D (GHBM), and the ViVa 2016 (ViVa). As a standard response curve comparison method, the Correlation Analysis (CORA) method was used to provide a dimensionless rating. The model with the best CORA score was the THUMS v3 with a CORA of 0.74, followed by the THUMS v5 with a CORA score of 0.68.

The high CORA score from the THUMS v3 is due to the THUMS v3 response crossing the mean experimental curve, whereas the THUMS v5 evenly follows the experimental response with a stiffer offset. Therefore the THUMS v5 is considered to have the best IVD response, and is valid to be used in the regimes in which the experiments were conducted. Looking to see if any of the models are unfit for application in this loadcase, the interquartile ranges were compared between the experiments and each of the five models. As all of the models have at least some overlap with the experimental corridors, none can be considered an outlier, and as such unqualified for further investigation.

In Chapter 4 functional spinal units (FSUs) were investigated as being one hierarchical level more complex than the IVDs investigated in Chapter 3. The FSU consists of a single IVD as well as the two vertebral bodies (VBs) adjacent to the disc, and the ligaments connected to both VBs. These ligaments include the anterior and posterior longitudinal ligaments, the supraspinous ligaments, the interspinous ligaments, the ligamenta flava, and the intertransverse ligaments . This investigation was done using experiments performed by Christou [25] as a reference. These experiments were performed using a drop tower to apply a pulse to the FSU, and then measuring the force transmitted to a transducer located below the specimen. For these simulations no CORA analysis was performed as not enough experiments were performed to be able to construct the necessary corridors. Instead peak force was compared between the experiments and simulations. Again THUMS v3 has the closest response when compared with the experimental values, and all other HBMs show a conservative estimate of what was observed in the experiments. By numerically disabling contact between the two VBs, a situation where the facet joint has been excised is simulated. For this configuration only the IVD is transmitting force, and results similar to those found in Chapter 3 were observed. The difference between the simulations with and without facet joint contact shows the importance of the facet joints in FSU loading. The coarse mesh geometry in these models leads to blocking which artificially increases the stiffness of the joints. The use of a drop tower in the physical experiments also led to an increase in uncertainty in the modelling of the simulation experiments. Material testing experiments have much higher confidence levels for a validation, as they can be more easily described and documented to the degree of detail which validation simulations require.

In Chapter 5 whole lumbar spine reference experiments from Demetropolous et al. [33] and Stemper et al. [109] were taken as the basis for both quasi-static and dynamic compression, as well as quasi-static flexion bending. For the IVD and FSU loadcases, the orientation of the specimen relative to the orientation of the testing apparatus is important, but the for the whole lumbar spine reference experiments, the orientation of the vertebrae in a single specimen also becomes important, this is referred to as the specimen posture, for which a non-ambiguous description was proposed. For the whole lumbar spine investigations four separate THUMS v5 postures were studied: the posture as delivered, a posture extracted from the THUMS v5 in a reclined seating setup, the reclined posture extended to be more lordotic, and the reclined posture flexed to be more kyphotic. For the quasi-static axial compression case [33], all of the HBMs bar THUMS v4 lie within the experimental corridor, in line with what was observed for the IVDs. For the quasi-static flexion bending load case however, all of the HBMs are too stiff. That the bending response needs to be further validated was also seen in the FSU validation. For the dynamic drop tower tests described in Stemper et al. [109] the kinematic behavior as measured by the angular deformation of the IVDs is best matched by the THUMS v5 model. This is due more to the initial geometry of the the THUMS v5 than to other modelling parameters, as can be seen in the response of the other various THUMS v5 postures. The force response as measured by a transducer located below the specimen is always overestimated by the HBMs, largely due to an oscillatory behavior, that although present in the experimental data, is greatly exaggerated in the simulation results.

In Chapter 6 the volunteer sled tests performed by Muehlbauer [77] were used as a validation basis. In these tests a single individual was tested in an upright seating position as well as varying angles of recline. For these low speed pulses, the simulation time had to be increased to capture all of the HBM movement. Additionally a gravity settling phase had to be included because gravity loading was found to be on an equal order of magnitude to the loading from the applied pulse. The global kinematics of the HBM simulations differed from what was observed in the Volunteer testing. These differences can be due to the modelling of belt prestress, and the lack of validation of the soft tissues for low speed HBM applications.

Chapter 7 looks at a high speed reclined seating configuration, with a focus on how various initial postures effect the peak forces and kinematics in the lumbar spine [35]. Different postures were found to have different lumbar spine kinematics and forces, while at the same time having only minimal affect on the global external occupant kinematics. As no widely accepted limit currently exists for lumbar spine loading in vehicle occupants, research is needed to define a criterion which protects occupants to the same level for which they are protected in other existing loading scenarios. This criterion must be developed to be seating configuration agnostic as many future interior scenarios are not only very different from one another, but also potentially modular, meaning that the traditionally defined seating position metrics must be reevaluated for use in these new load cases.

Given the observed influences of the spine posture and anatomy on the response in reclined seating, HBMs are expected to play a major role in understanding injury risks in such occupant load cases. In order to fully enable HBM-based risk assessment, more experimental data is needed, in particular on whole-lumbar spine level and full-scale level.

Chapter 1

Introduction

1.1 Introduction

Car crashes claim millions of lives every year, and in 2015 the World Health Organization reported road injury as one of the top ten causes of death world wide [121]. In the United States alone in 2016 37,461 people lost their lives, incurring an estimated economic costs in the hundreds of billions of dollars [80]. Preventative measures are an important part of automotive safety, but passive safety will continue to be a critical part of automotive packages in the meantime. The study of impact biomechanics informs how the body can behave under the large forces and accelerations experienced in the automotive environment. These interactions are important to allow new safety systems and countermeasures to be designed, and also hopefully, to predict where safety problems might arise in new vehicles. Accident analysis and reconstruction looks at historical trends to see where the biggest improvements in safety can be made. Since the advent of the automobile at the beginning of the 19th century, cars have been getting more features which have had the goal of making cars safer.

The history of biomechanics began long before the advent of the automobile, this is because people have been curious about how things work long before cars were invented. Like many things, the beginnings of biomechanics begin with Aristotle, whose book "De Motu Animalium was concerned with the movements of animals [44] [71]. The roman scholar Galen is the next scientist to delve into biomechanics, his book *On the Function of the Parts* was one of the first books on anatomy, and one whose influence lasted for hundreds of years afterwards [71]. Galen was interested enough in anatomy to perform vivisections and dissections of animals in order to understand the functions of various bodily systems [19]. After Galen the next leap in biomechanics came from Leonardo da Vinci. Da Vinci studied human and animal physiology in order to inform his art, and to find inspiration for his inventions. His inventions copied mechanical principles and forms in order to mimic what he observed in nature [72]. Galileo Galilee also made contributions to the science of biomechanics: Galileo observed that animal size doesn't scale proportionally to their mass. He also noted that bones have a tubular profile in order to efficiently address this phenomenon [71] [72]. During the industrial revolution the study of biomechanics was further advanced though the use of new inventions such as the moving picture, and new novel ways to measure forces. In 1939 the *Bioengineering Centre* is founded at Wayne State University in order to study blunt impacts to the head. This work would later become the basis for the Head Injury Criteria which is still used as an automotive safety indicator [116].

The history of automotive safety can be traced to August 31st 1869, where Mary Ward becomes the first documented death caused by an automobile accident [73]. Before this accident others had already been considering automotive safety safety, for example by equipping automobiles with brakes and steering wheels. This particular accident is considered the first because it was documented, and the documentation preserves it in the historical record and would allow future automotive engineers to use its example to design safer cars. The first crash test against a barrier was performed by general motors at Milford Proving Ground in Michigan in 1934 [74]. In 1953 Hugh DeHaven, a former pilot who had survived a fall from a large height and then tried to explain why, founded an automotive and aviation safety research group at Cornell college, which would recommend various ways to make cars safer.

The fields of biomechanics and automotive safety converged in the 1940s and 50s in the form of Colonel John Stapp, whose research started as a way to investigate human tolerance to injury with motivation coming from the military aviation field [107]. Experiments which were deemed too dangerous by Stapp necessitated the need for a stand-in for a human, and thus the concept of a crash test dummy was born [9]. Crash test dummies, also known as Athropomorphic Test Devices (ATDS) have continued to improve since their initial inception and have like many other aspects of modern life gone digital, in the form of Finite Element (FE) models. These models eliminate many problems associated with physical crashes such as sensor failure and calibration that must be considered when using hardware dummies.

This dissertation is concerned with the newest technology to come to the dummy front; namely, Human Body Models (HBMs). HBMs are digital finite element models of the human body, modeled as accurately as feasible, which can be used in simulations instead of doing physical experiments on human subjects. HBM have the advantages of the digital world such as safety, cost effectiveness, and repeatability, combined with the accuracy of real world data. A human body

model for example can exhibit much more human-like behavior than a crash test dummy without the need for actually testing a human subject.
HBMs are an emerging technology and still have many unresolved questions. The most challenging issue of HBMs is their validation and verification, because in order to say they can be used as substitutes for humans, first a measure of how accurate the models are must be made.

1.2 Background

1.2.1 Simulation

In the automotive safety industry simulations play a large role in the design of new systems and proof of concept as a complement to hardware tests [122]. Hardware tests consist of full-scale car crashes or sled tests with instrumented Anthropomorphic Test Devices (ATDs) used as a stand in for human occupants or pedestrians [45]. The ATDs, also referred to colloquially as crash test dummies, or simply dummies, have been an integral part of automotive safety over the past decades and will continue to play an important role into the foreseeable future [45] [42]. But ATDs are not perfect and have limitations that can be addressed using newer more suitable technologies. Crash test dummies are, per definition, not human. They circumvent the need to test safety technologies on living people by providing a reasonable approximation of of the human body which can be put into harm's way without endangering any living people. But being able to enduring many crash events throughout their lifetime, ATDs must also be built to be very tough and robust. The human body, on the other hand, is not very robust when compared with the standard ATDs: humans require protective restraint systems and airbags to avoid injuries in sever crashes [43], whereas the ATDs can withstand multiple of these events before even recalibration is required, let alone failure.
Simulations play a large role because they cut out the expense associated with hardware testing: geometry and materials can be changed quickly and cheaply in a simulation; whereas to fabricate a one off component for testing can be very expensive [111]. And because safety tests are by their very nature destructive, these expensive components have a very limited lifespan. Simulation on the other hand can save variants of components or configurations and apply them to different test setups. Also simulations are inherently repeatable, which is not always the case for hardware testing [99]. The biggest limitation for simulation is that simulations depend on hardware testing to calibrate how accurate the simulation results are. With no yardstick of what the true response is, it would be impossible to tell if a simulation is performing correctly of not [125].

The most common type of simulation for passive safety in vehicle is the so-called Finite Element Method (FEM). More specifically a specific type of FEM called explicit FEM which allows for the fast and accurate simulation of highly dynamic events [110].

There are multiple methods of approximating partial differential equations, depending of course on the characteristics of the equations to be solved. Finite Differences are often used on rectilinear grids, and have the advantage of a simple and highly diagonal stiffness matrix which remains relatively the same for a given problem type [105]. Finite Volumes are used primarily in fluid mechanics type problems because of their convenient formulation of the flux terms, and inherent three dimensional construction[105]. Finite elements are used most commonly in solid mechanics applications, for historical reasons, as well as because finite elements are good at describing the types of geometries one finds in solid mechanics [17].

The commercial finite element solver LS-DYNA will be used to perform the simulations for this work. As seen in Figure 1.1 finite elements can be represented as a series of interlinked equations and unknowns. The advantage of using a code like LS-DYNA is that is allows for the quick changing of equations classes and parameters, with no additional programming. This thesis focus on finding a suitable material description of adipose tissue, which in the mathematics of the Tonti Diagram, corresponds to the box labeled 'constitutive equations'. In LS-DYNA there are over 200 different material models which can be tried out with the exchange of keywords in an input file. LS-DYNA also has different element formulations which alter parameters and equations corresponding the remaining boxes, and even options such as contact which are not represented in such a straightforward Tonti diagram [70].

LS-DYNA also has a long history in crash simulation. It was originally developed by Lawrence Livermore National Labs as a way to simulate explosions, and in its early years was quickly adopted for use in auto crash simulations [14]. It has continued to be one of the premier dynamic FE solvers used in auto crash simulations, and has been specialized somewhat in the direction of automobile safety, offering models for airbags, seat-belts, and other automotive safety features [70]. In addition to these historical reasons, another very important consideration also makes LS-DYNA a good choice the simulations performed in this work: all of the commercially available human body models are developed in LS-DYNA. Because the models are all delivered in the native LS-DYNA format, the use of any other solver would necessitate the translation of the models, which might cause aberrations in the model results due to varying features and methods in various FEM Solvers.

1.2.2 Submarining and Lumbar Spine Injury

One of the largest trends in the modern auto industry is the race to develop Highly Autonomous Vehicles (HAVs) [75]. These vehicles themselves in turn will take over part or all of the navigating and piloting, which would allow the passengers to perform other tasks whilst they are taxied about. One thing that is strongly associated with HAVs is the possibility to offer new seating positions [65]. The thinking goes that if the passenger does not have to be alert, then why not offer a comfortable position in which they can read the newspaper, or answer emails? Futurists would also argue that HAVs will be so advanced and have such strong active safety features, that passive safety will no longer be of importance [20]. This is lofty thinking, and may very well one day come to pass, but for the foreseeable future mixed traffic and the problems associated with an emerging technology dictate that passive safety systems will still be needed. What's more, these passive safety systems will have to protect occupants in new seating positions and possibly in new crash scenarios that will emerge from mixed modal traffic [81].
The question then becomes how to protect the occupants of the near future? Traditional passive safety measures have been developed by analyzing accident data to see where the largest benefit can be made [45], but this is not an option when trying to predict how things will be with HAVs. The solution then is to project aspects associated with HAVs onto the current accident scenarios. An illustrative example is reclined seating. Many people associate reclined seating with HAVs [65], and many OEMs have concept cars which include reclined seating [76]. If one looks at a reclined occupant in a standard frontal accident situation it becomes clear that the mechanics and the biomechanics are very different between the two, see Figure 1.2. In the frontal case the lab belt is the primary means of restraint, and the upper body pivots around the lap belt. In the reclined position, the occupant is restrained by the seat pan, and there is much less pivoting and rotation of the upper body. On the one hand if the seat pan is at the wrong angle, is might not be sufficient to restrain the occupant. If this is the case, submarining will be the most probable result. On the other hand if the seat pan is the primary means of restraint, most of the force will then flow into the seat of the occupant and then into the spine, which could in turn cause spinal injury. A visualization of the differences between these two seating configurations can be seen in Figure 1.2.

Submarining

Submarining is when, during a frontal type accident, the lap belt slides off the pelvis and then into some soft tissue, usually in the region of the lower abdomen.

Submarining is also usually accompanied by some sliding of the occupant relative to the seat and or the lap belt [6]. The reason that submarining is of concern in new seating positions is because in a reclined position the lap belt has less projected area onto the pelvis, which would seem conducive to the submarining process. In the literature and in the accident databases, there is a relatively small number of accidents in which the occupants have been seated in a reclined position [21]. Production seats in cars on the road today can already recline, but it could be the case that no major epidemic of submarining has occurred because most occupants choose to sit in a fully upright position, due to societal norms or some other reason. Because of this lack of data it is hard to draw conclusions about how reclined seating will actually affect the injury rates of occupants. However, in simulations and in dummy tests of concept seats, it can be clearly seen that the kinematics with a reclined seat are different from the the kinematics in standard seating positions as demonstrated in Figure 1.2. This paucity of information is also a motivating factor to use HBMs to analyze the problem. With a properly validated HBM reclined seats and other autonomous driving postures can be investigated without the expense of performing PMHS tests.

Lumbar Spine Injury

Another aspect which new seating positions could exhibit, is that the load is directed from the seat up the spinal column, which does not occur in today's seating positions. As with submarining, there is very little data with which one could draw conclusions, but ongoing dummy tests have shown much higher axial spine forces when reclined as compared to standard seating positions [103]. If this is indeed the case, one would expect the critical part of the spine to be the lumbar spine, which would be the first region of the spine to experience the loading as it is the closest part of the spine to the pelvis, and thus the seat and the load. Currently lumbar spine injury is relatively uncommon in automotive accidents [78] but when it does occur it is more likely to occur during frontal accidents than other types [63]. Lumbar spine injuries are also somewhat of an oddity because although the prevalence of most other injury types has been decreasing (i.e. cars in general are getting safer,) [59] the prevalence of lumbar spine injuries has been more or less unchanged [93] [118]. Different authors postulate that this may be for difference reasons: [93] write that they believe pulses transmitted through new vehicles have a significant effect on the occurrence and location of lumbar injury. [118] hypothesizes that advances in diagnostic technology and better reporting are finding injuries which would have gone unreported in the past. What is undisputed is that currently, there is no definitive lumbar spine injury criteria, and because of this lumbar spine kinematics are ignored in most safety testing. The public database of crash tests published by NHTSA has no crash data where the dummies were mounted with lumbar spine sensors. It makes sense that if there is no limiting criteria, and no one is asked to prove that lumbar spine safety is met for a new vehicle, then the result will be uncontrolled for, and could very well yield something dangerous for the lumbar spine region. Here is another area where a properly validated HBM could prove very useful, maybe even to the point of having a lumbar spine safety criteria developed to be evaluated using HBM simulations

1.2.3 Lumbar Spine Physiology

The human spine consists of 25 bony vertebra which are held apart from each other via the soft tissue intervertebral discs. The discs consist of a gel-like nucleus pulposus, which is surrounded by the fibrous annulus fibrosa. The most distal 5 vertebra, or those 5 closest to the pelvis are the lumbar spine [15].

Bone

Bones are the structural elements of the human body. In the spinal column the vertebra are the solid anchor points which are articulated by the intravertebral discs. The spine also forms the basis via which all of the other parts of the skeleton are joined together. The vertebrae form a ring around the spinal nerves which serves to protect the spinal cord. Each vertebra consists of porous trabecular bone covered by a hard thin layer of cortical bone. The hard cortical bone provides impact protection while the lighter spongy trabecular, sometimes called cancellous, bone distributes the load over the bone [15]. In the spine the bones do not deform as much under loading as the disc, but they still do deform and eventually fracture [104], [29]. Bones are strain rate dependent, experiencing a hardening behavior as well as an increase of yield strength and fracture strength with increasing strain rate [96], [117].

Nucleus

The nucleus pulposus is at the center of the intervertebral disc. It consists of a soft gel-like material. The nucleus has a high water content which allows it to bear large compression loads, while also allowing it to change shape as the spine is flexed, extended or bent [15]. In adults the nucleus has very a very limited supply of blood, leading some to name it the largest avascular structure in the body [101]. This limited ability to exchange nutrients and waste most certainly means that injuries to the nucleus are often slow to heal [101]. The intervertebral disc as a unit has been found to be strain rate dependent [66], but it is hard to isolate the material behavior of the various components. The major building block for soft tissues in the human body is collagen, and collagen is known to be strain rate dependent [52], so this can be taken as the basis for components such as the nucleus pulposus. Due to its high water content and the availability of pressure data, the nucleus has been modeled as a constant pressure body [25].

Anulus

The anulus fibrosus is the tough fibrous outer layer of the intervertebral disc. The anulus fibers help to constrain the motion or deformation of the nucleus. It is when the anulus thins or weakens, that the nucleus can penetrate it, causing a herniated disc, also known as a slipped disc [15]. The fibers of the anulus have a very clear orientation, which is related to their load bearing characteristics. The only blood supplied to the intervertebral disc is to the outermost layers of the anulus. Similar to the nucleus, the anulus is strain rate dependent [66], but isolating exactly how strain rate dependent, and to what extent, is very difficult task to quantify experimentally.

Ligaments

Ligaments connect bones to bones, and in the lumbar spine help to constrain motion [15]. Ligaments are composed of collagen and elastin, which give them strength and resilience [15]. Because of their makeup, ligaments are also strain rate dependent [12]. In the lumbar spine, there are five main ligaments: anterior longitudinal ligament, posterior longitudinal ligament, ligament flavum, interspinous ligament, and the supraspinous ligament. Each ligament has an individual tissue structure and geometry, and thus serves a specific purpose for the lumbar spine [94].

Load Bearing Characteristics

The lumbar spine is the link between the upper and lower body. Also being the most distal part of the spine, it carries the highest compressive loads in everyday tasks, such as standing, walking, or lifting objects. Because in physiology form usually follows function [30], the lumbar vertebra are also the largest in the human body [55]. Normal lumbar loads in everyday activities have been reported to be in the range of 0-1500N [36], [79], [119], [22]. For these everyday activities the loads are applied on the timescale of seconds and thus can be considered quasi-static. Lumbar loads measured in crash are highly dynamic, being applied over thousands of times faster than the everyday loads. The values gathered from looking at simulations in dummies suggest loads with magnitudes up to 5-10 times greater than what is experienced in everyday activities.

Load sharing across the various components is very complex and load dependent. In [25] the authors investigate dynamic axial loading and find the load to be shared roughly equally between the anulus fibrosus and the facet joints. The remains, and slightly smaller, portion of the load is carried by the nucleus pulposus, as seen in Figure 1.3.

Range of Motion

The lumbar spine exhibits the largest range of motion in flexion, followed by extension and lateral bending, which exhibit similar levels, and is the least flexible in torsion. For all motion directions the range of motion decreases with age [114]. The reason for these limits lies in the physiology. In extension, for example, the bony spinous processes come into contact across the facet joints, limiting the motion. In flexion the limiting factors are the ligaments attached between the spinous processes. In lateral bending the ligaments between the transverse processes act to limit the range of motion. Of course the stiffness of the intervertebral disc also plays a role in each loading pattern [53].

Common Injury Patterns

The main injury mechanisms associated with the lumbar spine are differentiated based on the primary loading that causes the injury [124].

- Burst Fracture: this type of injury is due to purely axial loading, and is described by a fracture of the vertebral body in a homogeneous nature.
- Anterior Wedge Fracture: this type of injury is due to a compression bending loading, and is characterized by a localized fracture of the vertebral body on the anterior side
- Flexion-Distraction Injury: this type of injury occurs with pure bending, and is when the posterior ligaments and intervertebral tissues are damaged due to the bending.

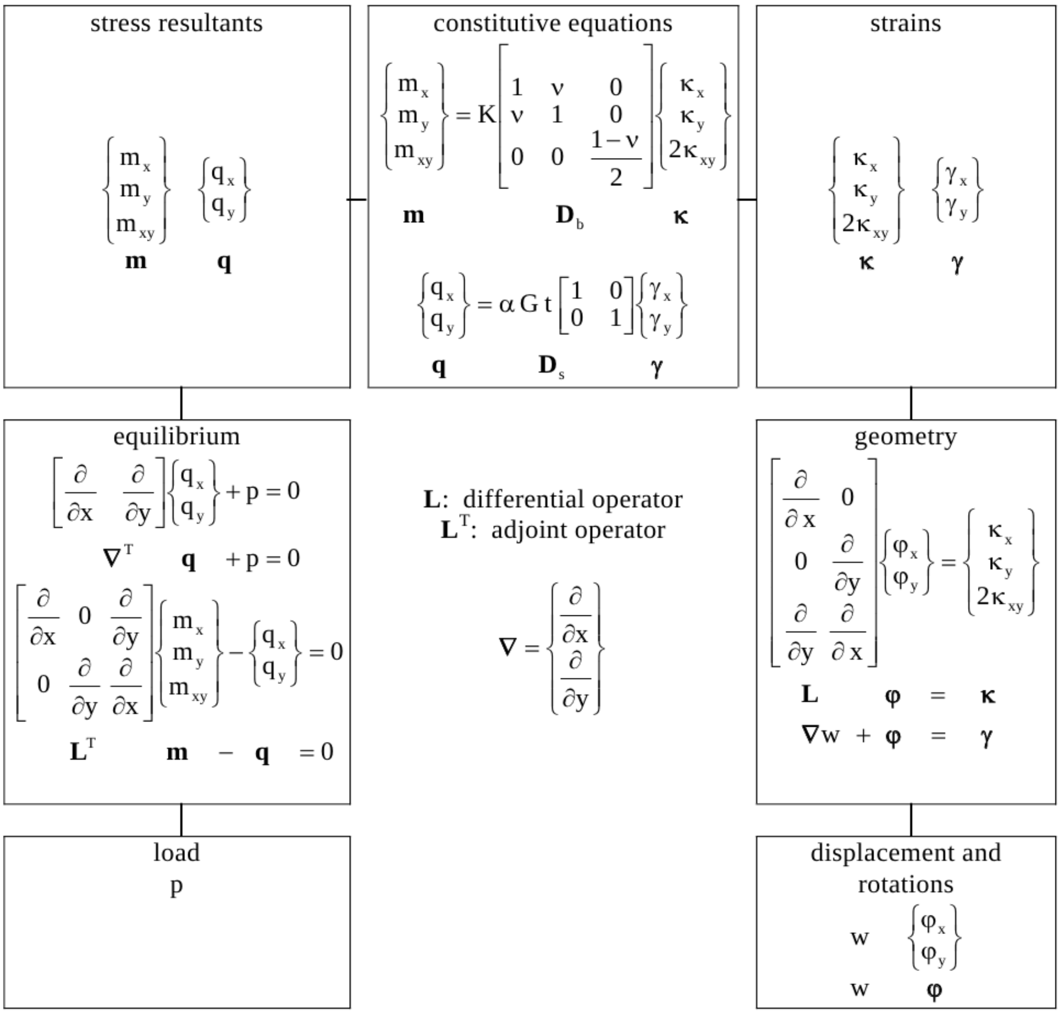

Figure 1.1: A Tonti diagram showing the relationships of various equations for a shell element formulation with shear. Figure from [17]

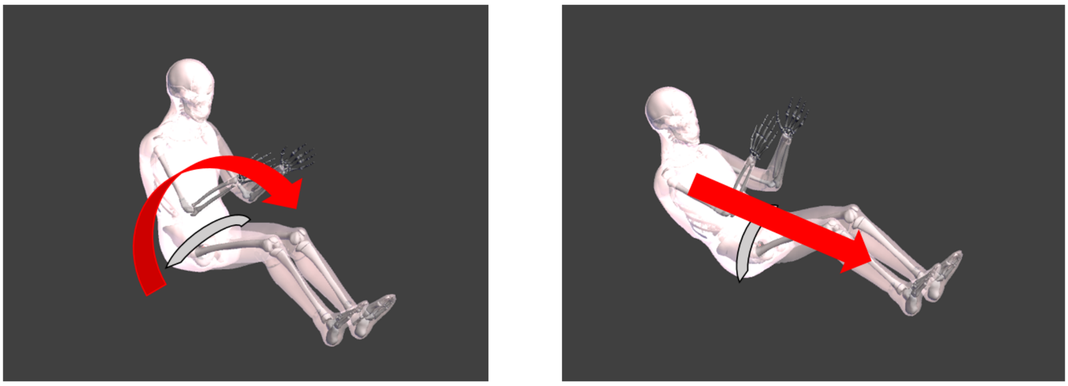

Figure 1.2: A comparison between standard seating, left, and reclined seating, right. The red arrows signify the dominant body motion for each load case

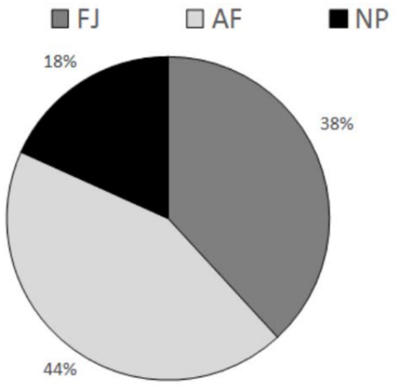

Figure 1.3: A comparison the loads seen over the Nucleus Pulposus (NP) Anulus Fibrosus (AF) and Facet Joints (FJ) [25]

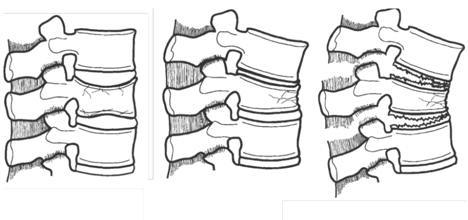

Figure 1.4: Injury mechanisms of the lumbar spine. From left to right: burst fracture, anterior wedge fracture, and flexion-distraction injury [124]

Chapter 2

Research Question and Definitions

2.1 Introduction

2.1.1 Research Questions

The main point of this dissertation is to investigate the biofidelity of the lumbar spine in current state of the art Human Body Models. This question has applications for the auto industry as discussed in Chapter 1. The important questions to be addressed in this work are namely:

- How biofidelic are the lumbar spines in current models?
- How is this biofidelity quantified?
- How does one use this information?

2.1.2 Definitions

These questions will be answered primarily via the mechanism of evaluating validation cases from the literature. In these validation cases the simulation should match the literature as closely as possible. Having such a broad goal makes the process of achieving said goal difficult: it makes the choice of where and how the simulation is evaluated trivial, but not unexacting. The simulation should be conducting, evaluated and analyzed in such a way to match the literature as closely as possible. For automotive applications which are currently being developed there is no template to copy from the literature so new evaluation schemes must be considered. For the purposes of this dissertation measurements of the Lumbar-Thoracic spine shall be considered. But the

question still remains: what should be measured, and how should it be measured? My simple answer to all of these questions is: as much as necessary. One might argue that the current line of Athropomorphic Test Devices (ATDs) should be used as a template for HBMs in general, and this is a good point as it allows comparisons between the two. One of the biggest advantages of the HBM though, is exactly that it is not an ATD, so I will argue that HBMs need measuring schemes appropriate to their construction and for their intended use. For example in the lumbar spine the geometry of all of the current ATDs being used is nowhere close to the human geometry. And having one or two sensors is nice, but the beauty of virtual simulation is that costs barely rise with more sensing (post-processing time does though).
As one can see in 2.1, the geometry of the dummy is also quite different than the geometry seen in a person. The geometry in the HBM is much closer to the the physiological reality, although still not perfect. It is perhaps a philosophical question to be argued by someone else if a single human body model with a single set physiology can be used to represent a large chunk of the population the way crash test dummies are currently used.

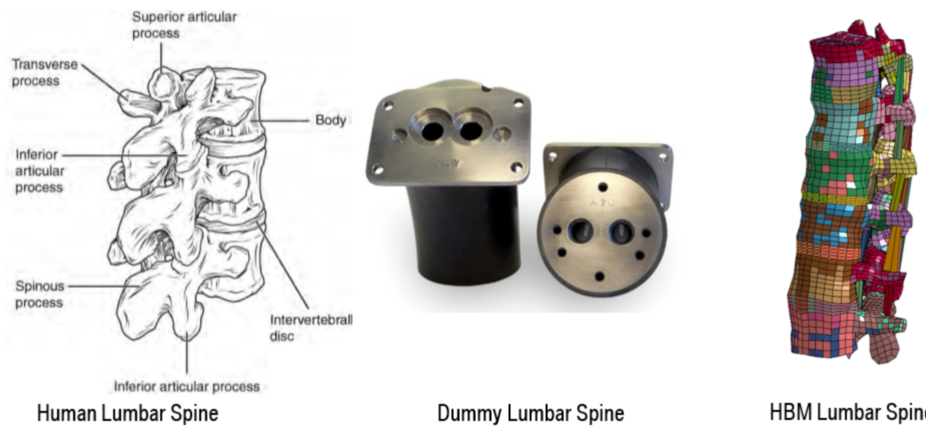

Figure 2.1: A comparison of the lumbar spine, from left: a sketch of two lumbar FSUs in vivo, a Hybrid III dummy lumbar spine, and a THUMS v5 lumbar spine [15] [38]

2.2 Method

2.2.1 Validation Approach

There are many ways to validate various kinds of models. For the validation of numerical models through the use of physical data one method of validation involves constructing a hierarchy and using this structure to ensure a model is valid [86]. The hierarchy helps models to be validated according to their application. For human body models the eventual application is the development of auto safety systems or subsystems, and this application is an incredibly complex one. The interaction between human physiology and the engineering materials seen in automotive safety involves many scales, including large differences in stiffness, occurring on many changing timescales. Using a hierarchical approach allows this complexity to be broken into smaller problems where the reduced complexity can be addressed [86]. Applying verification and validation techniques to biomechanical systems has its own issues and challenges as discussed in [54]. One difference is that even using a hierarchical approach to reduce complexity, biological systems are still very complex. To qualify a model of a tissue sample it can be impossible to eliminate all the sources of uncertainty to the level required in traditional solid mechanics, and do some model assumptions must be made, such as using single curves to represent populations, or assuming variables have normal distributions. Another problem that is often encountered in the validation of biomechanical systems is the validation is performed indirectly, meaning that the experimental data being used for the validation was not originally intended as a validation experiment. This often means that much of the data required for validation is missing. More specifically the challenges involved in validating HBMs for use in automotive applications is that the end scenario is pre-defined. In other fields of biomechanics it might be enough to say that, for example, a femur is the total system, and that is the final area of interest. In automotive crash we always care about the occupant, so the models must be of the entire person. In [46] the author proposes a hierarchy for validating the thoracic region, which can be seen in Figure 2.2. This particular hierachy shall be used as a template for this dissertation, but instead of the region of interest being the thoracic region, the main interest of this work shall be the lumbar spine.

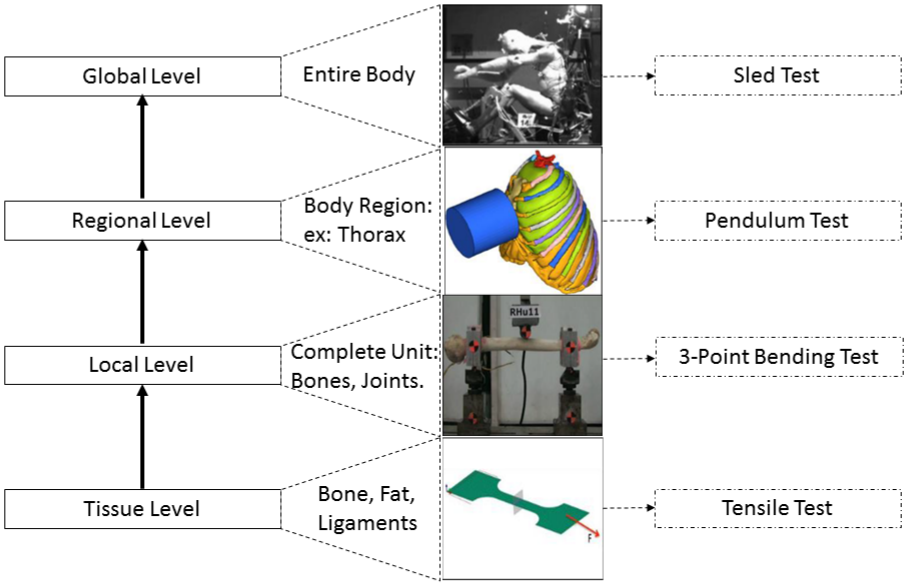

Figure 2.2: Description of the validation hierarchy according to [46].

2.2.2 Measurement Quantities

In order to develop a protocol for the various outputs of the models, the first question should be, what do I want to measure? The second question should be, are my measurements feasible? For example forces and accelerations can be measured quite easily in hardware, and are commonly found in the literature as dependent variables. Stresses and strains on the other hand, while being readily available in finite element models, are extremely difficult to measure in vivo. So the outputs which shall be considered are:

- Forces
- Moments
- Displacements
- Angles

Another important inquiry to make would be, where should I measure what? Looking at the example of the FSU one can begin to make informed decisions. In order to measure the forces and moments transmitted through the spine, the first intuitive idea would be to measure the force at the intervertebral disc and at

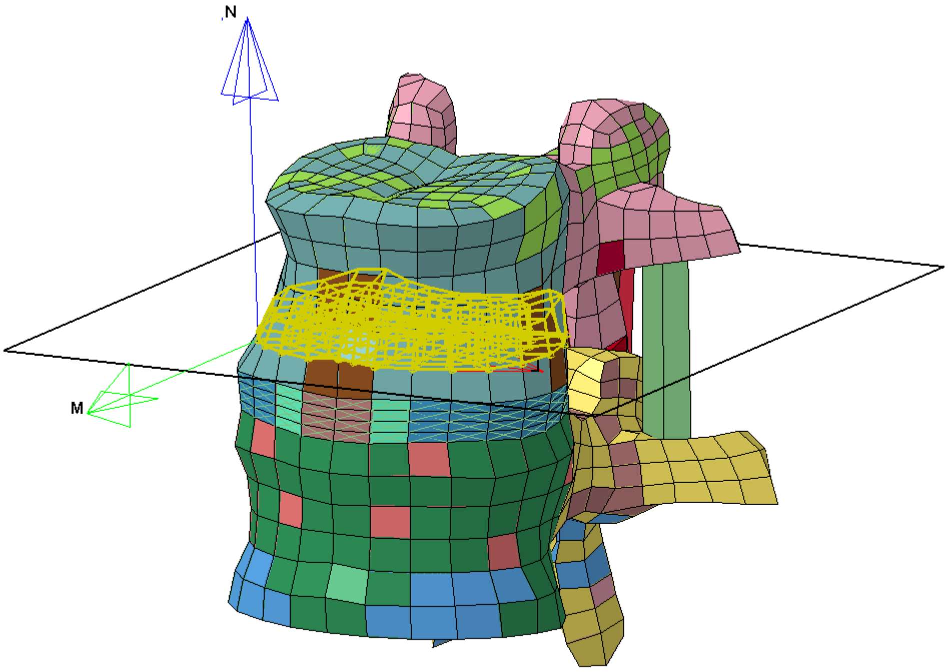

Figure 2.3: Output Definitions and Their Locations as Defined on an FSU

the facet joints, as these are the two structures via which the forces are transmitted. The disc, however is one of the more deformable structures in the FSU, and these large deformations tend to make measurements difficult. When different parts of the disc deform in different modes or when certain parts of the disc deform more than others, it becomes difficult to know which forces are the result of which deformations, and sometimes even in which direction the forces are being applied or transmitted. Measuring forces at the vertebra solves these issues because, while being deformable, the vertebrae in the THUMS v5 are much stiffer than the disc and can be said to exhibit approximately rigid body behavior for most loading conditions. The interesting force transmission through the disc can be captured by measuring forces in the vertebrae directly above, and directly below the disc. For the loading conditions which are the most motivating for this dissertation, namely compression and flexion, the disc global deformation is also of interest. This will be investigated by looking at the displacements of the two end plates, as this is something which can also be investigated in hardware by using video analysis. The end plates where taken as the critical measure as opposed to something like bulge, because the bulge can dependent strongly on the mesh quality in the simulation and can be difficult to measure in vivo. The other main areas of interest are the various spinal ligaments. The ligaments will also use global displacements as their outputs, again due to the straightforward nature of the measurement experimentally. Global ligament strains can also be calculated from these displacements in order to compare them with failure strains from the literature. It should be noted that using the global strains as calculated from global displacements has an analogue with how ligaments are tested experimentally. This contrasts to using the element strains, which would be like attaching a strain gauge to whichever ligament should be investigated. There are two common ways to measure forces and moments from a simulation: by outputting the contact forces or by defining a cutting plane, through which forces are translated. Contact forces will be used to measure the forces in the facet joint, but should only be present in compression and extension, when the facet joint is itself undergoing compression. Contact can also be used to see how much force is transmitted between the posterior elements during extension, if there is enough extension to cause contact. Contact will also be monitored between the vertebral bodies, because although such contact is physiologically impossible without some sort of disc failure, it is numerically possible, and because of this, needs to be controlled for on simulations where it might occur. Outputting forces and moments with a cutting plane is a straightforward process: the user defines a plane where the forces and moment shall be measured. In LS-DYNA this plane can be defined by either choosing a node set and associated elements, or by defining a normal vector and specifying which parts should be included in the calculation. Both of these methods where investigated to see if there was a difference between them.

Figure 2.4: Reference Point Locations as Defined Over the Entire Spine. From Left: the Cervical Spine, the Thoracic Spine, and the Lumbar Spine

The kinematic movements of the spine are also very interesting quantities to evaluate after a simulation. The kinematics can be described by tracking points through time and space. The choice for the kinematic tracking points were chosen as the node closest to the center of the vertebral body. This decision was made for practical reasons. Ideally the tracking points would relate to the exact center, but this is infeasible to achieve: first certain reference points would need to be defined, and then calculations would interpolate the the tracking points based on the position of the reference points. The issue is that for most FE HBMs the mesh quality is not good enough that the reference points match the anatomical descriptions. One can circumvent this by choosing the node closest to the true reference point, which leads back to the original problem[1]. A description of the kinematic tracking points can be seen in Figure 2.4

[1]This incorrect definition of reference points is only a problem for anatomical reference points. For functional reference points, such as the center of a joint, these can be accurately extracted even from rough meshes because the the physics of the coarse mesh will be dependent on the geometry described by the mesh.

2.2.3 Evaluation Methods

After a simulation has been run, the task of evaluating it must also be considered. What is a good result? And how can this be objectively measured? One common way to assess the accuracy of a simulation is through the so-called goodness of fit of the simulation results to some proposed mark which as taken as being correct, or as being reality. In most the cases from this work this will be to compare output quantities from the simulations to results published in the literature, usually in the form of curves. The goodness of fit would then refer to how well the simulation curve matches the curve from the literature. There are many ways to go about comparing two curves, each of course with their own pros and cons. One major method that stands out is Correlation Analysis, or CORA [48]. This method is used by many in the field of impact biomechanics to compare different result curves [61] [126] [92]. In a CORA analysis a corridor consisting of an upper boundary and a lower boundary is a prerequisite for the base data. Corridors can be constructed in numerous ways [48]. To obtain the total corridor rating the test curve is treated as a collection of test points. The total rating is calculated by taking the average over all of the points in the entire test curve. Each of the components of the cross-correlation score are calculated independently of one another and combined into the final rating. Sometimes the shape score is also called the progression rating [112].
The CORA rating is just one of many evaluation methods [**?**]. It was developed to attempt to minimize the amount of expertise or subjectivity involved in comparing simulations to experiments [48], but this is still not fully automated; at the present time some sort of engineering judgment or expert opinion is still required. Whenever my judgment or expert opinion is expressed in this work I will attempt to clearly explain my reasoning and to provide objective evidence as support.

2.3 Results

The output protocol is defined only for the lumbar spine, and can be exemplified through the example of a single FSU. The disc deformation is measured by tracking the nodes of both of the adjacent end plates, and then by comparing their relative displacement. These nodal outputs are also used to find the deformation angle of the disc. Other nodal outputs are defined for of the following spinal ligaments:

- Anterior Lateral Ligament (ALL)
- Posterior Lateral Ligament (PLL)

- Interspinous Ligament (ISL)
- Supraspinous Ligament (SSL)
- Intertransverse Ligament (ITL)

For all of the ligaments the relative deformation of each of their end nodes is calculated, this of course is only meaningful when the ligament is in tension. Cutting planes are defined in the vertebral body along the transverse plane. Three cutting planes are represented: one close to the superior vertebral end plate and another close to the inferior end plate. A third cutting plane is defined to cut through the entire vertebra including the posterior elements. An additional cutting plane is defined through the soft tissue of the facet joint, in order to measure tensile force in lateral or flexion type movement. Cutting planes are also defined through each of the aforementioned ligaments in order to help visualize the load path of the complete system.

The questions to be addressed in this chapter relate the various output strategies used by LS-DYNA as well as the calculation methodologies used to post-process the outputs. The main question being, how does LS-DYNA output a cutting plane force, or as it is referred to in LS-DYNA, a section force? There is an option to define the plane as a vector or as a set of nodes and elements, what are the differences between each variant? There is also the option to define a local coordinate system for the cutting plane, what effects does this have? For the nodal quantities it is also interesting to deal with coordinate system questions, in which coordinate system should the results be calculated, and what is the best way to calculate them?

Several different load cases were considered in order to address each of these questions. A single FSU loaded in flexion and extension was used to investigate the differences between a plane defined geometrically versus a plane defined based on a mesh definition, as can be seen in Figure 2.5. The entire lumbar spine loaded in flexion was used to investigate the effects of defining local coordinate systems.

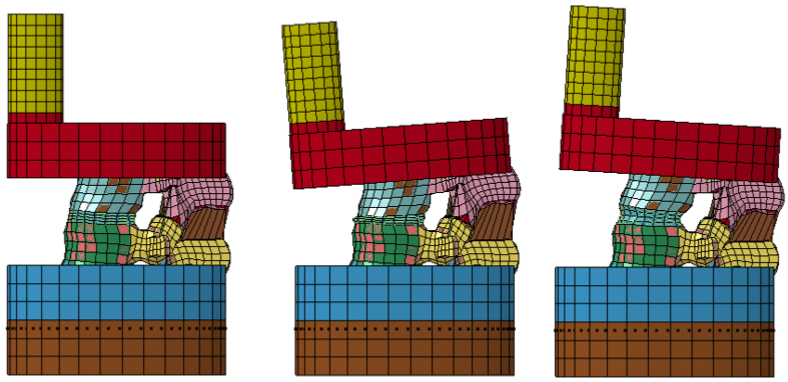

Figure 2.5: Visualization of the Simulation Used to Investigate Cutting Plane Definitions

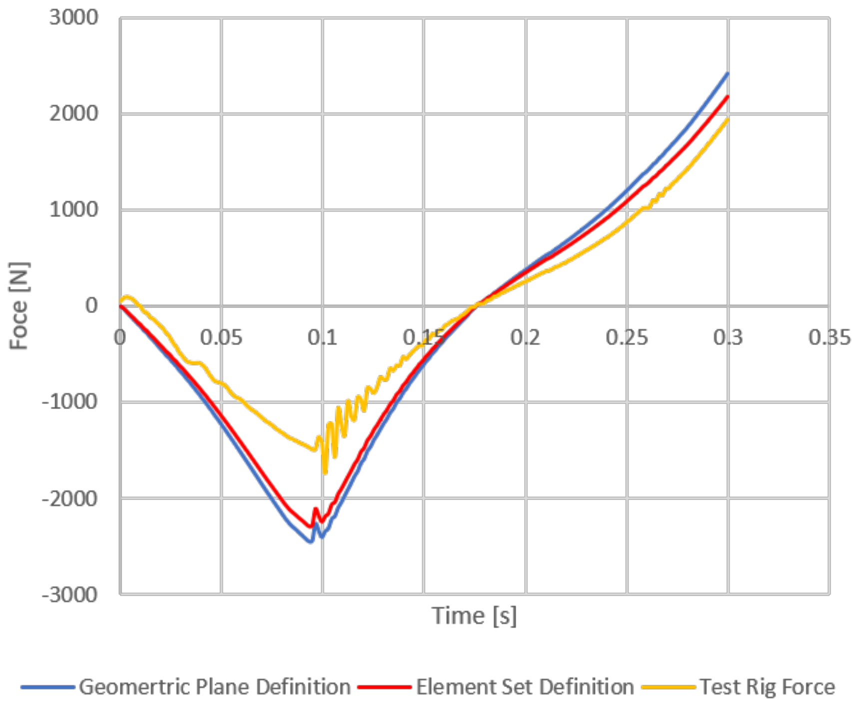

Figure 2.6: The results of the simulation investigating the separate cutting plane definitions. Force in the Z axis, corresponding to the transverse plane, is plotted

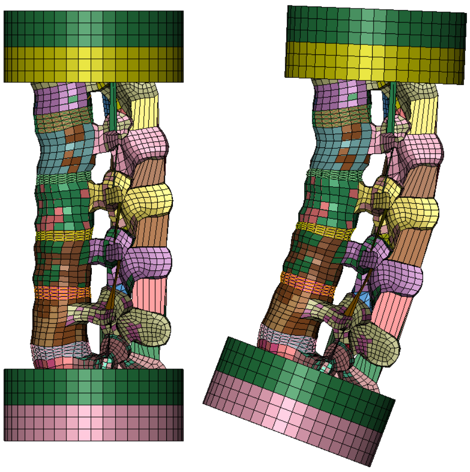

Figure 2.7: Visualization of the Simulation Used to Investigate Coordinate System Definitions

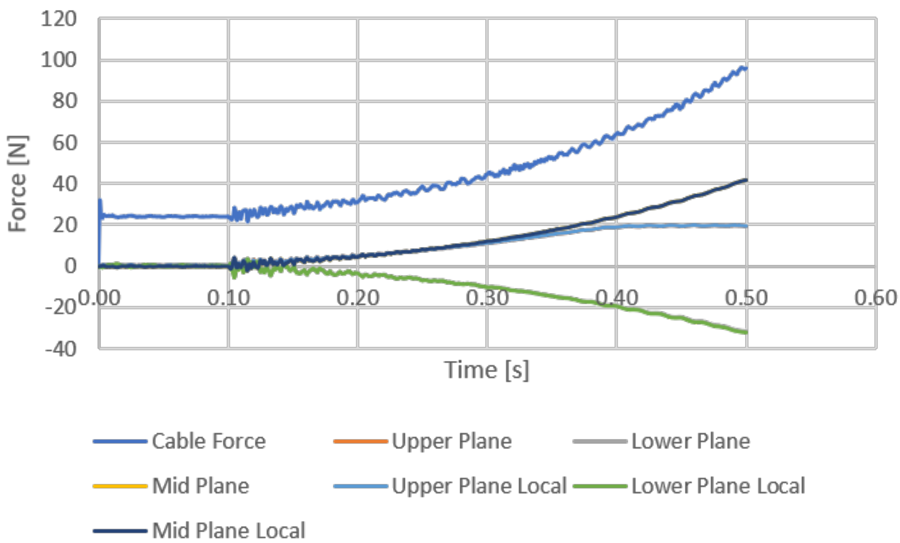

Figure 2.8: The results of the simulation investigating the separate cutting plane coordinate system definitions. Forces measured in the L1 vertebra in the X direction, corresponding to the coronal plane, are plotted

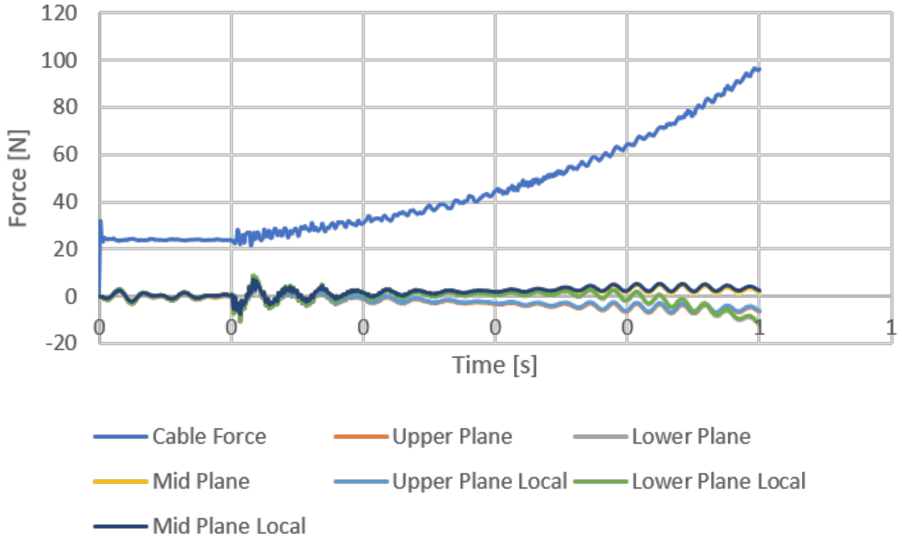

Figure 2.9: The results of the simulation investigating the separate cutting plane coordinate system definitions. Forces measured in the L1 vertebra in the Z direction, corresponding to the transverse plane, are plotted, with the cable force still axial along the cable, which is mostly in the X direction

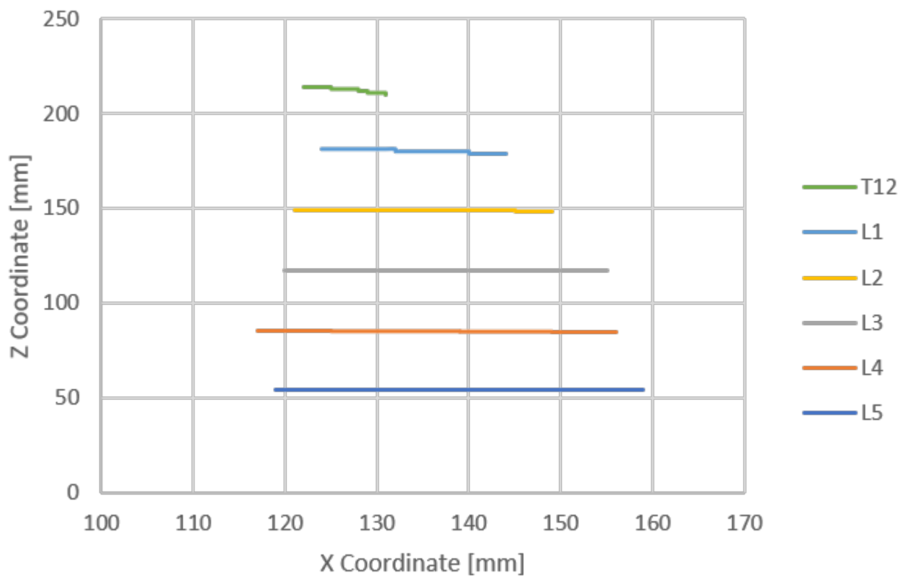

Figure 2.10: The results of the simulation investigating the kinematic tracking of the lumbar vertebrae

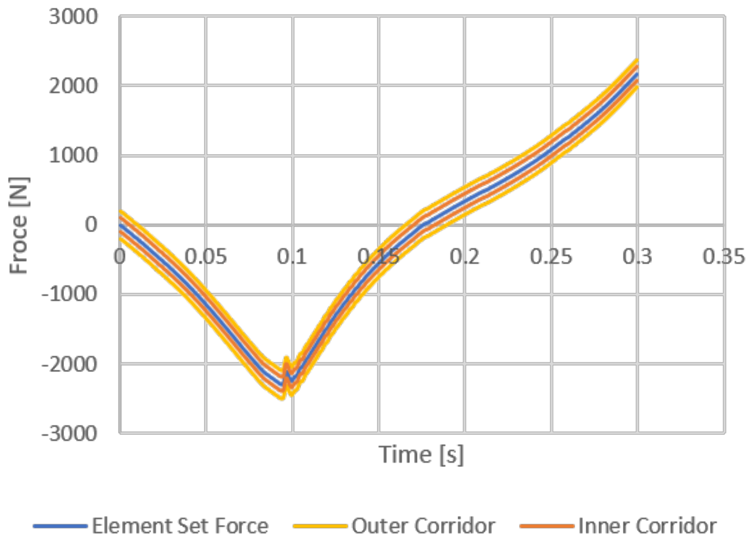

Figure 2.11: The CORA analysis of the simulation investigating the separate cutting plane definitions

An example using a CORA analysis is performed on the results of the study of different section force definitions in Figure 2.11.
In Table 2.1 the quantity C1 describes the corridor rating. A rating of 1 describes the best rating. For this example a rating of C1=0.81 shows the most of the reference curve falls within the inner corridor around the reference curve. The next step in the CORA analysis is the cross-correlation. The size, shape, and phase alignment of the reference and the test curves are compared, disregarding the corridor definitions.

C1	Shape	Phase	Size	C2	C3
0.81	0.99	1.00	0.97	0.99	0.90

Table 2.1: The results of the CORA analysis of the simulation investigating the separate cutting plane definitions

A diagram showing the expected coordinate system transformation from the rigid body rotations can be seen in Figure 2.12

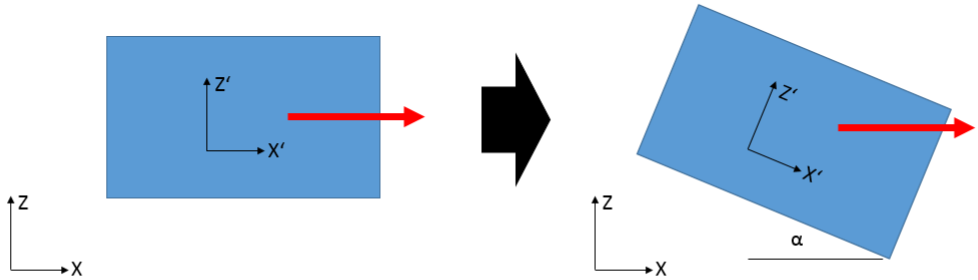

Figure 2.12: A diagram showing the undeformed state with the local and global coordinate systems as aligned, left, and the deformed state where the local coordinate system is rotated to have the applied force more oriented towards the z axis, right

2.4 Discussion

The FSU in flexion and extension was chosen as the load case to investigate the difference between defining a cutting plane using geometrical quantities such as vector normals and defining the planes using mesh quantities such as elements and nodes, because the change in orientation of the cutting planes, no matter how they were defined, should help to elucidate how the cutting plane outputs are calculated in LS-DYNA.

As one can see in Figure 2.6 there is a discrepancy between both cutting plane definitions, with the geometrically defined cutting plane having larger peak values. The output of the test rig cutting plane was included for scaling purposes; one would think that the overall force measured at the ground should match the overall force transmitted through the vertebrae. However as this simulation has not, and will never reach its steady state, this assumption proves false, the curve is included nonetheless. It is interesting that both of the internal cutting planes reach a higher force than the ground cutting plane, energy absorbed by the disc deformation could be responsible. Both the geometrically defined and the mesh based cutting plane show the same general shape, and both cross the axis at the same place, which means they are somehow related by a scaling factor. It is unclear which is more accurate, and as there is a noticeable difference between the two, it is clear that one method must be consistently used in order to compare like to like. For the context of this dissertation it has been decided that the mesh-based definition shall be used. It is clear that in a finite element context the forces and moments must be calculated at the nodes, because that is where the force quantities are defined. With this knowledge, one can assume that the geometry based cutting plane is simply a way of selecting the nodes closest to a given plane. The decision to use the more straightforward definition using the nodes themselves rather than an algorithm which chooses them, is largely just a way to be able to eliminate unknown quantities from the modeling.

An example using a CORA analysis is performed on the results of the study of different section force definitions. In Figure 2.11 this example has been illustrated. To compare the two curves representing the geometric cutting plane definition and the finite element based definition one of them is taken as the reference curve (in this case the definition of the plane using the finite element definition) shown in Figure 2.11 as a solid red curve. In this example the definition of the reference curve is arbitrary, because in this example both of these curves are simulation results[2]. Around the reference curve an inner and an outer corridor are constructed. For this example both of these corridors are artificial and made by adding or subtracting a constant value from the reference curve, seen in Figure 2.11 as dashed and dotted red lines. The reason why these corridors are artificial is discussed in the previous footnote. The first part of the CORA analysis compares a sample test curve, in this example the curve showing the geometric cutting plane results shown in Figure 2.11 as a solid blue curve, to the established corridor. A good match is defined as when the test curve fits entirely withing the corridor. In this example the shape, phase, and size ratings are 0.99, 1.00, 0.97 respectively which considering a maximum possible score of 1.00 suggests that in all three fields both curves are extremely similar. The C2 score is a weighted sum of the shape size and phase ratings and so is also almost perfect at C2=0.99. The weights are chosen to fulfill a partition of unity which ensures that the best possible score for the cross-correlation remains 1.00. The final score C3 is the overall CORA rating and is a weighted sum of C1 and C2 with the weights also chosen to ensure that a score of 1.00 can not be exceeded.

An overall score C3 of above 0.8 suggests that the curves show a good agreement [106]. Looking into the component parts and seeing that the cross-correlation score C2 = 0.99 this suggests that all of the sources of disagreement between the two curves arises from the corridor score C1. Not using any sort of formal analysis criteria one can see that the element set curve and the geometric plane curve are only different in their scaling. They even cross the x axis at the same point, suggesting that the scaling has no offset. The reason why the corridor treats this scaling as a source of dissimilarity is because the corridors were constructed using arbitrary constant values. With a a large enough value one could force the corridors to be large enough to capture all of the data. Another option would be to use sigma-based corridors [48] which change their width

[2] Usually CORA analysis is used to compare simulation results to experimental results, this exercise is an example to illustrate roughly how the CORA analysis works

dependent on where they are applied to the curve. With sigma-based corridors the variation has a more physical meaning, such as upper and lower corridors coming from separate experiments.
The second investigation concerning the coordinate system definition was conducted after the first, which means the cutting planes it uses were defined using the mesh quantities. In this case the entire lumbar spine was considered under flexion because it achieves a larger variation in angle than the FSU could. This difference in orientation would be able to emphasize the difference between the local and global coordinate systems, as one would be able to see a phase shift, increasing with increasing angle.Consider that in this test setup a force is applied constantly in the x direction and the vertebra are all free to rotate. This would mean that in the deformed state the vertebra would be experiencing the global x force oriented more towards the z local coordinate, which can be visualized in Figure 2.12. One can see from Figures 2.8 and 2.9 that there is no sizable difference between the two curve classes. The question then becomes, are both curves in the local coordinate system, or are both curves in the global coordinate system? It would stand to reason that the default for the system would be to have a global coordinate system, so it shall be assumed that the outputs which are displayed are all given in the global coordinate system. To output the forces in the local coordinate system can be done in post-processing.
To summarize, all cutting planes will be defined using mesh quantities, such as nodes and elements. The output forces and moments will be given in the global coordinate system and then transferred to the local coordinate system in post-processing.

Chapter 3

Validation of the Intervertebral Disk

3.1 Introduction

The most local level of the investigation into the influences of the submarining phenomenon will be conducted on a functional spine unit (FSU). But seeing as how the FSU itself is a complex structure composed of bones, multiple ligaments, facet joints, and an intervertebral disc (IVD), in order to reduce complexity, one of the FSU's components shall also be validated. It was chosen that the IVD would be this validation, mainly due to the availability of data, but also because it carries a large portion of the load in an FSU [25]. Sensitivity studies using finite element analysis (FEA) have also shown that IVD parameters have a large effect on overall spine response [102] [27].

The IVD was chosen as the smallest level of validation for several reasons. One can of course start at the cellular level, but in general for human body models, or finite element type validation this is generally seen as an impractical level of detail because the cellular structures are modeled as a continuum [16]. What is more typically common, is validation starting at the tissue level [85, 115]. The local level is chosen over the tissue level for this thesis because the main point of interest concerns the kinematics and injury mechanisms in the lumbar region, including injuries and kinematics which relate to submarining. The IVD plays an important role in all of the spinal degrees of freedom, namely: forward flexion, extension, lateral flexion, and axial rotation, [15] and it is these motions which are of interest to help investigate the cause of injury during submarining, and in new seating positions.

The IVD is composed of a fibrous annulus fibrosis, which surrounds a gel like nucleus pulposus. The IVD is bound to the vertebrae via a hyaline cartilage endplate [98]. The annulus is composed of 15-25 concentric layers of lamellae, where each layer is composed of parallel collagen fibers oriented at an angle of 60° to the longitudinal axis [98]. The annulus exhibits a nonlinear, viscoelastic behavior, which is strongly anisotropic, and strongly dependent on the location of the specimen tested [39]. Mostly made of hydrated aggrecan [98], the nucleus pulposus also contains collagen fibers, but they are oriented randomly. The nucleus also exhibits viscoelastic behavior, at low strain rates resembling a fluid, while under more dynamic loads it shows more solid-like mechanical properties [58]. The endplates consist of a thin layer of cartilage, with collagen fibers in it running horizontal and parallel to the vertebral bodies [98]. The endplate properties are difficult to isolate from the vertebral body, although it has been observed that properties are strongly location dependent [51].

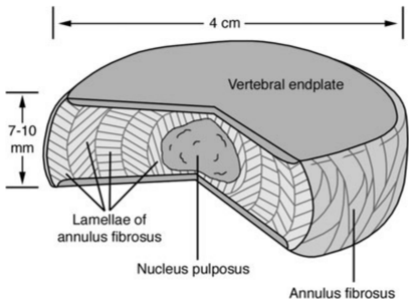

Figure 3.1: The anatomy of the intervertebral disc [98]

The objective of using many different HBMs to investigate the IVD is to analyze how the models differ, and to investigate if any systemic errors exist in the models as compared to the reality of the component tests. Additionally, just as each human is different in their response to an impact load, each HBM also provides a response different from the other HBMs. An interesting research question is to see if the HBMs show more or less variability than their analogous human counterparts for any given study.

3.2 Methods and Materials

Description of the HBMs investigated

The HBMs investigated are the THUMS v3.01 TUC v2 2016 (THUMS v3), the THUMS v4.01 (THUMS v4), the THUMS v5.02 (THUMS v5), the GHBM v4.5-D (GHBMC) and the ViVa 2016 (ViVa). In general the THUMS models all model the anulus, anulus fibers, and nucleus as separate materials, each attached to the other with shared nodes, while the GHBM and ViVa models model the entire

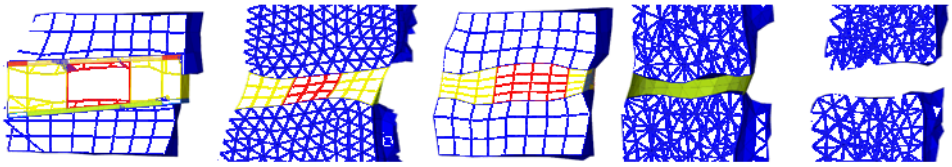

Figure 3.2: Cross sectional view of the five human body models investigated for the IVD load case. From left: THUMS 3, THUMS 4, THUMS 5, GHBM, VIVA. The vertebral bodies are shown in blue, the nucleus pulposus is highlighted in red, and the anulus fibrosis is colored in yellow. Note that the models have the posterior elements excised.

Table 3.1: Table describing the various selected modelling conventions used in the HBMs under investigation

	THUMS 3 (TUC)	THUMS 4	THUMS 5	GHMBC	Viva
Nucleus Material Model	Linear Elastic	Elastic Plastic	Hyperelastic	6 Degree of Freedom Curves[1]	6 Degree of Freedom Curves[1]
Annulus Matrix Material Model	Linear Elastic	Visco-elastic	Viscoelastic	NA	NA
Annulus Fibers Material Model	Linear Elastic	Linear Elastic	Nonlinear Elastic	Linear Elastic	NA
disc Height [mm]	8.7-10.5	5.6-9.8	5.3-8.2	7.3	NA
Mean disc Area[mm]	1110.46	1098.07	1161.5	1161.92	NA
Mean Nucleus Area [mm]	203.3	217.83	414.84	NA	NA

disc complex through use of non-linear elastic 6-degree-of-freedom curves[1]. The approach used by GHBM and ViVa appears superficially thus to have no IVD (although the GHBM model has shells surrounding the disc geometry (seen in Fig. 3.2 in green), which have no analog in human physiology). The HBMs can be seen in Figure 3.2, and a more detailed description of their differences can be seen in Table 3.1.

[1]The 6 degree of freedom curves are used instead of having the tissues between the vertebrae, this is a purely kinematic description, analogous to a spring that has different stiffnesses depending on the direction of loading

Description of the Reference Experiment

In order to validate the response of the IVD, the experiments conducted by Newell et al. [84] were considered. In this experiment twelve human spine segments with the posterior elements removed were tested in compression at different strain rates. Four lumbar motion segments were obtained from four human cadaveric specimens (40 ± 18 years old) and were fresh frozen directly after harvesting. All human tissue was obtained via Imperial College Tissue Bank ethics committee (Ethical approval number: 12/WA/0196). The specimen displacement was measured using two Linear Variable Displacement Transducers (LVDTs) mounted to the pots holding the specimens. Another LVDT was placed horizontally in order to measure the disc bulge under compression. A pressure transducer was placed into the nucleus in order to measure internal pressure. Reaction forces were measured by the Instron machine (8872; Instron, Canton, MA,USA) used to apply the displacements. All experiments were also filmed. This reference experiment applies constant velocity displacements up to a strain rate of $1s^{-1}$. The maximum displacement of approximately 15% strain was chosen so that the specimens would not be damaged, this allowed for multiple tests on each specimen. This was ensured by testing a test specimen to 15% strain and then letting it rest for five minutes. After this recovery period the specimen was again tested to 15% strain. As there was found to be less than a 5% difference in peak force between the response curves between the two tests, it was shown that testing to 15% strain caused no injury.

Finite Element Simulation

The various reference experiments were then simulated in LS-DYNA, where care was taken to model the experiments exactly as described in the literature. The first step towards modeling was to process the experimental data into a more useful form. The experiment used Linear Variable Displacement Transducers (LVDTs) to measure the disc displacements. These displacements were averaged across all donors and specimens in order to provide the displacement boundary conditions for the FE models. Upon analyzing the time displacement curves for all subjects, it was found that for the L4-L5 level the time scale was much shorter than for other experiments. Because of this discrepancy only 12 of the possible 16 tests were used to construct the boundary condition data. And because these four tests were excluded from the inputs, they were also excluded from the calculations of the corridors used as outputs.
The modeling was undertaken with five different human body models, namely the THUMS TUC v3.01 [60], which was used under license at BMW, the THUMS v5.02 [61] also licensed by BMW, the THUMS v4.01 [67], the GHBMC

v4-5 [47], both of which were used under license from the LMU Institute of Legal Medicine, Biomechanics, and Accident Analysis, and the ViVa HBM [87], which is an open source model.
The relevant components of the HBM were isolated using standard pre-processing software by excising the components not directly relevant to the experiments. This directly analogous to how the specimens were prepared for the physical experiments. For this IVD investigation, the posterior elements and all muscles were removed, leaving the disc intact with all of its ligaments and structures.
In all models, rigid body definitions as well as shared node parts were used in order to join the HBM specimens to the plattens where the forces and displacements are defined.

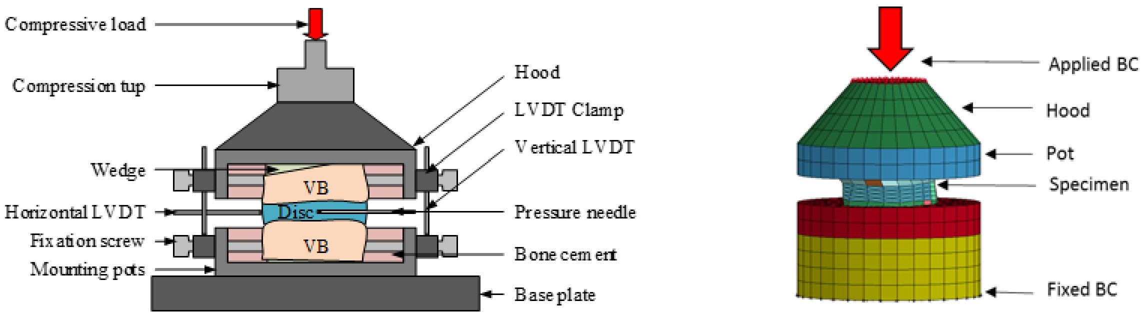

Figure 3.3: A diagram of the reference experiment (left from Newell [84]) and the finite element model of the reference experiment

The models are positioned using the specimen experiments as the reference data, with the mid-plane of each disc held perpendicular to the direction of testing. In the experiments this is accomplished through the use of 3D printed wedges based on the data from CT scans, in the simulations the angles are defined using numerical boundary conditions. The specimens were positioned in the testing device in such a way as to minimize the applied bending moments: they were aligned such that the center of the testing device cross-head was aligned at 1/3 of distance from posterior to anterior of the disc, from the posterior-most aspect along the mid-sagittal plane of the disc. It is a simple process of translation to align the HBMs in this manner.
Model result corridors are constructed using the method according to Newell [84], who performed the original experiments.The model variation across experimental levels is added to the average of the model response across levels in order to obtain a corridor. Analysis of the model fit as compared to the experimental corridors is performed using a CORA analysis [48]. In the CORA analysis, V is a progression rating which rates how well the shapes of two curves match, P corresponds to a phase shift rating, and G is a rating of how similar the

two curves are in size. A value of 1 corresponds to a perfect match, where 0 indicates curves have nothing in common. A cross correlation score C2 is derived by weighting V, P, and G. The corridor score C1 indicates if the test curves from the FE Models fall within corridors derived from the experimental curves, with again a score of 1 being the best. Both C1 and C2 are aggregated into a total score C3, with a score of 1 being best.
Additional corridors are constructed using the interquartile range multiplied by a scaling factor instead of the standard deviation.These corridors are constructed in order to perform an outlier analysis, as suggested by Hoaglin [56].

3.3 Results of the IVD Validation

The results from the simulation study can be seen in Figure 3.4. The shaded regions represent one standard deviation about the mean value, which is plotted as a solid line. The variation observed comes from simulating different lumbar levels, which corresponds to the method with which the experimental corridors were constructed. There is overlap between the different model corridors and experimental corridors, showing a diverse range of responses between the models. The results from the CORA analysis can be seen in Table 3.2[2]. In addition to the model corridors being plotted analogously to how the experimental corridors were constructed, they were also plotted with the corridor width corresponding the the interquartile range, which can be seen in Figure 3.5. In these corridors there is more overlap than in Figure 3.4

	C1	C2	V	P	G	C3
THUMS 3	0.82	0.67	0.97	0.00	0.94	0.74
THUMS 4	0.01	0.49	0.97	0.00	0.33	0.25
THUMS 5	0.68	0.68	0.99	0.00	0.93	0.68
GHBM	0.06	0.53	0.97	0.00	0.47	0.29
ViVa	0.35	0.58	0.73	0.00	0.96	0.46

Table 3.2: The results of the CORA analysis of the various simulation

[2] V is the progression rating which rates how well the shapes of two curves match, P corresponds to a phase shift rating, and G is a rating of how similar the two curves are in size. The cross correlation score C2 is derived by weighting V, P, and G. The corridor score C1 indicates if the test curves from the FE Models fall within corridors derived from the experimental curves. Both C1 and C2 are aggregated into a total score C3. For all values 0 is the worst fit 1 is the best fit

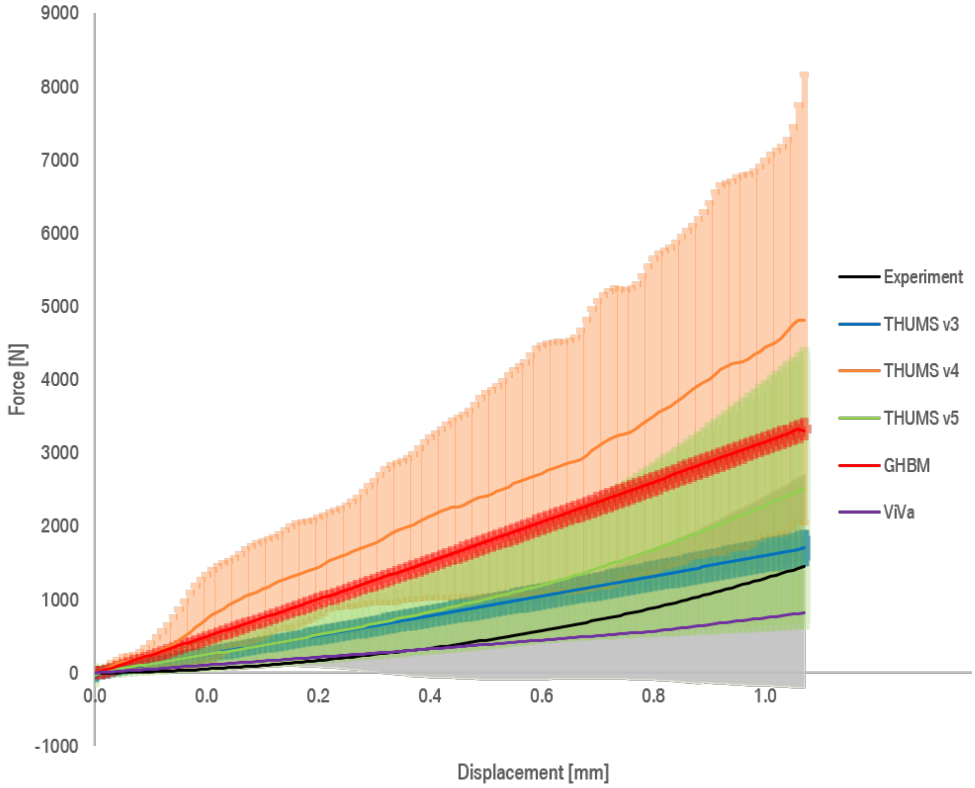

Figure 3.4: Results comparing the simulation results to the reference experiment. Solid lines represent the mean response seen for both the experiment (in black) and the HBM simulation, and the transparent corridors around the mean are the variability from the experimental results and FE simulation results, respectively

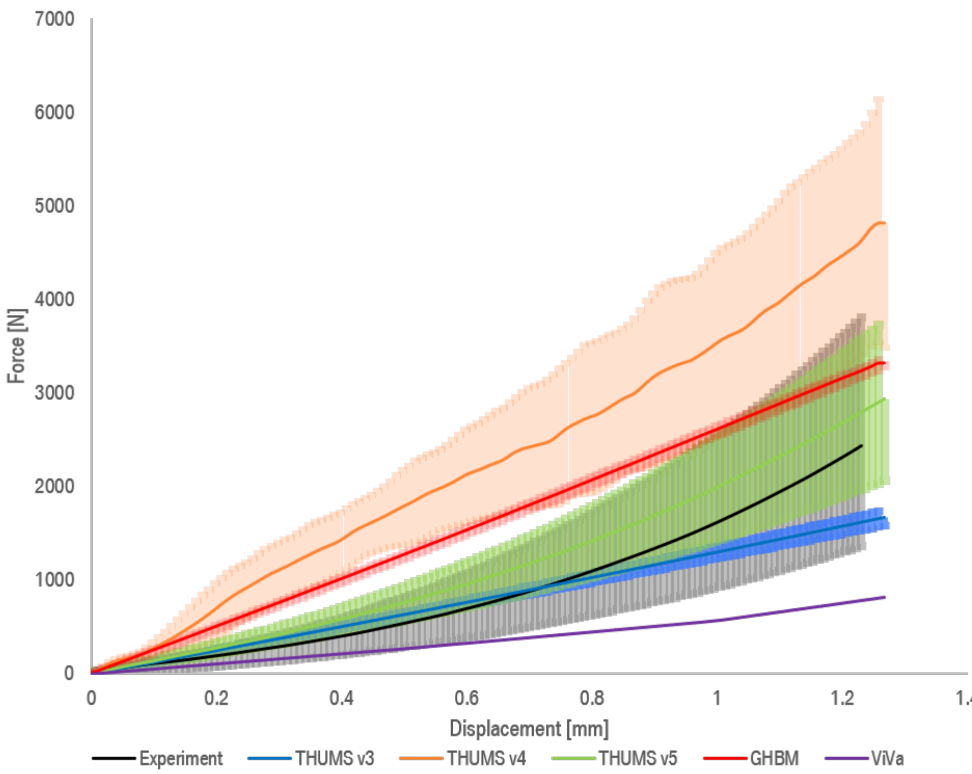

Figure 3.5: Results comparing the simulation results to the reference experiment. Here the corridors represent a region 2.2 times the size of the inter-quartile range for each each curve set to see if any particular FE curve can be considered an outlier with respect to the experimental data [56]

3.4 Discussion

This reference experiment applies constant velocity displacements up to a strain rate of $1s^{-1}$, which is where according to Race et al. [97], strain rate is negligible. Only the THUMS v4 and THUMS v5 have strain rate dependency, but as both use viscoelastic models this strain rate dependency can not be calibrated to the strain rates observed in physical experiments.
The experiment used Linear Variable Displacement Transducers (LVDTs) to measure the disc displacement. This is more accurate than using the material testing machine itself as the LVDTs record displacements at the region of interest, whereas the testing machine might also measure displacements in the fixtures or in the testing machine itself which have nothing to do with the region of interest.
Rigid body definitions were used in order to join the HBM specimens to the plattens where the forces and displacements are defined. This approach is assumed to be a valid modeling simplification because the relative stiffness of the bones and test frame is much greater than that of the IVD.
Based on the results presented in Section 2.3 one can see that of the current HBMs there is a very wide range of responses: over 500% difference between peak median values and over a 300% difference in the peak variation as measured by the interquartile range. Larger variations are observed between the different HBMs tested than seen within the experimental results between individuals, which suggests that at least some of the HBMs investigated do not give a realistic response for this IVD loading regime. That being said a sample size of only four individuals might also not show the kind of variability seen in the entire population. One reason it is interesting to compare multiple HBMs is to see if there are some kinds of systemic trends on display. For example if all of the HBMs were found to be much stiffer than the experiments this could be seen as a problem in general with HBMs: they could be said to have too stiff lumbar discs. This is however not the case. As seen in Figure 3.4 there are always at least two HBMs which are softer than the level based upper experimental corridor. Having the HBMs spread on either side of the corridor likely means that in general the HBM modelling conventions are sound, and that the HBMs with the more extreme response, i.e. further away from the corridors, are the ones which have the least accurate modelling for this particular load case.
Looking at Figure 3.4, one can see that the only simulation models which falls completely within the experimental corridors are the THUMS v5 model and the THUMS v3 model. Both THUMS v4 and the GHBM Model exhibit behavior stiffer than the experimental corridor, while the ViVa model is softer than the experimental corridors. A relevant question to ask at this point would be if that means the other simulations which lie outside of the corridors are usable data

representing the bounds of what is realistic, or are they outliers which have no physiological relevance. One way to test this is to look at the inter-quartile range of the physical experiments [56]. After building a corridor which represents the scaled inter-quartile range from the median of all of the experimental and simulation curve clusters, one can see there is indeed overlap between all of the clusters, as seen in Figure 3.5. This scaling was done using a factor of 2.2 which Hoaglin suggest as appropriate for the large number of data points being considered [56] This overlap is inconclusive; by comparing like curves as in Figure 3.4 one can see larger discrepancies between the models and the experiments, most notably for the THUMS v4 and GHBM. It should also be said that any sort of outlier analysis for these simulations is limited. At each experimental level there are only four specimens, which makes construction of a box plot ambiguous. Also the small range of loading could influence the results: loading to two or three millimeters might cause the experimental corridors to align better with the stiffer models leaving the softer ones as outliers.

The accuracy of the THUMS v5 model is likely due to the inclusion of multiple FSU validation load cases [61], which help the model to fulfill corridors of a similar nature to the analyzed reference experiment. It is logical to assume that if the model was designed using criteria similar to what is being investigated in this experiment, then the response should be similar. In addition to the inclusion of this validation data, the THUMS 5 model also has the most detailed disc modelling of all the HBMs investigated. It has the finest mesh, as well as material model definitions which can capture the hyperelastic, nearly volume conserving behavior associated with IVDs.

There is no published data for the THUMS v3 validation cases, but the THUMS v4 uses a validation case which considers the entire lumbar spine in compression, in addition to other loading directions. No matter which validation cases THUMS v3 had used, it is interesting that it exhibits such a different behavior to both the THUMS v4 and the THUMS v5. The THUMS v3 and THUMS v5 share a common lineage, with the THUMS v5 acting as an update to the THUMS v3, with many updates being presumably informed by the development of the version 4 which came between. The spine, including the discs are noticeably different from THUMS v3 to v5, the THUMS v3 discs are modelled as linear elastic, and the spinal mesh is much coarser than that of the THUMS v5.

As mentioned above, THUMS v4 was validated using component data, so it is surprising that the model is stiffer than this particular reference experiment. One possible explanation is that the increased complexity of some of the validation cases convolutes the behavior of this simpler reference experiment. Another explanation could be that the THUMS v4 model is also stiffer compared to its lumbar validation corridor. Due to its finer mesh quality and the use of material models which do not conserve their volumes the THUMS v4 Model is also the most robust model in terms of deformation. The increased stiffness could have something to do with this phenomenon might also be another factor which adds to this robustness.

The GHBM is also stiffer than the corridor and shows a very linear response. It is unclear which reference experiments were used in the calibration of the model, but judging from the response shown in Figure 3.4 some similar reference experiments were likely used to obtain a response which is not far from the observed experiments. The interesting aspect of the GHBM response is its linearity. The model is defined with a kinematic joint, one with different stiffnesses in all of its degrees of freedom. These stiffnesses are defined via curves with a relatively coarse discretization, which might explain the linear response.

The model with the softest response is the ViVa model, which like the GHBM is defined as a multi degree of freedom kinematic joint. The ViVa model uses different validation tests to the THUMS models [87], but it is unclear if the validation only considers female specimens, or the difference in the model response is solely due to differences in the reference experiments. The model also exhibits a linear response, which similarly to the GHBM model, might also be due to coarsely discretized stiffness curves.

The overarching conclusion which can be drawn from this analysis is that the disc for at least the THUMS v5 can be considered to give a physiological response for the ranges of motion applied and for the range of loading considered for these reference experiments. Where the intervertebral disc cannot be said to be valid is in its failure mechanisms and proclivity towards injury. The experiments used for this validation did not go to failure, so it would be impossible to use them to predict injury risk. Another area of interest would be loading in the physiological range in other modes of loading. Of particular interest for the automotive safety field would be experiments in flexion and extension.

During the IVD validation two models stood out as having the best CORA scores: The THUMS v3 with a total score of 0.74 and the THUMS v5 with a score of 0.68. In general CORA scores greater then 0.58 are often considered to be an adequate fit [11], and specifically for HBM applications CORA scores above 0.65 are suggested as indications of good biofidelity [95]. A CORA score of 1.0 would be a perfect fit. Based on the results of the CORA study, as well as on qualitative analysis of the corridors, the THUMS v5 model was found to match the experimental results the closest. Both models have very high V scores, which measures how well the shapes of each curve matches the reference data. This is a bit misleading, because looking at the response curves the upward curvature seen in the experiment is captured only by the THUMS v5 and not by the THUMS v3, which has a linear response, as seen in Figure 3.4. This linear response also helps

THUMS v3 to achieve a higher G score than the THUMS v5. The G score measures how well a sample curves size matches the reference curve, as measured by comparing the respective areas under the curves. The linear THUMS v3 response intersects the reference experiment, yielding a smaller error in the size rating than the THUMS v5 response which has a constant offset to the reference experiment. This linear response would be a poor indicator for injury prediction, as it would overpredict injury at displacements less than 0.7 mm but underpredict injury for displacements greater than 0.7 mm. It must be said that the constant offset seen in the THUMS v5 curve means its response is more conservative, which at lower levels of compression the THUMS v3 is not. These observations show potential limitations in the application of objective ratings to HBM validity assessment.

The largest model differences seen for the IVD experiments can be attributed to the various modelling approaches used to construct discs. The vertebral geometries have no effects as no contact was seen anywhere between the vertebrae, which had their posterior elements removed. In THUMS v3, GHBM, and Viva, the vertebrae are all modelled as rigid, and as such have no influence on the compliance measured during the simulations. THUMS v4 and v5 have deformable vertebrae, but they are modelled with materials orders of magnitude stiffer than those found in the disc. In the simulation results this is reflected with vertebral displacements orders of magnitude smaller than the disc displacements, at 15% strain in the disc for the THUMS 5 Simulation, the Vertebral Body experiences a strain of 0.008%. Other modelling factors such as contact did not play a role in the IVD simulations as there was no contact observed between bony structures in the simulations, which agrees well with the experiments.

However, there are geometric as well as material differences in the modelling of the discs. In Figure 3.2 the geometric differences can be seen, and they are described in greater detail in Table 3.1. Two models, the GHBM and the VIVA, model the disc using load-displacement curves to define the stiffnesses with respect to the various modes of deformation. This approach is flexible, as only the curve stiffness values must be changed to vary the model response; for example keeping the flexion and extension stiffnesses constant while changing the compressive stiffness. However, the point at which the forces and moments interact is rigidly fixed, which means the instantaneous center of rotation (ICR) cannot translate as it does in reality. Gertzbein et al. [49] described the ICR as translating anteriorly and cranially, and then posteriorly and caudally when going from extension to flexion, using experiments performed ex vivo. Aiyangar et al. [7] found that for in vivo lumbar spines the ICR translated posteriorly when going from flexion to upright, with large variations in caudal/cranial movement depending on the applied load. The three THUMS family models all have solid meshed discs, but all with different geometries, mesh densities, and material modelling. The material modelling likely accounts for the majority of the variation between THUMS models, as geometric differences as measured by the disc cross sectional areas vary less than 5% between models, which is much smaller than the -65% to +109% differences seen in the peak force response. A notable difference which can be seen in Figure 3.2 is the nucleus of the THUMS v5 model covers 35% of the total disc area compared with $\tilde{2}0\%$ disc area for THUMS 3 and THUMS v4. THUMS v5 also uses a hyperelastic material model for its nucleus, which perhaps helps to contribute to the convex curvature seen in the THUMS 5 average curve in Figure 3.4. THUMS v5 is the only model which exhibits the same kind of convex curvature also present in the experimental results.

Chapter 4

Validation of the Functional Spine Unit

4.1 Introduction

The functional spine unit (FSU) was chosen as the next unit of validation at the component level for several reasons. The FSU is still relatively simple when compared to the complete spine: It consists of two adjacent vertebrae and the intervertebral disc (IVD) connecting them. Also present in the FSU are all of the ligaments which help to keep the joint stable. The ligaments are also important as they constrict the range of motion of the FSU. Especially in the forward flexion motion, which is common in frontal crash type accidents, the interspinous ligament and the supraspinous ligament limit motion. A second reason that FSUs lend themselves to analysis is that they are the smallest complete joint in the spine. Looking at the isolated IVD one can deform it arbitrarily and get a response, but that does not mean each response is physiologically possible. The posterior elements and ligaments add constraints to the IVD which give it boundaries describing what is normal, what is possible, and in extreme cases show what can be harmful. FSUs also lend themselves for use in a validation load case because they have been well studied in the literature, but unfortunately what has been primarily studied have been under quasistatic loading [3], or have been investigating range of motion [90, 32], which are both very dissimilar kinds of loading expected to be seen in automotive applications, where soft tissue strains can reach 30%, strain rates can be between $1\,\mathrm{s}^{-1}$ and $-10\,\mathrm{s}^{-1}$, and axial forces can be on the order of 1-10 kN.

The FSU consists of two vertebra and the intervertebral disc between them. In Figure 4.1 one can see how the different components of the disc are situated in relation to the vertebrae. In addition to allowing ranges of motion in flexion,

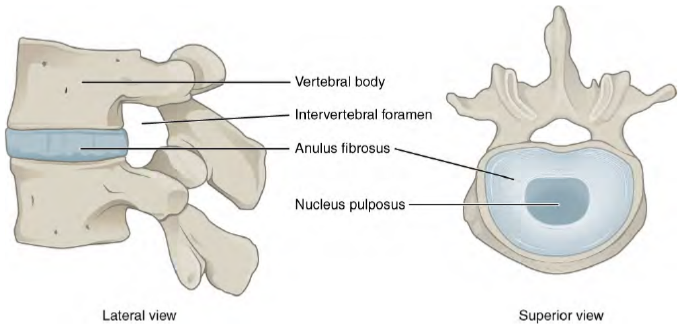

Figure 4.1: The anatomy of a functional spine unit [15]

extension, lateral flexion, and axial rotation, the disc also acts as a padding material between the vertebrae and allows for a certain amount of compression and tension between the vertebrae [15], for the case of impacts loading the spine in the long direction or the standard forces associated with normal activities.

4.2 Method

The reference experiment to be modeled was first presented by Christou et al. [24] and consists of an FSU specimen being loaded by a drop-tower impact. The experiments were performed on two FSUs isolated from the same lumbar spine specimen, one consisting of an L2-L3 segment, the other of an L4-L5 segment. Each specimen was tested multiple times at different drop heights. After each drop height a minimal impact was performed as a control for injuries. These minimal impacts were performed from a drop height of 5 cm, corresponding to an impact velocity of 1 m/s. This impact velocity is the upper end of what was investigated by Newell et al. [84] for the IVD investigations discussed in Chapter 3, and as such make a good segue into testing the model validity going towards higher force levels. A description of the model setup can be seen in Figure 4.2. In order to model the experiment using a finite element analysis, high speed videos of the experiment were utilized in order to extract the specimen motion using FalCon eXtra version 9.22.0000 (Graefelfing-Locham, Germany). More specifically the motion of the upper and lower pots were extracted and then applied to the corresponding components of the finite element model as boundary conditions. The finite element model was constructed to match the dimensions of the experiments, again using the high speed videos as the comparison metric. A picture of the FE model of the FSU experiment can be seen in Figure 4.3

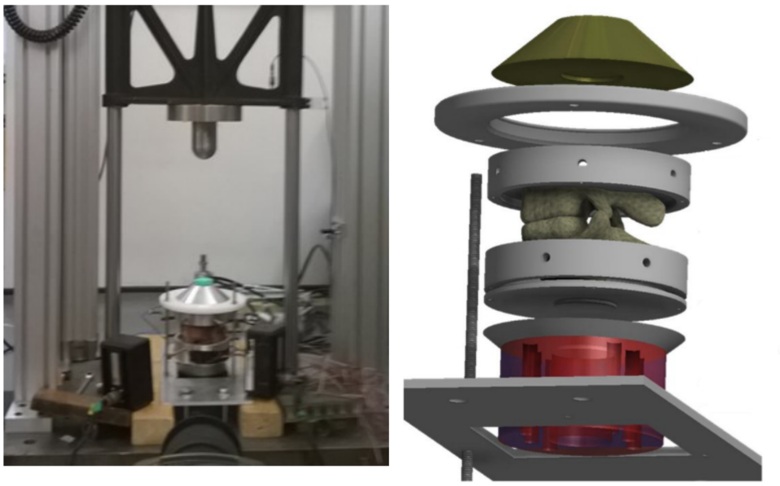

Figure 4.2: Diagram of the FSU drop test experimental setup performed by Christou [24]

Figure 4.3: The Finite Element model of the FSU reference experiment

In order to better quantify the experimental uncertainties, various sensitivities were performed using this model setup, using the THUMS v5 HBM. The sensitivities investigated included varying the initial position and orientation of the HBM specimen in relation to the pots, changing the vertical distance between the pots (the gap width), and changing the boundary conditions associated with the pots by changing the orientation of the applied accelerations. An overview of the parameters can be seen in Figure 4.4, and are detailed in Table 4.1.

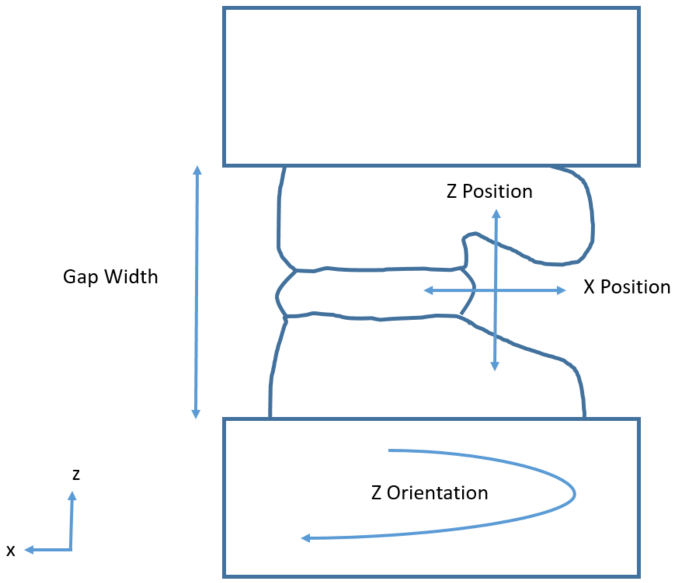

Figure 4.4: Description of the FSU reference experiment sensitivity study, with the adjusted parameters labeled

Configuration	1	2	3	4
Orientation	0°	15°	30°	45°
Gap Width	-10mm	0mm	10mm	-
X Position	-10mm	0mm	10mm	-
Y Position	0mm	10mm	-	-
Z Position	-10mm	0mm	10mm	-

Table 4.1: Table of sensitivity parameters investigated

The models were all ran with and without the inclusion of all vertebral contacts. This was to mimic the simulation of only the IVD, but using the FSU boundary conditions, and to allow for a finer grained model comparison.

One additional boundary conditions was investigated using the THUMS v5, namely the effect of having a fixed or free lower pot. In the experiments the lower pot was free to move, and did during the rebound phase. By fixing the lower pot to the test fixture, it can be investigated if this motion in the rebound phase has an effect on the observed forces. In order to look into these effects a contact boundary condition is used instead of an applied acceleration from the video analysis.
After the simulations have been performed the results are then compared with the results obtained from the IVD analysis in Chapter 3 in order to see how the increased complexity associated with the FSU affects the observed response.

4.3 Results

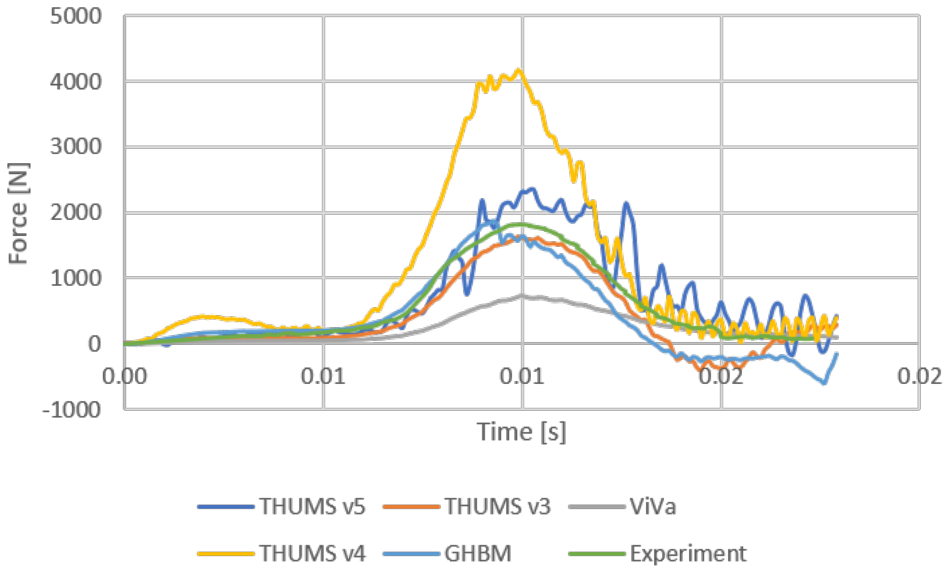

Figure 4.5: Comparison between the FSU models run without contact

In Figures 4.5-4.6 the results from the investigations of the model with and without facet joint contact are presented. The THUMS v4 behavior does not change with or without contact, but all of the other models show significant differences in peak force response depending if they are modelled with contact or not.

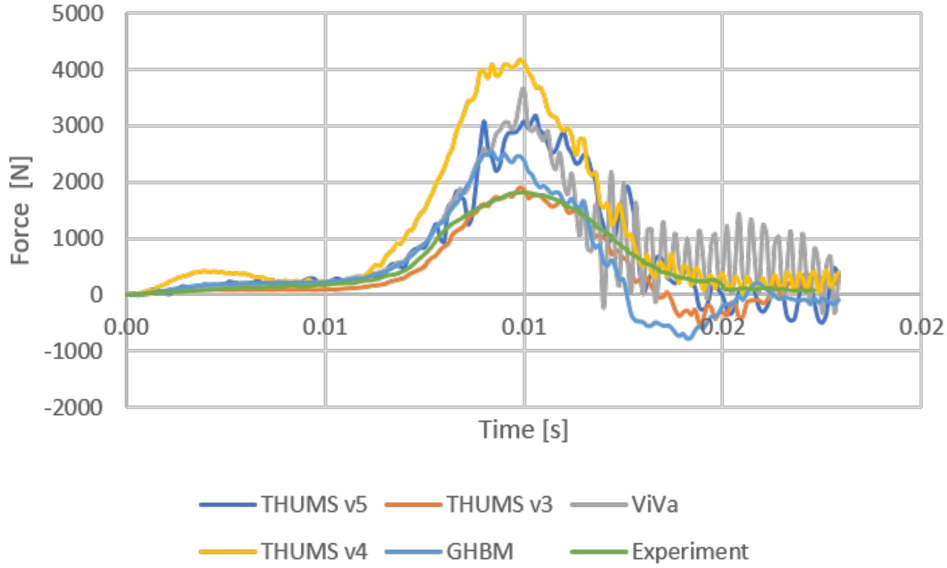

Figure 4.6: Comparison between the FSU models run with contact

One noticeable difference between the material testing machine approach used to test the IVDs and the drop test approach used to test the FSU is the intensity of the energy brought into each system, which the drop tower bringing more energy, and applying said energy faster than the material testing machine equivalent. These energies and energy intensities can be measured by proxy using the strain seen in the IVD and the equivalent strain rate seen in the IVD. Table 4.2 shows the observed strains and strain rates as measured in the THUMS v5 FE simulations.

	Peak Strain	Peak Strain Rate
IVD	14.6%	$1.16s^{-1}$
FSU	7.6%	$36.4s^{-1}$

Table 4.2: Strains and strain rates as measured in the FSU and IVD simulations

The sensitivity study which was performed in order to see which model parameters yielded the following curves:

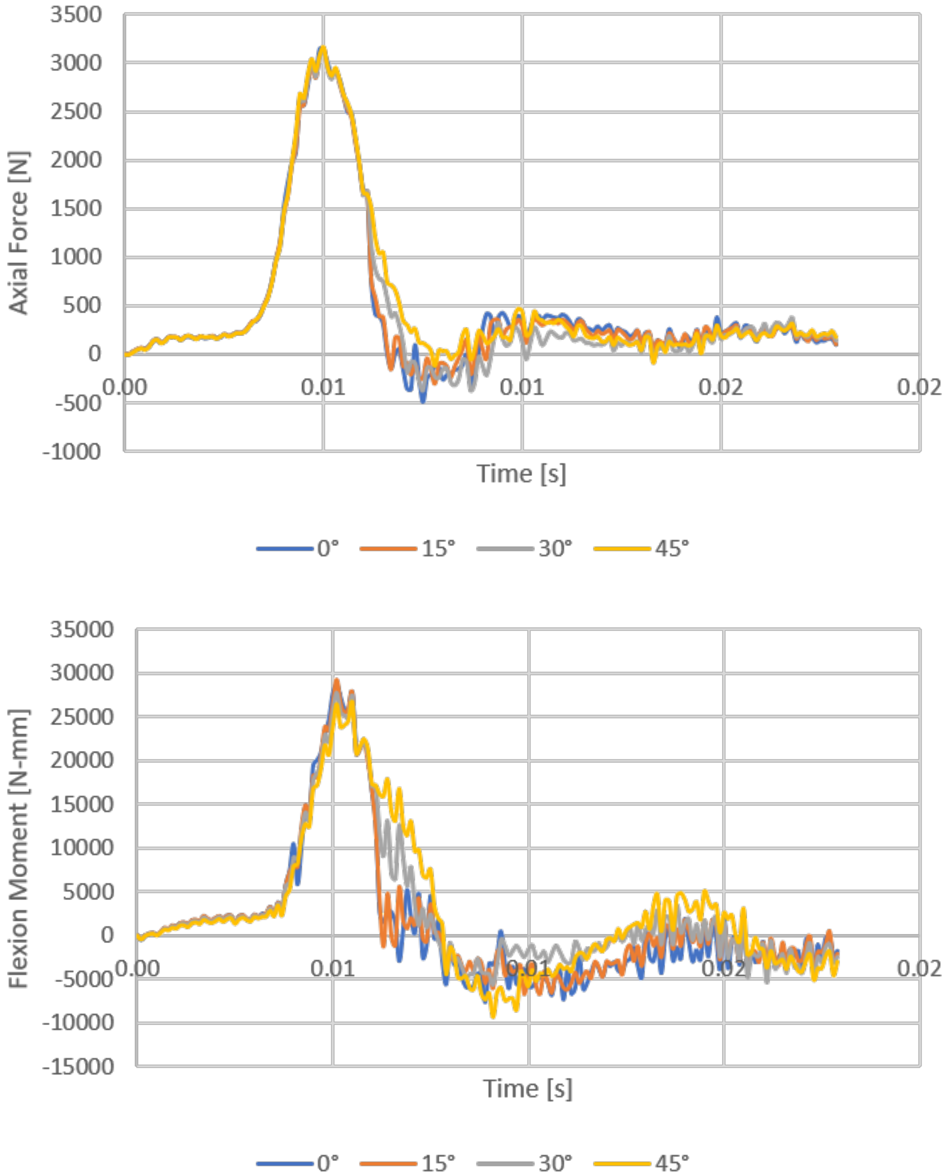

Figure 4.7: Simulation results for various initial FSU orientations for the 5cm drop test FSU load case

In Figure 4.7 the results from orienting the FSU at an angle along its vertical axis can be seen. For both the force and moment response little difference is seen for the peak value.

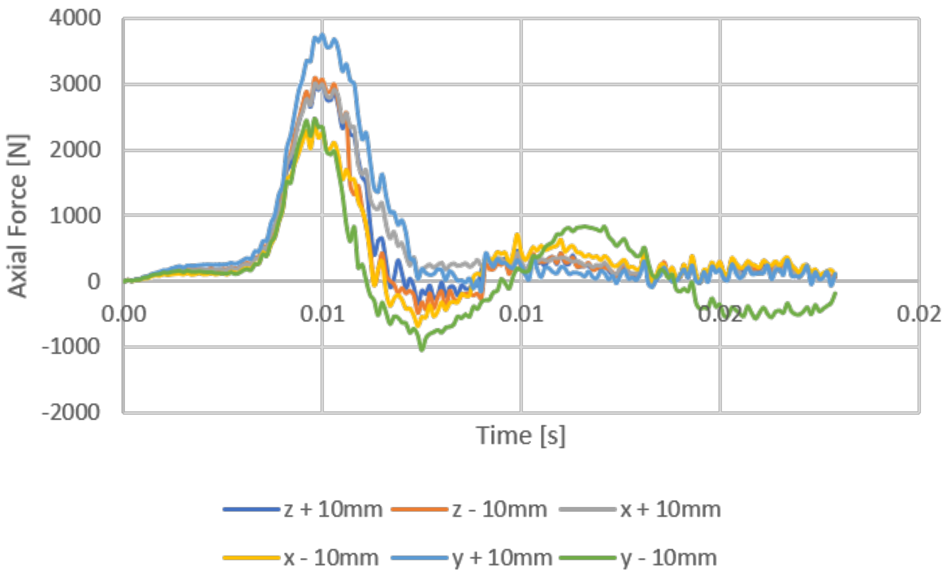

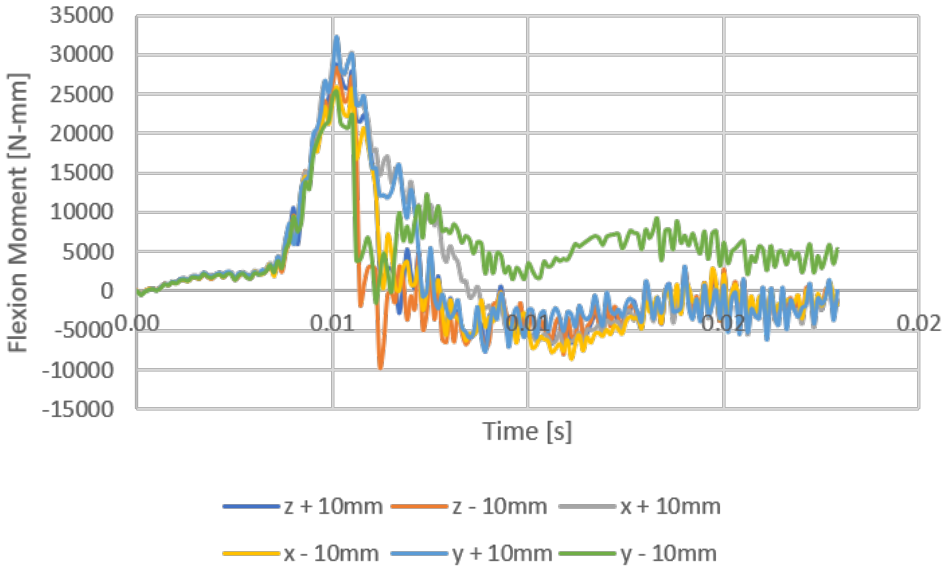

Figure 4.8: Simulation results for various initial FSU positions for the 5cm drop test FSU load case

In Figure 4.8 the results from positioning the FSU in the test setup by translating it by a given amount in each direction can be seen. Large changes in the peak force values were observed, but no large changes happened to the peak moment values.

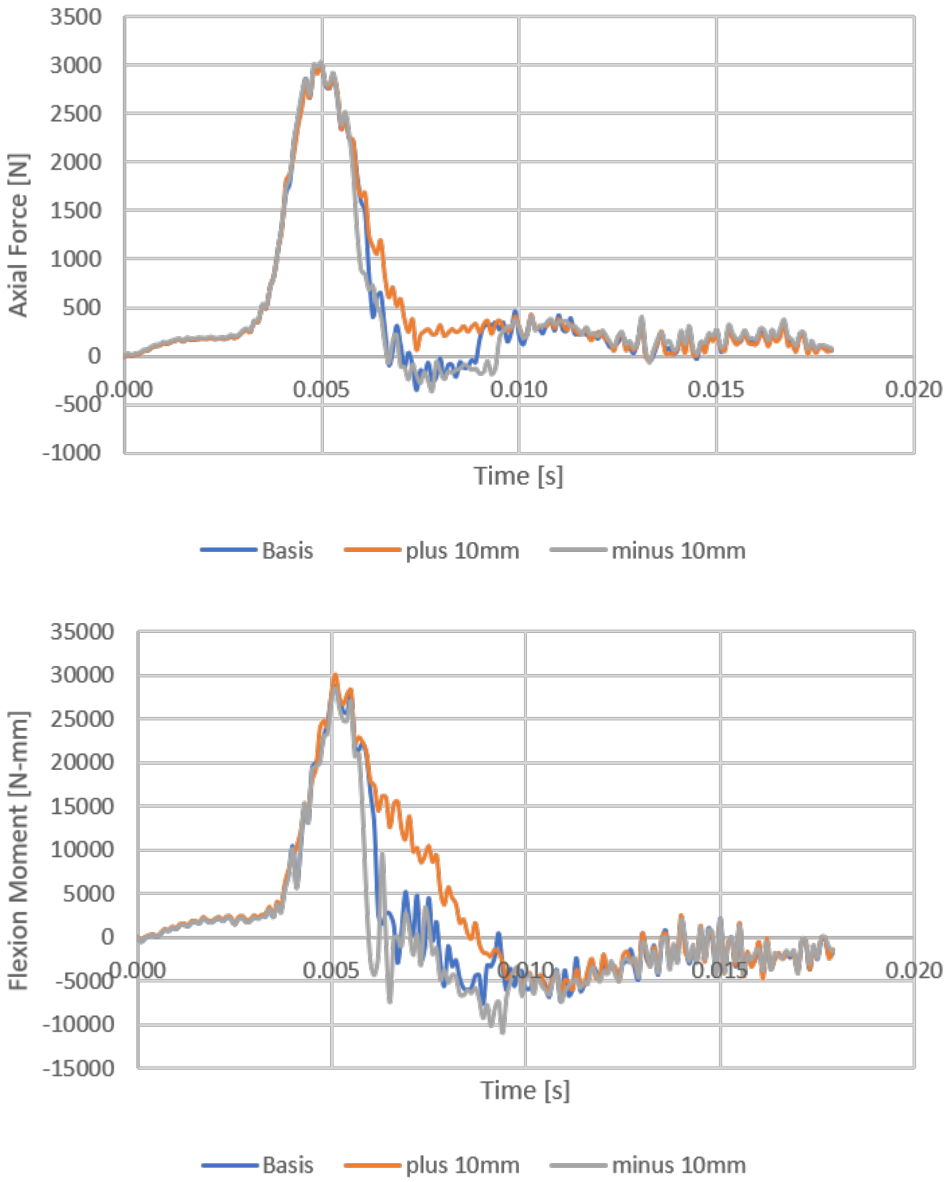

Figure 4.9: Simulation results for various initial FSU gap lengths for the 5cm drop test FSU load case

In Figure 4.9 the results of varying the gap width of the test setup are displayed. Changing the gap width has no large influence on the peak force or peak moment response.

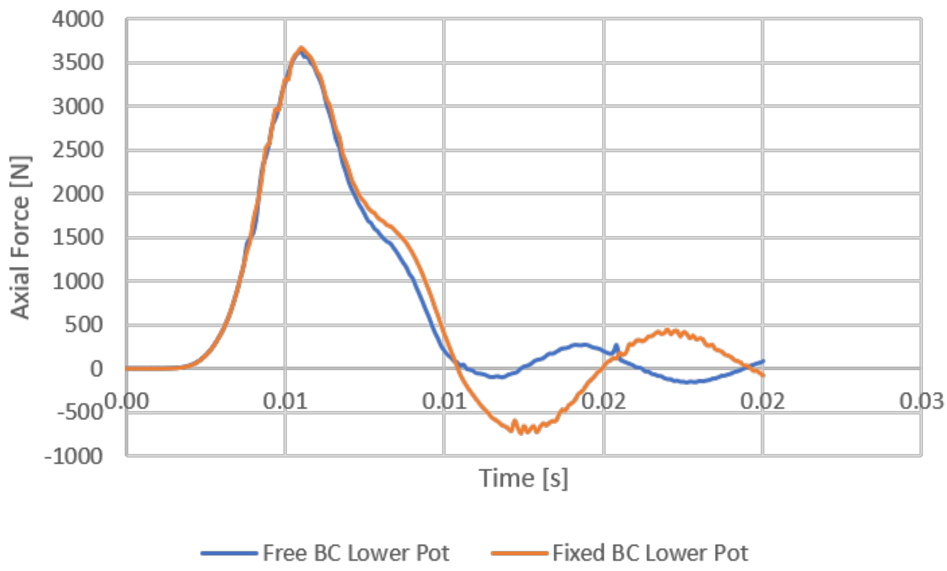

Figure 4.10: Simulation results for various boundary conditions for the 5cm drop test FSU load case

The force over time results for the case study investigation of whether having the lower pot bonded to the force transducer can be seen in Figure 4.10. Having the potting model connected or not connected to the force transducer makes no difference in the peak value, but introduces disparate characteristics in the late unloading phase.

4.4 Discussion

For the FSU simulations, a difference of approximately 50% can be seen between the simulation and the experimental force response, as seen in Figure 4.6. The kinematic response as seen by visually comparing the simulation to the video shows good agreement between the model and the experiment. Discrepancies arise both due to how the discs are modelled as well as from facet joint contact. Comparing this too stiff response to the response seen with contact turned off for the HBMs investigated, as seen in Figure 4.5, explains much of the over-stiffness: with model contact turned off all of the models except for the THUMS v4 show an improved force response. The THUMS v4 shows no difference in having its contact activated or deactivated because for this load case the part of the model that in other HBMs comes into contact, namely the facet joints, remains separated for the THUMS v4 under this loading regime.

If the contact between the facet joints appears to be making the models too stiff, then turning off the contact would be a logical solution. However, eliminating contact for these HBMs is not a realistic modelling decision. Facet joints do have contact, and it must not be ignored. Instead the contact must be represented in some way in order to bestow more biofidelity. In all of the models tested the mesh around the facet joints is very coarse, which might be negatively conducive to generating penetrations, and the high forces that come along with penetrations. In models where the vertebra are modelled as rigid (THUMS v3, GHBM, and ViVa), any bony contact will be artificially stiff as rigid bodies cannot deform, and thus lead to high contact forces. The cartilage which the facet joints are composed of has been modelled in some of the HBMs, but always as a shell layer, which might be an oversimplification for how much the facet joint locally deforms. Combing any of the aforementioned issues probably leads to effects which are greater than the sum of their parts.

If the contact is indeed taken into account, the next possibility is that the HBM FSU models are too stiff. If the models show good alignment with zero-level contact forces, and contact forces are in reality greater than zero, that the non-contact part of the response must be lower in order to have a good response when considering all components. The THUMS v5 IVD response, for example, showed a force response very similar to was seen in an Instron type IVD experiment, as discussed in Chapter 3. However, the FSU reference experiment, being a drop tower experiment, has a different profile. These differences can be seen in both the strain and strain rate development between the two experiments, as seen in Table 4.2. Although the FSU experiment reaches a lower global strain, its peak strain rate is more than an order of magnitude larger than the strain rates seen for the IVD reference experiments. These strain rate differences are likely to have an effect on the force output quantities. Most viscoelastic materials exhibit a strain-rate hardening behavior, which is also the case for biological tissue [10, 23]. This strain hardening which could describe the discrepancies seen in Figure 4.6. According to Race [97] the viscoelacity of the human IVD should remain constant at strain rates above $1\,s^{-1}$, however the material models found in THUMS v5 have no mechanisms with which to implement that observation. The material models used are traditional viscoelastic and hyperelastic materials which have a strain hardening description.

Another possibility is that the numerical models are not capturing some of the physical behavior which is occurring in the boundary conditions of the experiments (i.e. the parts which are not HBMs). One of these phenomena could be the elasticity found between the specimen and the pot. In the simulation this was modelled as a rigid connection, as the potting material as well as screws into the specimens were described in the reference literature as having no slip. But of course, in reality even a very strong connection is not ideally rigid. This observation is of lower importance in quasi-static loading and develops more influence with increasing loading rates. However from the available data there is no way to quantify how rigid (or not) the experimental setup actually is.

Other sources of boundary condition influence were investigated in the sensitivity studies whose results are shown in Figures 4.7-4.9. By making changes to the boundary conditions and seeing how these changed affect the response, one can get a general feel to which parameters have an outsize influence, or may be causing incorrect responses. For this sensitivity study the translational position of the HBM, as seen in Figure 4.8, relative to the test setup was the only parameter to have a significant influence over the force curve. This information is useful, but difficult to use. In an ideal world, these simulations could be checked to ensure that the positions of the HBM specimens match those of the PMHS specimens used in the literature. Unfortunately these positions were not documented in the literature, and as such, cannot be more closely investigated. A posteriori one can use the knowledge that the position has a large influence in order to build a corridor around the simulation results and use this corridor to determine how well the simulations match the experiments. Unfortunately again, without a baseline, this could mean artificially inflating how well the results fit, and so shall not be performed.

Looking at the model sensitivity to the initial orientation, as documented in Figure 4.7, one would expect more influence than what is actually measured. In the physical experiments if the specimen was rotated about its vertical axis, all else being equal, the instantaneous joint center would also be expected to move, and cause the force and moment response to vary. That this is not the case is because of how the simulations were modelled: the prescribed motion boundary conditions intrinsically describe the joint motion, and thus the influence of the HBM itself on the joint motion is limited. This is an unrealistic simplification, but it is seen as the best ground truth fit to be extracted from the experiments. The high speed video which was used for the analysis is much finer grained than the associated accelerometer data, and allows for a very trustworthy validation cross-check. It would be better to model the experiment as it was performed with a contact condition, but the experimental data required to bring a simulation to the adequate point to be believable was not available.

It is a similar case for the gap sensitivity, as seen in Figure 4.9. The sensitivity in the force and moment response should be higher, as a larger gap will have a larger lever arm, and thus cause different kinematics, which would then lead to different forces and moments, but any change in the gap distance will only be fractionally represented in the lever arm, so these changes should be small. However, using the prescribed boundary conditions precludes this being possible. It was noted during analysis of the high speed videos that a separation occurred between the lower potting and the force-moment transducer. This is an interesting observation, because before watching the video the simulation setup was modelled with having the potting bonded to the transducer, and therefore not allowing for separation. This discrepancy provided the opportunity to make a small case study to see the influence of the separation. First a comparable model must be built. All of the simulations discussed until now had prescribed potting motion which would already preclude separation. A model was build modelling the contact of the drop tower. This contact was not tuned to be used to compare to the experimental results, but rather purely to investigate the separation, so it is more qualitative than quantitative. The results of these simulations are shown in Figure 4.10. Until the peak both curves, with and without potting/transducer separation are identical. As the peak value and the curve behavior until the peak value are the primary quantities of interest, it can be said there is no difference between these two conditions. The difference in the unloading is likely due to differences in mass and inertia. Although it makes no difference, this sort of conditions should still be documented. Having a fixed setup that does not allow for separation is the condition which better to simulate as it eliminates uncertainties arising from the contact between the two bodies.

Chapter 5

Validation of the Total Lumbar Spine

5.1 Introduction

The lumbar spine consists of the five lumbar vertebra [15], and sometimes the sacrum and T12 are also included in order to form the so-called thoraco-lumbar spine.
The total lumbar spine is much more complex than the individual FSU not only because it consists of several stacked FSUs, but also due to the new degrees of freedom that this stacking realizes. A total lumbar spine can exhibit instabilities, and the initial posture has been shown to play an important role in the kinematic and force response [35]. Due to these reasons however, the lumbar spine is also a very difficult specimen to test experimentally, and accordingly only very few data exist for whole lumbar spine tests [109, 33, 123].

No criteria currently exists to evaluate lumbar spine injury for vehicle crashes. In the aerospace industry, a limit is given for which lumbar forces must be under during the event of a crash landing [18], but this criteria is based on regressions of ejection seat injuries, which have a different acceleration profile than automotive accidents [34], and so might not be applicable for automotive applications. The main reason that the lumbar spine has not been extensively studied, is because in vehicular crashes lumbar spine injuries are relatively rare [64, 93, 5]. And when they do occur they are normally non-life threatening.

In this chapter simulations will be conducted to compare the existing human body models to some existing experiments from the literature and try to draw the parallels how the IVD and the FSU modelling affect the total Lumbar Spine response. For each of the reference experiments to be validated, first five state of the art Human Body Models (HBMs) are compared to the experimental results with the spinal posture in which the HBMs are delivered. This nominal position corresponds to an upright seated position normally seen when operating a vehicle [35]. A second sensitivity study is then performed using only the THUMS v5 HBM, where the nominal posture has been modified to have both more lordosis and more kyphosis. A diagram depicting the validation structure can be seen in Figure 5.1.

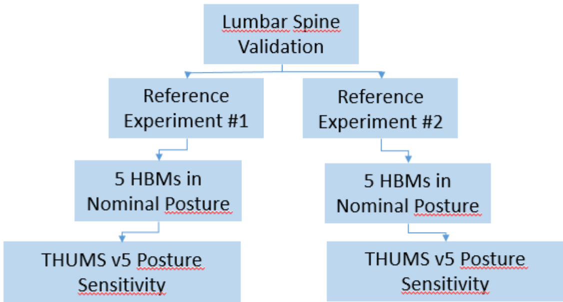

Figure 5.1: Structure of how the lumbar spine validation shall be performed

5.2 Method

5.2.1 Describing Spinal Posture

The full lumbar spine with its added complexity poses a possible variable: the variable of posture or position. Posture can be thought of as how an individual's spine is shaped, and position is than the more general form of any spinal shape. Posture varies naturally between individuals [62], and any changes caused by these various postures should be taken into account in a validation context.

Currently spinal posture is described using global angles, usually taken from x-ray images [8, 31]. These global angles have been used in the past in automotive injury studies to identify large global trends [62], but originally come from the study and diagnosis of scoliosis [26]. The global angles can be very useful, but they lack the detailed information needed in order to properly position a spinal model vertebra by vertebra. In order to harmonize the validation of numerical Human Body Models (HBMs) with individual spinal postures as measured in vivo, the following method is proposed:

A Method to Identify the Position and Orientation of a Vertebra

It is important that this method work equally well on experimental data (in this case X-rays and three dimensional CT scans or MRI scans) as well as the finite element models used to recreate these data. Having a method to identify the position of both experimental data and finite element models eliminates one source of uncertainty, and ensures that the positions from both sources remain consistent.

The first step of the method is to identify both vertebral endplates and to assign a plane to them. For the finite element model this can be done by finding the best fit plane to all of the nodes associated with the endplate. For a 3D scan, this can be done by identifying points on the endplate and fitting a plane to them. The point associated with this plane shall be the area center of the endplate. A graphic showing how the planes look when identified on an FE model can be seen in Figure 5.2.

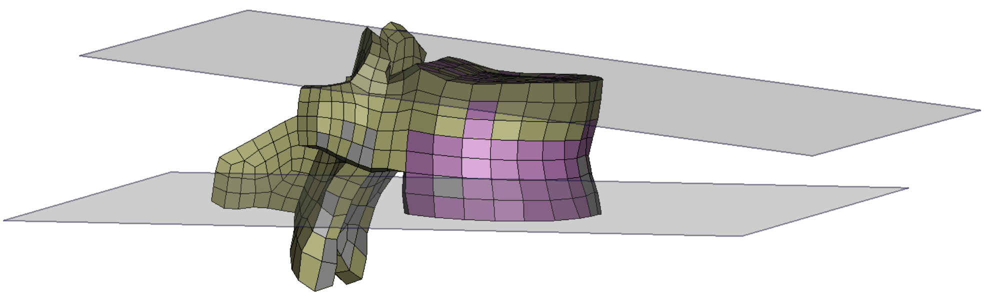

Figure 5.2: Description of how planes can be fit to the endplates

After the endplates have been identified, their associated planes should be averaged to find a new in between plane. The center points of these plans is also averaged. The normal of this new average plane describes the local Z orientation of the vertebra, and the new averaged plane vertex describes the center of the vertebral body. A graphic showing how the averaged plane looks when identified on an FE model can be seen in Figure 5.3.

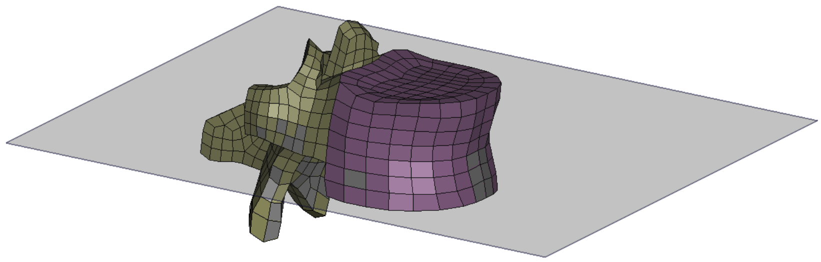

Figure 5.3: Description of how the average plane is defined

In this new plane the ring which contains the spinal canal can be identified. The next step of the method is to find the area center of the canal ring in the averaged plane. The vector going from this canal ring center point through the vertebral center point defined the local X axis of the vertebra. The local Y axis can be found via the cross product of the local X and Z axes. A graphic showing the local coordinate construction can be seen in Figure 5.4.

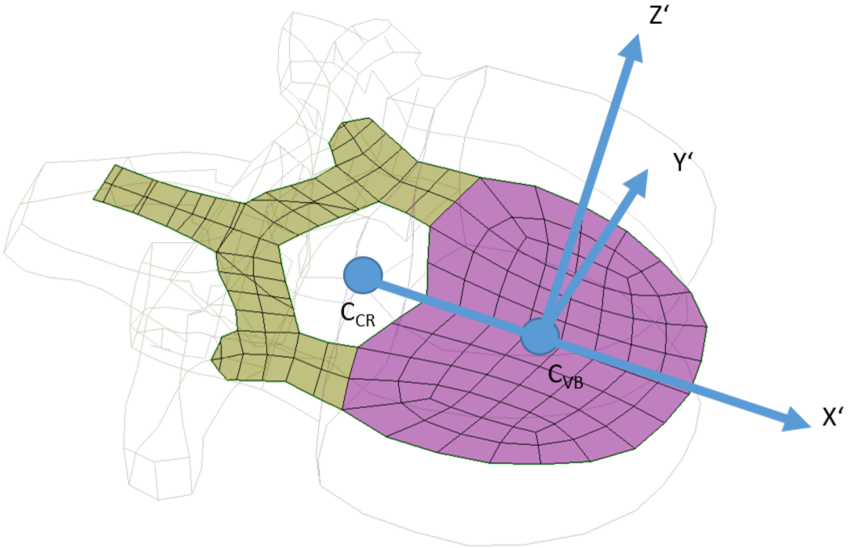

Figure 5.4: Description of how the vertebral local coordinate system is defined

With the posture being described in a quantifiable, unambiguous manner, the lumbar spine from various HBMs can be compared to experiments from the literature in an attempt to validate the HBMs.

5.2.2 Description of the THUMS v5 Sensitivity Study Postures

In order to better understand the influence of the spinal geometry on the simulation results, several THUMS v5 postures are defined. The first posture is the THUMS v5 lumbar spine as delivered, also referred to as the nominal or standard posture. The second posture is the lumbar spine extract from a THUMS v5 model which was fitted into a reclined seating position, as seen in Chapter 7, and is referred to as the reclined posture. Two additional spinal positions were derived by positioning the spine using the Piper positioning framework [13]. These two additional positions are herein referred to as kyphotic and lordotic. In direct comparison to the reclined position they are characterized by a modified curvature towards lordosis and kyphosis, respectively.

5.2.3 Comparison of Lumbar Spine Postures

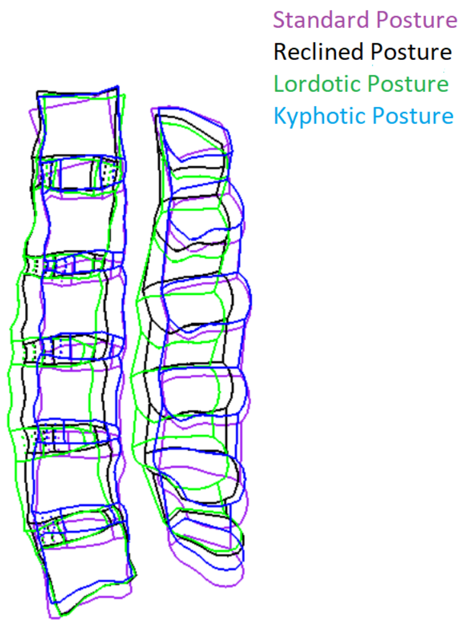

Figure 5.5: Overlay of the various postures investigated as seen in the saggital plane

A summary of the key differences between the postures investigated can be found in Table 5.1, where the pelvic angle is measured in the sagittal plane by drawing a straight line from the ASIS to the PSIS, relative to the global coordinate system. The Cobb angle is measured from the caudal aspect of L5 to the cranial aspect of T12. The maximum amplitude is measured perpendicular from each vertebra center of mass to the line connecting the S1 center of mass to the T12 centers, and the corresponding vertebra is also noted.

	Nominal	Baseline	Lordosis	Kyphosis
Pelvic Angle	51.5697	48.7617	47.3698	47.8247
Cobb Angle	10.8834	23.1592	33.9766	8.4249
Max Amplitude	6.3577 @ L1	13.89mm @ L4	19.96mm @ L3	8.83mm @ L5

Table 5.1: Selected anthropometry differences between the postures

These posture are described as in Section 5.2.1, which each vertebral body being represented as a point and a vector. The initial as delivered posture of the THUMS v5 lumbar spine from T12 to L1 can be seen in Table 5.2

Level	XZ Angle	X position	Y Position	Z Position
L1	80.25	8.61	45.56	35.53
L2	77.70	-0.35	45.56	5.62
L3	72.99	-10.34	45.62	-24.81
L4	76.32	-21.12	45.56	-55.45
L5	86.08	-28.95	45.56	-86.12
T12	84.58	15.81	45.56	69.55

Table 5.2: Center point and orientation vector for all vertebrae in the nominal posture of the THUMS v5 model

Level	XZ Angle	X position	Y position	Z position
L1	34.33	34.15	0.17	39.84
L2	35.68	6.81	0.11	24.03
L3	33.78	-20.64	0.05	7.08
L4	41.85	-47.86	-0.15	-10.98
L5	54.01	-70.37	-0.27	-32.59
T12	31.25	65.08	0.31	55.89

Table 5.3: Center point and orientation vector for all vertebrae in the reclined posture of the THUMS v5 model

Level	XZ Angle	X position	Y position	Z position
L1	30.21	34.88	0.15	38.12
L2	28.90	6.19	0.10	25.00
L3	33.31	-22.30	0.05	9.75
L4	49.27	-48.42	-0.15	-9.97
L5	56.14	-69.02	-0.26	-33.29
T12	28.91	66.62	0.28	52.38

Table 5.4: Center point and orientation vector for all vertebrae in the lordosis posture of the THUMS v5 model

Level	XZ Angle	X position	Y position	Z position
L1	40.52	34.31	0.20	37.74
L2	34.21	8.73	0.17	21.51
L3	30.05	-19.20	0.10	6.17
L4	37.29	-46.73	-0.19	-9.20
L5	45.47	-71.47	-0.35	-28.14
T12	37.19	63.08	0.30	56.77

Table 5.5: Center point and orientation vector for all vertebrae in the kyphosis posture of the THUMS v5 model

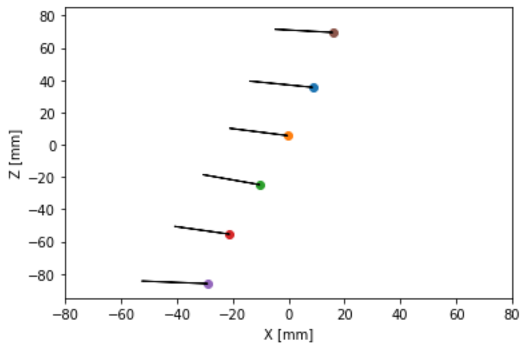

(a) Nominal Posture

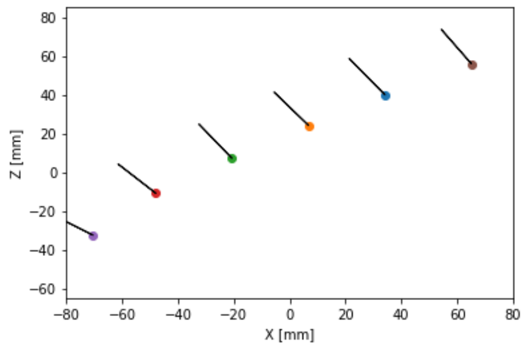

(b) Reclined Posture

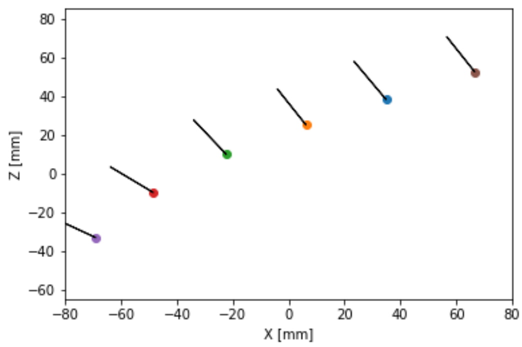

(a) Lordotic Posture

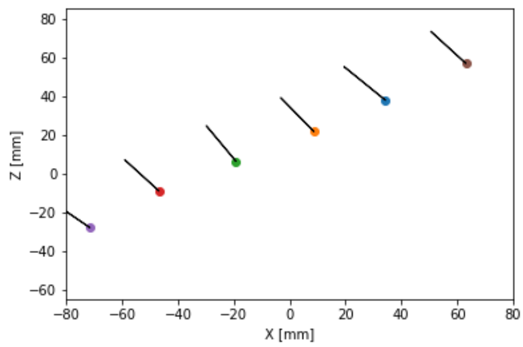

(b) Kyphotic Posture

Figure 5.6: Visualization of the spinal posture of the THUMS v5 as delivered (a), in the reclined posture (b), with the more lordotic posture (c), and with the more kyphotic posture (d)

5.2.4 Reference Experiment 1: Demetropoulos et al.

Description of the Experiment

This study performed by Demetropoulos et al. is a set of full lumbar spine experiments, and has been used in the validation of HBMs [67]. In this experimental setup n=10 lumbar spine specimens were extracted and tested in 8 different configurations: tension, compression, anterior shear, posterior shear, left lateral shear, flexion, extension, and left lateral bending. The compression and flexion load cases will be used as the references.

None of the tests went to failure in order to allow testing in all configurations. In order to best achieve this the authors state that they tested starting with the experiments least likely to cause damage. The tests were performed using a material testing device using a constant velocity of 100mm/s. An image showing the experimental setup can be seen in Figure 5.7.

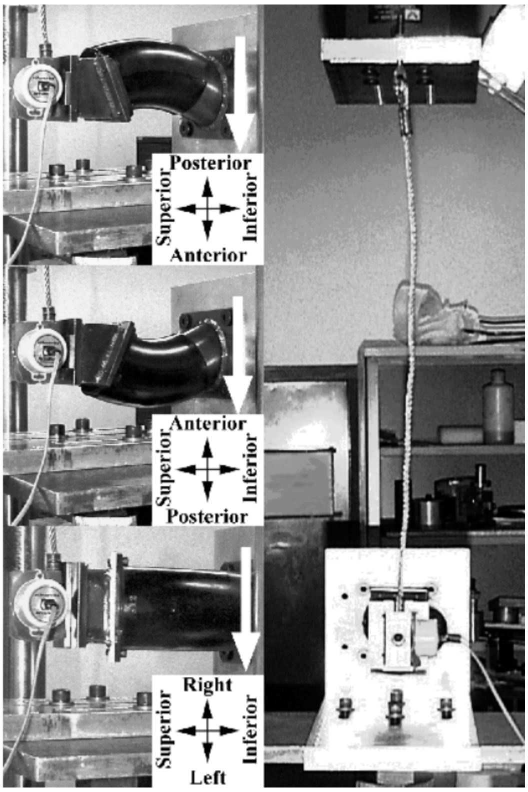

Figure 5.7: Photograph of some of the experimental setups from Demetropoulos et al. [33]

Preparation of the Specimens

All specimens were excised at the T12-L5 levels, with all bones, ligaments and discs intact. Care was taken to only remove muscle tissues. The specimens were potted into their pots using epoxy and screws. The fixtures to hold the pots were constructed such that both the specimens and the Hybrid III dummy lumbar spines could be mounted. Initial positioning for the specimens tried to eliminate any prestress by allowing the specimen to rest in their natural curvature.

Instrumentation of the Specimens

For these test the relevant outputs are forces, moments, displacements and angles. The forces were measured using a load cell, the displacements were measured using the internal displacement instruments from the material testing device, and the angles were measured using a clinometer. The moment data was generated from the force data.

Simulation of the Experiments

For the experiments of Demetropoulos et al. the most interesting load cases are those in compression and flexion. These load cases are interesting because they are the loads which are the most associated with frontal crash scenarios. The simulation for the compressive load case was performed by applying the constant velocity boundary condition to the HBM specimens as it was described in the paper. A picture showing the simulation setup can be seen in Figure 5.8. For the compression loadcase, five HBMs were tested, just as in the previous chapters. Additionally three postures which were realized using the THUMS v5 model were also simulated under compressive loading to see what the effects of posture are on the model response.

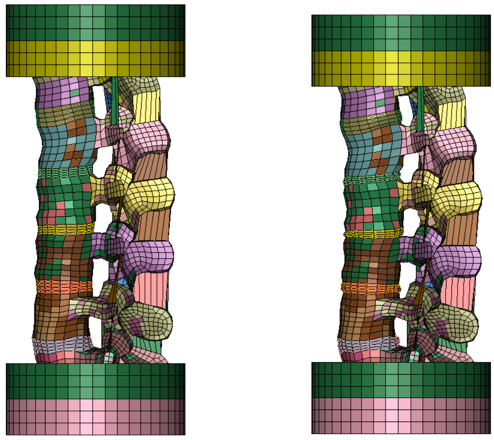

Figure 5.8: Diagram of the simulation setup in compression as described by Demetropoulos et al. [33]

For the flexion loadcase the same five HBMs were investigated as in the previous simulation studies. Additionally the same three postures which were realized using the THUMS v5 as described in the compressive simulation section were also simulated under flexion loading to see what the effects of posture are on the model response.
For both the flexion and compression load cases, forces and moments were output from locations in the simulation models corresponding to the force measurement locations from the experiments. The kinematics were also output for the tracking points located on the vertebral bodies.

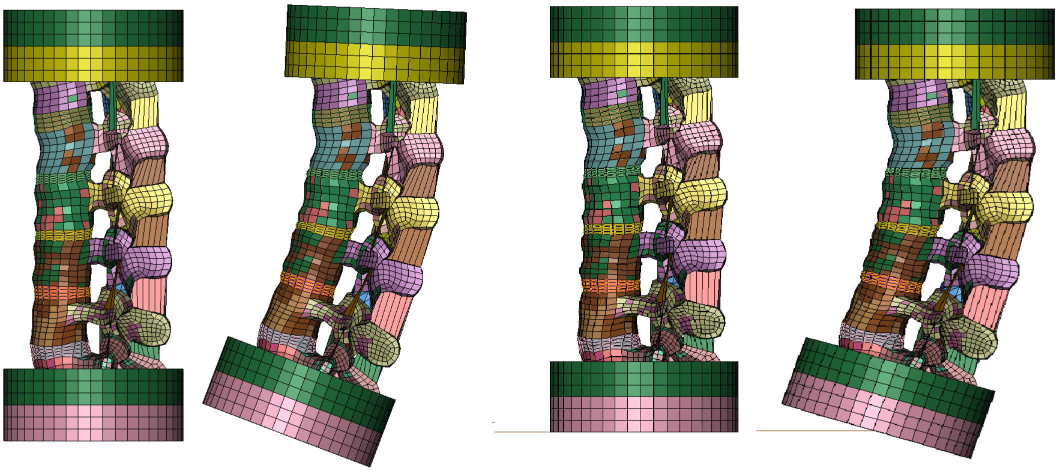

Figure 5.9: Diagram of the simulation setup in flexion as described by [33]

5.2.5 Reference Experiment 2: Stemper et al.

Description of the Experiment

For this study n=23 specimens were tested at subfailure and failure loads using a drop tower testing setup. The droptower was outfitted with linear rails to ensure that compressive flexion loading was achieved. A piece of foam was used to shape the acceleration pulse, and was located at the interface where the impact occurred. A diagram showing the experimental setup can be seen in Figure 5.10.

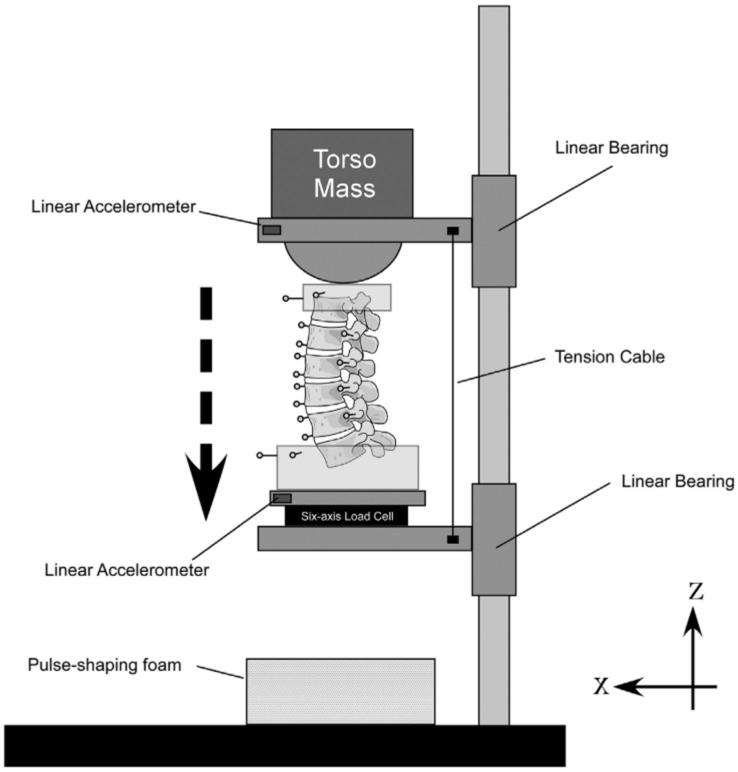

Figure 5.10: Diagram of the experimental setup from Stemper et al. [108]

Preparation of the Specimens

This experiment also used specimens at the T12-L5 levels, and potted them into polymethylmethacrylate (PMMA). Specimens which had osteophytes, degraded discs, or inconsistent alignment were not studied. During the potting procedure the target position was defined as having the L2-L3 disc as close to being horizontal as possible, while not changing the natural lordosis of the specimens.

Instrumentation of the Specimens

The experimental setup from Stemper et al. measured forces and moments using a six-axis load cell, as well as linear accelerometers places caudally and distally from the specimen, all of which can be seen in Figure 5.10. In addition to these engineering quantities, each specimen was also checked for injuries, both using x-rays after every test, and by palpation and range of motion checks.

Simulation of the Experiments

For the experiments form Stemper et al. [109], the accelerations measured in the experiment are applied to the lower specimen pot below the force transducer, allowing for accurate force measurement. A contact definition is used between the upper specimen pot and a cylinder which is positioned according to pre-test x-rays taken during the original experiments. A picture of the simulation setup can be seen in Figure 5.11.

Four of the HBMs investigated in previous sections were simulated under this loading setup. The three additional THUMS v5 postures previously described were also investigated using this drop tower setup.

For the drop tower load cases, forces and moments were output from locations in the simulation models corresponding to the force measurement locations from the experiments. The kinematics were also output in the form of tracking points located on the vertebral bodies, defined as described in section 5.2.1. The kinematics from the vertebral centers were then transformed into the kinematics at each disc, to be analogous to the kinematic data reported by Stemper et al. [109].

In order to be able to compare model variability to experimental setup variability a suite of simulations were carried out with the impacting cylinder at the cranial end of the HBM lumbar spine moved 2 mm to the anterior, and 2 mm toward the posterior of the model. The evaluation of these experiments was carried out as described above.

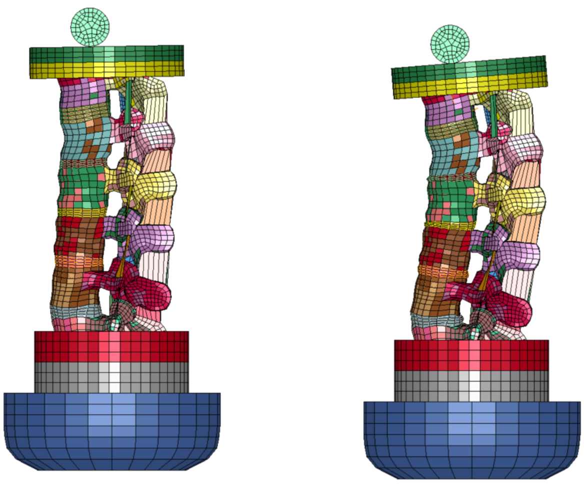

Figure 5.11: Diagram of the simulation setup as described by Stemper [109]

5.3 Results

Results from the Demetropoulos et al. Simulations

In the experiments performed by Demetropoulos et al. experimental corridors were reported comparing global displacement as measured by the material testing machine plotted against axial force. The same outputs were also calculated for each of the HBM simulations and plotted against the experimental corridors, as seen in Figure 5.12. Similarly for the bending tests performed by Demetropoulos et al. angle and moment are measured. The bending flexion corridors as well as the corresponding HBM simulation results are plotted in Figure 5.13. It is of note that for the flexion results all of the HBMs investigated are too stiff, which is not the case for the axial load cases. The comparison between compressive experiments of Demetropoulos and the simulations reconstructing them, as seen in Figure 5.8, provide the same model stiffness ranking which was seen for the IVDs (see Figure 3.3). By comparing the strains and strainrates of the Demetropolous setup to those of the IVD and FSU, one can see that with a strain rate of 3.64, the Demetropoulos strain rate is closer to the 1.16 strainrate seen in the IVD testing than the 36.6 s^{-1} seen in for the FSU testing.

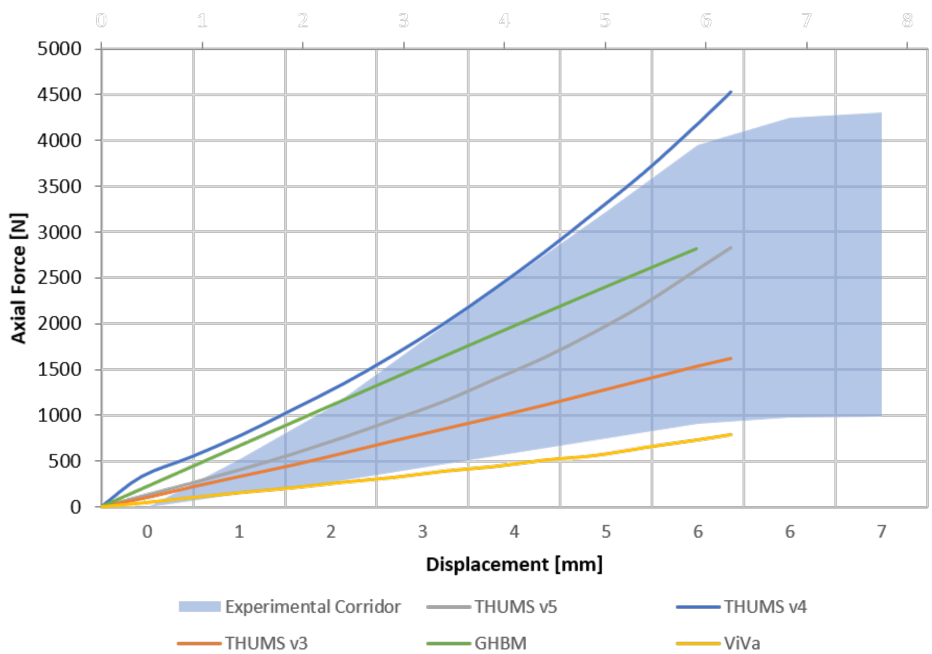

Figure 5.12: Simulation results plotted against experimental results for the Demetropoulos axial compression load case

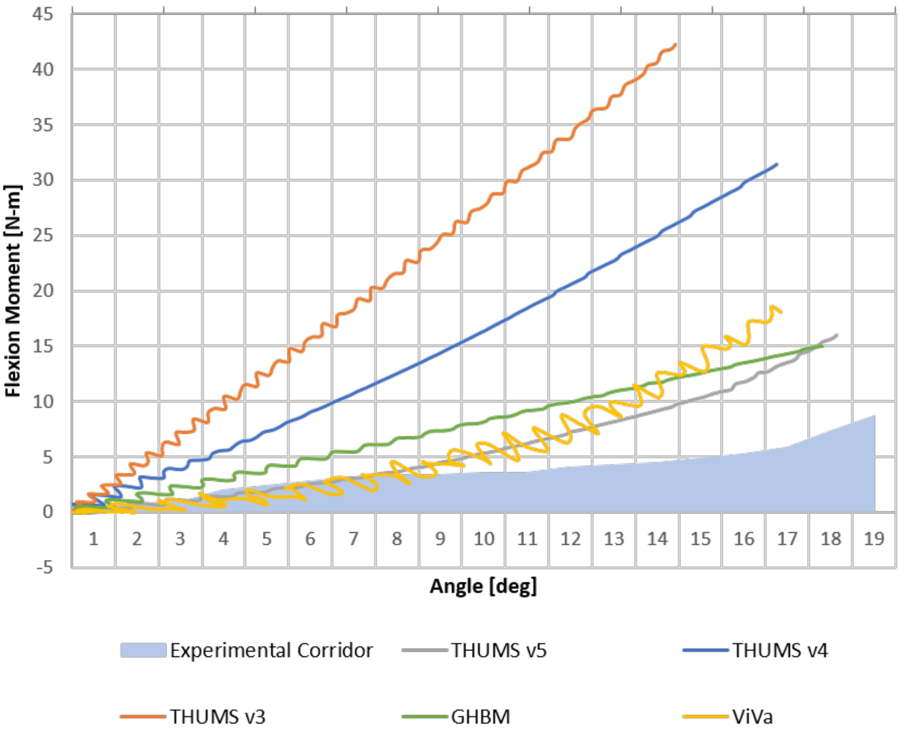

Figure 5.13: Simulation results plotted against experimental results for the Demetropoulos flexion load case

Although no kinematic data was published for these experiments it is still interesting to analyze the HBM kinematics and any differences that they can elucidate. Kinematic plots for the simulations mirroring the experiments from Demetropoulos et al. can be seen in Figure 5.14. In the zoomed view one can see that the initial difference in posture is the largest source of divergence between the models, and the spatial difference as measured in the sagittal plane is larger between the individual HBMs than the deformations in each HBM.

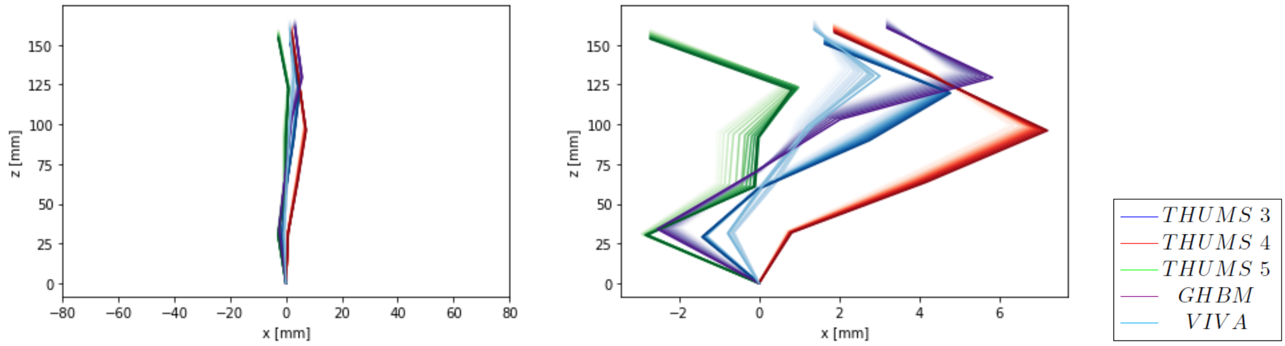

Figure 5.14: Sagittal view of the kinematic responses of the various HBMs under axial load as described in Demetropoulos et al. [33]. The kinematics were tracked using nodes near the center of each vertebral body. The lightest colors represent the initial position, and become darker as time progresses. Left is a view of the kinematics to scale, and right is a zoomed view in order to better see the development.

Results for the various THUMS v5 postures investigated as part of the sensitivity study can be seen below. Figures 5.15 and 5.16 show the kinematic and force response results respectively for the various postures in the axial load case, and Figures 5.17 and 5.18 show the kinematic and moment response results respectively for the flexion loadcase. For the kinematic results of the postures, again the initial position remains the largest difference, with only small deformations occurring in the sagittal plane.

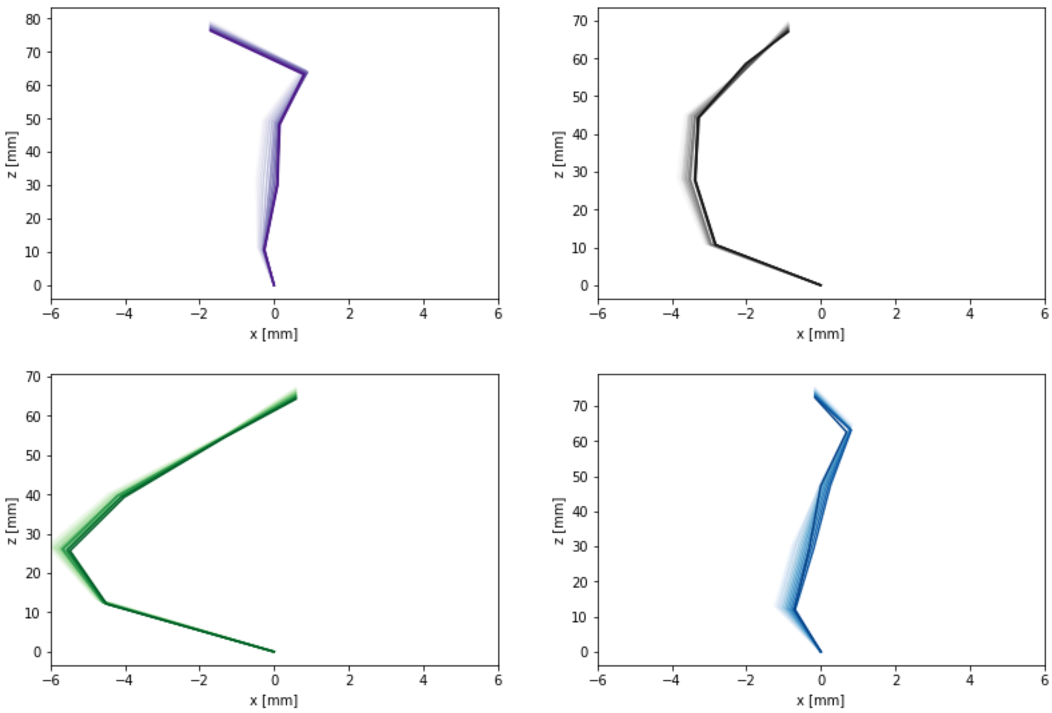

Figure 5.15: Kinematic sensitivities for the various lumbar spine postures which were investigated under axial loading as described in Demetropoulos et al. [33]: purple is the standard position, black is the reclined baseline, green with more lordosis, and blue with more kyphosis. Time 0 begins with lighter colors and the colors become darker until the final position is reached

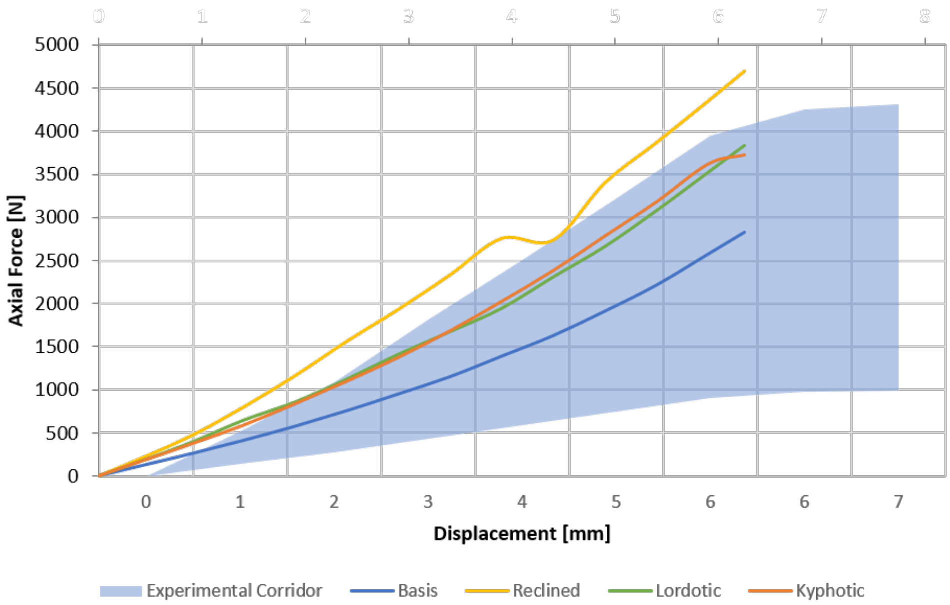

Figure 5.16: Axial force comparison of the positions investigated according to initial posture for the axial load case of Demetropoulos et al. [33]

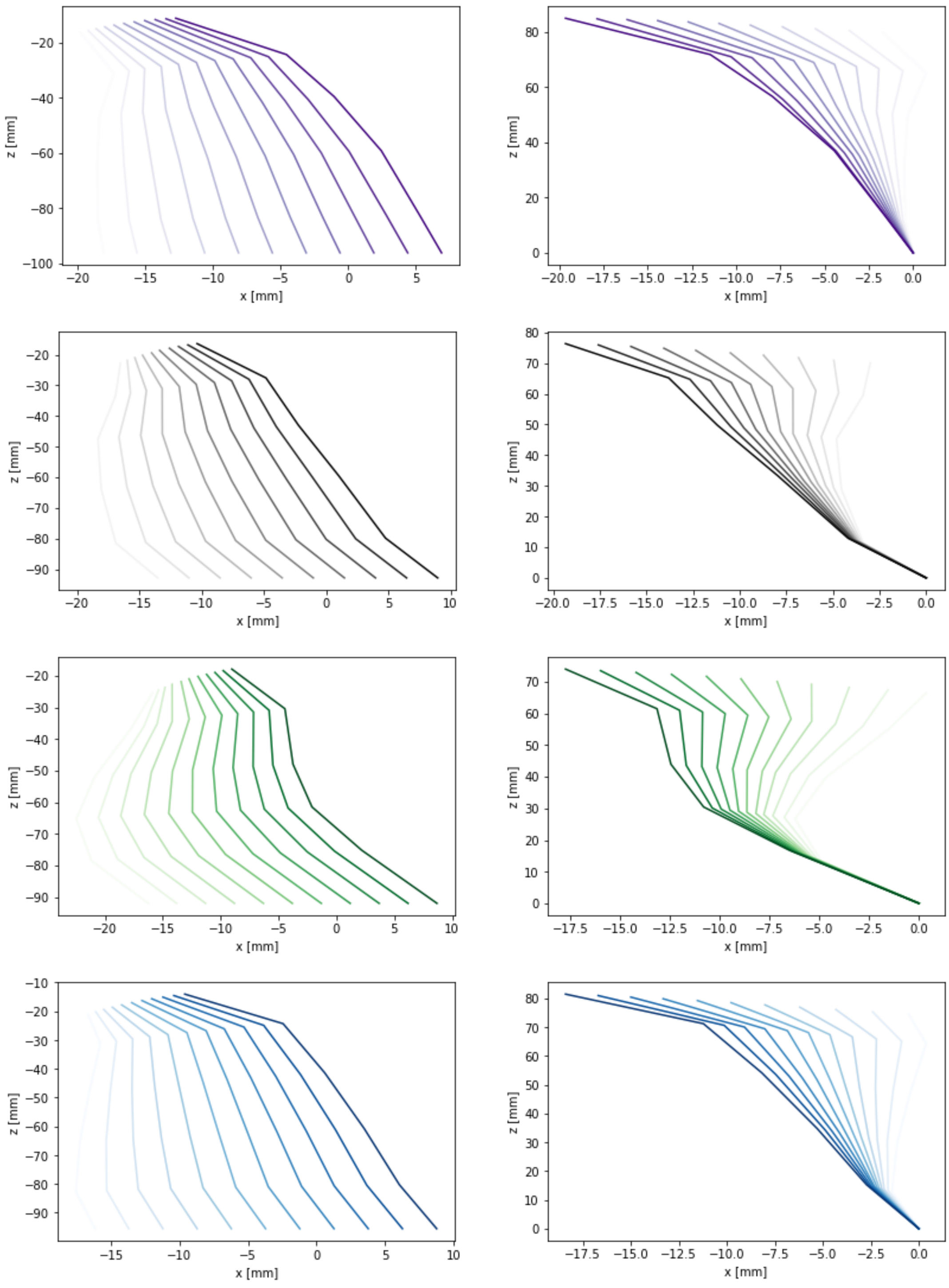

Figure 5.17: Spinal kinematics results from the posture sensitivity in flexion load-case per Demetropoulos et al. [33]: black is the baseline, green with more lordosis, and blue with more kyphosis. Time 0 begins with lighter colors and the colors become darker until the final position is reached. The left column is a global view; the right column is following lumbar spine pinned at L5

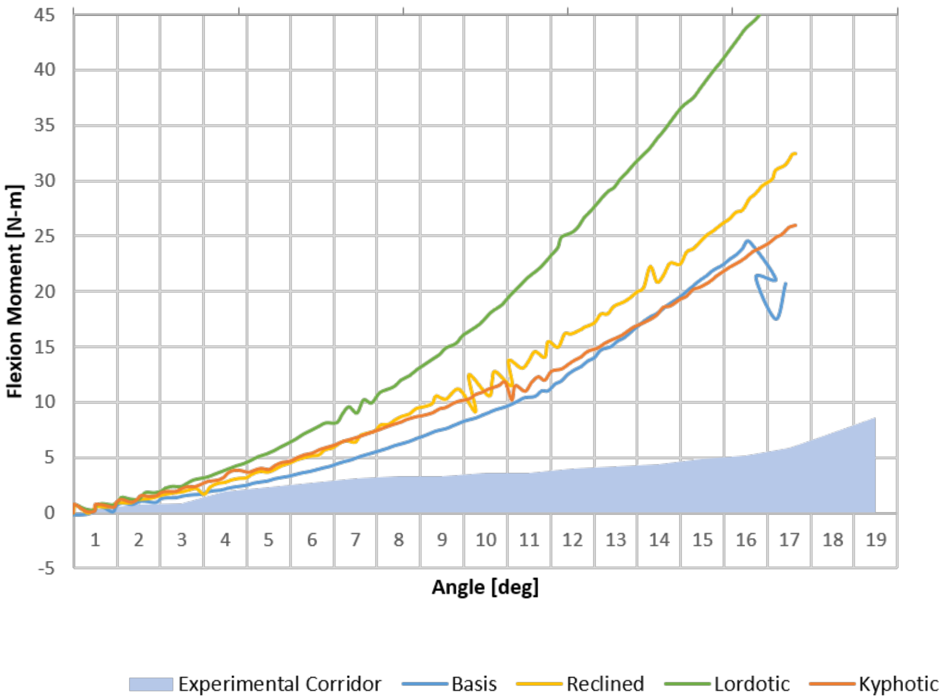

Figure 5.18: Flexion moment comparison of the positions investigated according to initial posture for the flexion load case as described in Demetropoulos et al. [33]

Results from the Stemper et al. Simulations

The results comparing the and the kinematic response across the five separate HBMs can be seen in Figures 5.19 and 5.20. The results comparing the force response across HBMs are depicted in Figure 5.21.

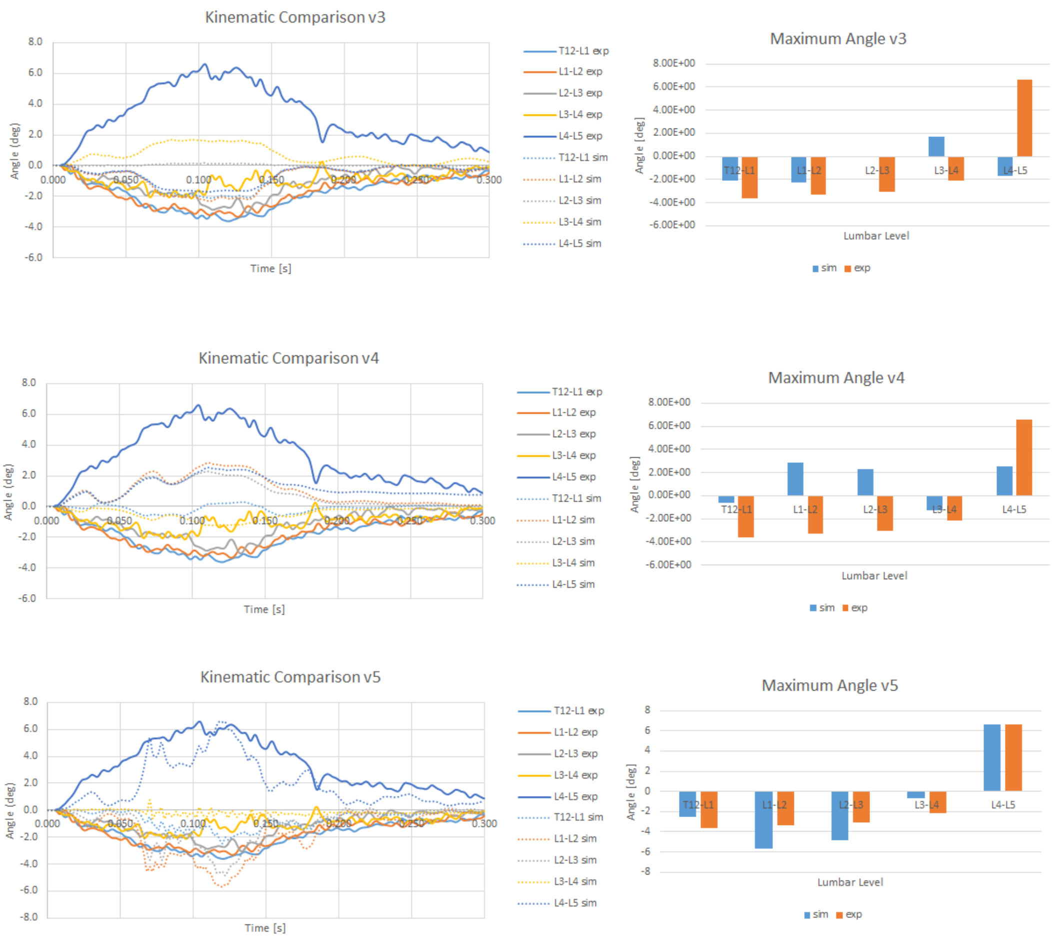

Figure 5.19: Sagittal view of the kinematic responses of the various HBMs under axial load as described in Stemper et al. [109]. The kinematics were tracked using nodes near the center of each vertebral body. Positive angles represent flexion, whereas negative angles represent extension.

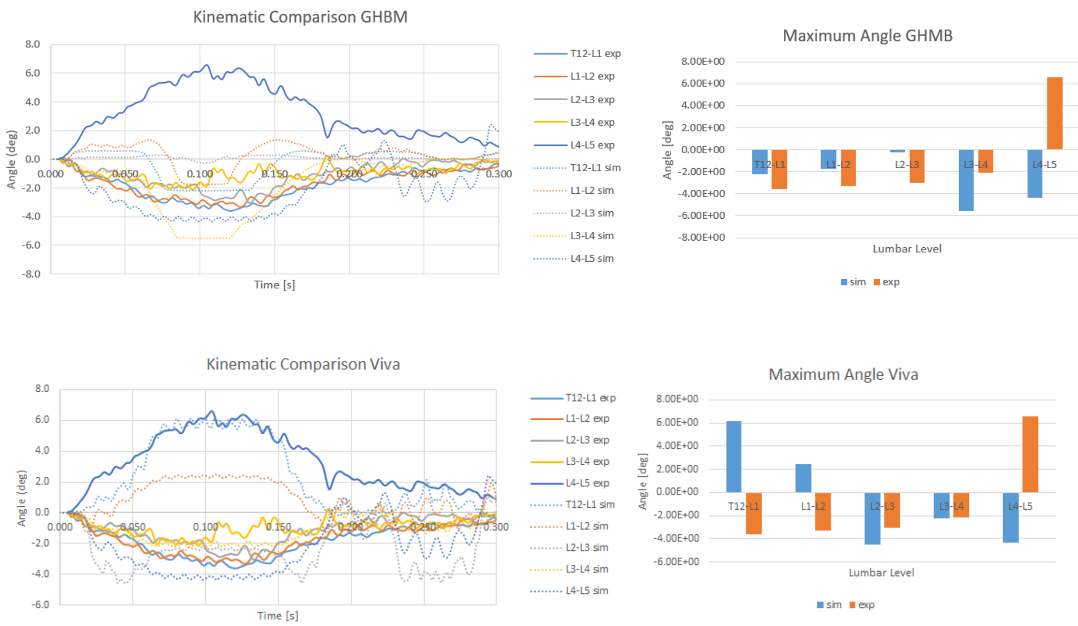

Figure 5.20: Sagittal view of the kinematic responses of the various HBMs under axial load as described in Stemper et al. [109]. The kinematics were tracked using nodes near the center of each vertebral body. Positive angles represent flexion, whereas negative angles represent extension.

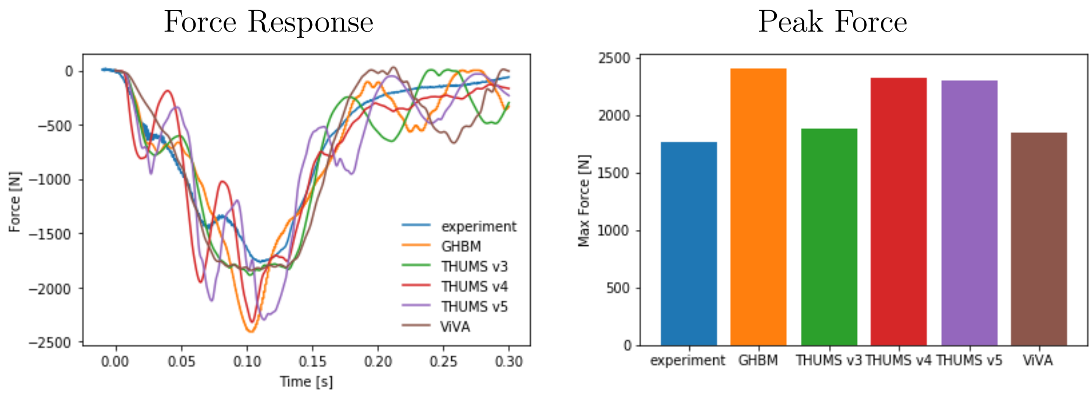

Figure 5.21: Force responses of the various HBMs under axial load as described in Stemper et al. [109].

Figure 5.22 shows the kinematic results of the simulations investigating the sensitivity of the Stemper et al. simulations to changes in the boundary conditions. Figure 5.23 shows the force response of the Stemper et al. simulations to the changes in the boundary conditions.

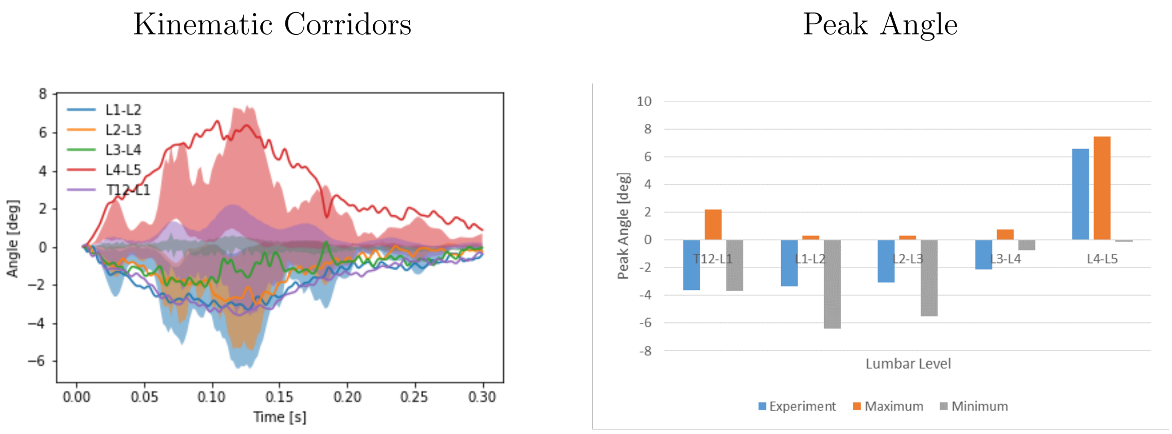

Figure 5.22: Kinematic response of the THUMS v5 HBM under axial load as described in Stemper et al. [109] with the point of load varied by ±2 mm. Solid lines represent the experimental values and the shaded corridors represent the range of simulated responses

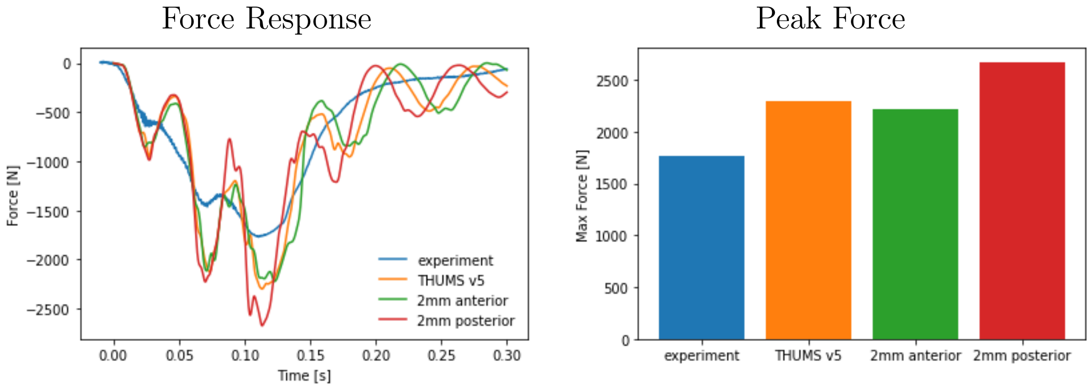

Figure 5.23: Force responses of the THUMS v5 model with ±2mm uncertainties (anterio-posterior) of the fulcrum point under axial load as described in Stemper et al. [109]

The kinematic results comparing the various THUMS v5 postures for the Stemper et al. drop tower experiment are shown in Figure 5.24. The force response for the various postures are presented in Figure 5.25.

Figure 5.24: Sagittal view of the kinematic responses of the various THUMS v5 postures under axial load as described in Stemper et al. [109]. The kinematics were tracked using the nodal coordinate systems as defined in Section 5.2. Positive angles represent flexion, whereas negative angles represent extension

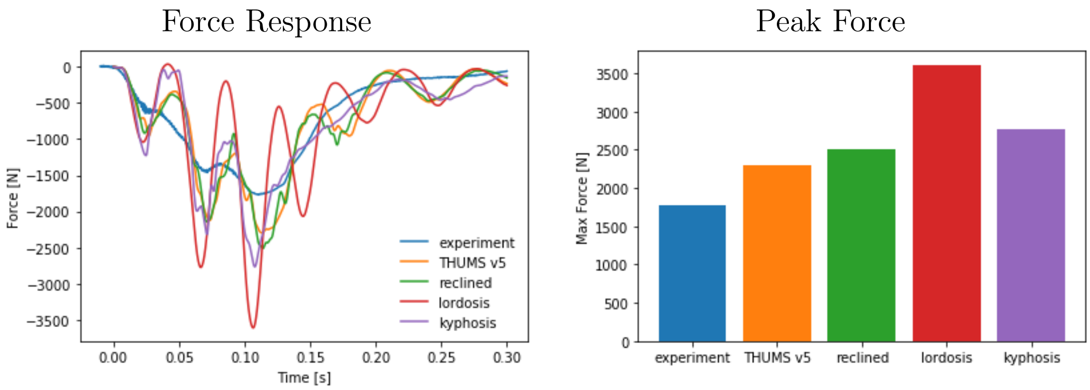

Figure 5.25: Force responses of the various THUMS v5 postures under axial load as described in Stemper et al. [109]

5.4 Discussion

5.4.1 Relevance of the Reference Experiments

These two experiments provide a good source of data for axial impacts across strain rates. They are similar to the two experiments from Chapter 4, one being at a constant lower strain rate applied using a material testing device, and one being at a higher strain rate achieved using a drop tower. They both also carry similar uncertainties as it relates to drop testing as compared with material testing devices in general. This mirrors the testing setup seen in Chapters 3 and 4, where the IVD was tested using a material testing device and the FSU tested using a drop test setup.

Comparison of Lumbar Spine Postures

As seen in Figure 5.5, the position with added lordosis has the most curvature. The reclined model has the second most curvature and the as delivered posture, and the kyphotic postures both have the least amount of lordosis. The kyphotic model is not truly kyphotic, as its lumbar lordosis angle remains positive. This is a limitation of the current study. According to Izumiyama et al. [62], in a population there are individuals with lumbar kyphosis. And the level of kyphosis can reach levels of lumbar lordosis as low as -10°. As this sort of posture could not be realized using the THUMS v5 within the context of this study, this is an area for future research, and cannot be commented upon using the current results. What is also unclear about the described postures is how well they describe individual lumbar curvature. Just because they lie with in corridors described by Izumiyama et al., does not mean that the posture taken as an individual is realistic. In order to have this kind of biofidelity access to CT scans or at the very least sagittal x-rays are required. With CT data the same methodology as proposed in Section 5.2 can be applied to have comparable postures in silico as in vivo.

The vertebral positioning as described in Tables 5.2-5.5 paint the same picture as the visualization of the postures, but allow for other researchers to recreate these postures with their own models allowing for a much more precise comparison in the future studies. The protocol which was used to define these postures, as described in subsection 5.2.1 is model and code agnostic, and also allows for comparison to radiological data sources. This means that future researchers can also compare any future postures investigated in individuals to the postures presented here. This standardized framework makes comparing across data sources, as well as within them, much more consistent.

Comparison to Demetropoulos et al.

All of the models except for the THUMS v4 and the Viva lie within the experimental corridors. These experimental corridors were constructed differently than those used in the IVD comparison. For the IVDs the corridors were constructed using the mean and standard deviation from the experimental setups, which also allowed for an analogous corridor to be constructed for each HBM. The corridors from the experiments of Demetropoulos, on the other hand, are the maximum and minimum response seen across all individuals [33]. Because only the maximum and minimum response make the corridors, and an HBM can be considered as one individual for comparison purposes, no corridors were able to be constructed for the HBMs. This difference in the type of corridor has an affect on the ability to validate. Statistically constructed corridors are more conservative than individual based corridors, as plus minus one standard deviation represents only 68% of a population, whereas the sample used in an individual type corridor is ideally representative of the entire population.

The THUMS v5 model notes in its documentation [113] that the Demetropoulos experiments are used as validation load cases, which is likely the reason the THUMS v5 model sits so squarely in the middle of the corridors. The THUMS v4 response is especially interesting as it closely mirrors the upper bound of the corridor, which comes from a single individual experiment. The THUMS v4 also lists the experiments of Demetropoulos et al. as being used for model validation [67]. With a larger sample size it would be possible that the THUMS v4 would also lie inside the corridors. The shape of the THUMS v4 curve also closely matches the shape of the upper corridor boundary.

The second case investigate from the study of Demetropoulos is the case of flexion. This is a novel case as it is the first time flexion is discussed in this work. Flexion has been investigated for IVDs and FSU by numerous researches [4, 89], but at the loading rates and levels seen for automotive applications, none of the experiments from the literature were deemed to have been described in enough detail to allow precise modelling using HBMs. If angular stiffness can be seen as being similar to compressive stiffness, than a comparison can be made between the ranking seen in Figure 5.8 and 5.9. For the flexion load case, all of the models show a too stiff response as compared to the experimental corridors. In flexion the facet joints do not play a large role in contact, as flexion cause the facet joints to separate from one another. More likely is that this overstiffness in flexion is due to numerical reasons. Looking at the THUMS family of models, until now the THUMS v4 has always been the stiffest, likely due to how its material modelling was chosen for the lumbar spine. For the case of flexion, however the THUMS v3 model is now the stiffest. The THUMS v3 model has the coarsest mesh for its IVD, with the THUMS v4 being the next coarsest, and with the THUMS v5 model being meshed the finest. Usually mesh refinement leads to a softer response, and that is what can be observed in the flexion response. That even the THUMS v5 is stiffer than the experimental results suggest that its mesh has not converged for the flexion loadcase. The GHBM and ViVa models, having curves to define their stiffness in flexion, rather than discretizing their geometry do not yield to the same mesh refinement logic as the THUMS models, and both these models are closer to the experimental corridors than either the THUMS v3 or THUMS v4 responses.

No kinematic data was published from the study of Demetropoulos et al. [33], but it kinematic comparisons can be made between the different models. In Figure 5.14 both in a "to scale view" of the kinematics and a "zoomed in view" of the kinematics can be seen for the axial compression load case. In the scaled figure one difference between the models is their initial position. This initial difference is the largest source of the kinematic differences, as measured by position in the sagittal plane. That the initial difference in position remains the biggest global difference in position throughout the axial simulations shows that an well documented initial position is crucial when comparing global kinematics of lumbar spine experiments.

When comparing the various lumbar spine postures described in Section 5.2.1, similar results are obtained. As seen in Figure 5.15, during the simulations there is relatively little kinematic motion seen, less than 1 mm in the sagittal plane at each vertebral level. The initial differences in posture however have up to a 6 mm difference in position at L3. These initial posture also have an effect on the model response. As seen in Figure 5.16, the original posture as the model is delivered falls in the middle of the experimental corridor, but the posture from the reclined position is stiffened to the point that it lies outside of the corridor. Both the lordotic and the kyphotic posture lie within the experimental corridors, but are stiffer than the original posture. This suggest that the original posture is a local stiffness minimum, as deviation from this posture in both flexion and extension causes the results models to be stiffer.

Comparison to the experiments of Stemper et al.

Comparisons Across HBMs The experiments of Stemper et al. are simulated using the accelerations measured in the experiments as applied boundary conditions for multiple models and postures. The kinematics of the various HBMs were first compared with the experimental results, as seen in Figures 5.19.

The kinematics of the THUMS v5 shows the same trends as the experimental data, with bending in flexion occurring at all levels except for the L4-L5 level. Good correlation of the general direction of bending however only goes so far;

differences in the peak angle range from less than 1% to 72%. The largest peak differences are found at the L3-L4 disc, which experience the smallest absolute angles at 0.7° for the simulation and 2.1° for the experiments, yielding an absolute difference of 1.4°. The largest absolute angular difference occurs at L1-L2 with a delta of 2.3°. That the overall bending directions at each disc level are correctly observed, but that the absolute amount of bending seen shows a wide variation shows that the THUMS v5 model has the potential to correctly approximate the lumbar spine under high rates of axial load, but that more validation work is needed. The differences in the angles could be due to a too-coarse mesh causing a too-stiff response. In the IVD and FSU validations in previous chapters the THUMS v5 model was found to be in good agreement with the data, but both of these load cases were purely axial, whereas the experiments of Stemper et al. also have bending element. Before the models are evaluated in bending at the total lumbar spine level in bending they should also have an established baseline for the IVD and FSU cases in bending. This can also be seen in the results discussed in Section 5.4.1: for the axial load cases three of the models lie within the experimental corridors, with the remaining two being close the the experimental limits, but for the bending loadcase none of the models remain fully within the experimental corridors.

The GHBM shows the correct kinematic tendencies across all levels except for L4-L5, underestimating the flexion at T12-L1, L1-L2, and L2-L3, and overestimating the flexion at L3-L4.

The THUMS v4 model has kinematic trends which match the experimental data at the T12-L1, L3-L4, and L4-L5 levels, which show peak percent differences of 83%, 42%, and 61% respectively. The THUMS v4 model always shows less movement than the experiments, meaning at the levels which bend in the same directions as the experiments, the THUMS v4 model is too stiff. This stiffness however might be due to the levels where the model bends opposite to what was observed in the experiments of Stemper et al. For the IVD load case THUMS v4 was seen to be the stiffest model, but for the bending case of Demetroupolos et al., the THUMS v4 has the softest response. The combined axial and bending of the Stemper load case mixes elements of both bending and axial loading, making it more difficult to separate the two effects from each other.

Both the THUMS v3 and ViVa models predict the kinematic directions correctly at two levels. The THUMS v3 at the T12-L1 and L1-L2 levels and the ViVa model at the L2-L3 and L3-L4 levels. For the ViVa model the simplified disc models are not able to correctly model the physical behavior of the lumbar spine under compression. As the load is transferred to the T12 vertebra, it can be seen to rotate about the predefined disc axis, which is statically defined close to the center anterior to posterior of the vertebral body. For the THUMS v4 and v5 models which have modelled the discs as solid elements this initial contact eventually leads to flexion bending at T12-L1 because the other discs take some of the load which causes the T12 lever arm to shift anteriorly. For the ViVa model however this cannot happen, due simply to how it is modelled. The THUMS v3 model experiences the opposite phenomenon, that its discs shift the load too far anterior, causing the reversal of kinematic directions towards the caudal end of the lumbar spine. The THUMS v3 discs are modelled as solids, but only have one element row of deformability. This coarseness hinders any bending which is wont to occur. The THUMS v4 and v5 have differing kinematics even though they are both modelled using solid element discs which are finely mesh enough to avoid the over-stiff response in bending seen in THUMS v3. Part of this difference can be attributed to the differences in disc stiffness between the two models. As seen in Figure 3.4 the THUMS v4 disc has a 67% stiffer average response than the THUMS v5 disc. The disc stiffness alone makes the entire lumbar spine stiffer as can be seen in comparing the THUMS v4 and THUMS v5 responses in Figure 5.8.

For the case of the drop tower experiments from Stemper et al. however there are additional degrees of freedom when compared to the experiments of Demetropoulos, namely in the anterior-posterior directions, allowing for anterior shear and flexion bending. All else being equal, stiffer discs would equate to less bending, but for the case of the THUMS v4 and v5 models, the difference in stiffnesses comes not only from differences in their material properties, but also from their geometries, as summarized in Table 3.1. The differences in disc geometries have an effect on disc stiffness which in turn has an effect on global stiffness and therefor kinematics. However the model geometries are not only difference in the discs. The THUMS v4 has a L1-L5 Cobb angle which is 21° more flexed than that of the THUMS v5, which leads to it also having a larger moment arm. In order to ascertain whether the disc material, disc geometry or the global geometry is the dominant factor for the model kinematics, more work is needed to validate the discs in bending. Experiments have been done on lumbar IVDs in bending in the past [2], providing very useful data. However these experiments were not carried out with the intent of validating finite element models and the data they provide are thus incomplete, especially as it relates to the kinematic descriptions of the discs in bending.

The force response of the various HBMs shows a different trend than the kinematic data, as seen in Figure 5.21. The experimental data shows an oscillatory behavior in loading with a frequency of 125 Hz, and the three THUMS models also show oscillations of around 125 Hz. The Viva Model, however, shows a smooth loading response with a plateau first peak followed a second peak at 270 ms. The GHBM has a smooth, non-oscillatory ramp up with a single peak, which is also the global maximum of 2413 N. Although the oscillations seen in the THUMS models have a similar frequency to the experimental values, the maximum amplitudes of the simulated oscillations are larger by a factor of 4.81, 15.55, and 21.87 for the THUMS v3, THUMS v4, and THUMS v5 models respectively as compared with the experimental values. This suggests that the models are correctly modelling whatever phenomenon is causing the oscillations in the experiments. The most likely source is the sudden onset of the force during the impact. That these oscillations are only seen in the high speed impact load cases rather than the material testing driven ones also supports this hypothesis. But because the amplitudes are larger in the simulations this suggest some aspect of the simulation is being incorrectly represented. Seeing slight phase shifts in the models and higher peak values could be due to a lack of damping. Many of the structures in human bodies are idealized in HBMs, which often leads to linear elastic instead of a viscoelastic behavior. The peaks of the force curves are all higher than the experimental values, with the THUMS v3 being 6.7% higher, THUMS v4 31.1 % higher, THUMS v5 29.8 % higher, the Viva model being 4.2 % higher, and the GHBM being 36.2 % higher. That the general trends of the force curves show less variation than the corresponding kinematic responses shows that validation experiments need to use both kinematic and force response data in order to provide useful results. That the THUMS v3 and ViVa models show the closest force response to the experimental values, but have kinematic responses that vary widely from the experiments means that caution should be taken using only force criteria to evaluate HBM behavior. This is because of how forces were measured in the experimental setup: by measuring the force of the impact underneath of the specimen, the specimen weight and inertia dominate the response, as any energy absorbed by the specimen as damage or deformation is much smaller than the kinetic energy of the specimen falling. In the HBM simulations it is possible to measure forces in the specimen itself, but this would be very difficult in a PMHS specimen. Certain studies have used pressure transducers mounted in the nucleus as a proxy for force [84, 100], but these types of measurements are also very difficult to validate and consequently correlate with the global forces as measured in the HBMs.

Comparisons Across Postures One way to tease the relationship between geometry and kinematics is to look at the same model in various postures. The THUMS v5 model was simulated in this setup with the postures described in Section 5.2.1. Because these models have the same material definitions with different geometries, any differences in model responses that they experience are due solely to their geometries. The kinematic response of the reclined posture is similar to that of the basis THUMS v5 with all of the peak angles in alignment with the experimental values. Where the basis model underpredicts the experimental values at T12-L1 the reclined model overpredicts. The reverse is true at the L1-L2 and L2-L3 levels where the reclined model underpredicts and the basis model overshoots. These two models perform similarly despite how geometrically different they are, with the reclined model having 13 more degrees of lumbar lordosis, corresponding to having its L4 vertebra 7 mm more anterior than the baseline model. The lordotic model shows diverging kinematics at the T12-L1 and L4-L5 discs both the other two postures, as well as to the experimental results. The lordotic position has the largest lumbar lordosis of all of the postures, which might be the reason there are higher amplitude oscillations in all of the measured disc angles as compared with the baseline and reclined models. The kyphotic posture has a different response than all of the other postures in that it has an extension response at the L1-L2 and L3-L4 levels, which was also not observed for any of the other HBMs investigated. This unique extension response, combined with a 218% larger flexion at T12-L1 than was reported in the experiments, causes a global shortening between T12-L5 that catches the kyphotic posture in a deformed state, not allowing the model to return to its t0 position. This behavior can be seen in the kinematic curves in Figure 5.24 where the kinematic curves do not return to zero.

The force responses of the various postures mirror their respective kinematics, with the basis THUMS v5 and the reclined posture having the most similar forces, being 29.7% and 41.9% higher than the peak forces measured in the experiments. The lordotic posture shows higher amplitude oscillations than the other models and the experiments, and due to these oscillations has a peak force which is 103.9% higher than the peak experimental force. The kyphotic posture here shows the second highest peak force 56% higher than what was reported in the experiments of Stemper et al. In this way the postures are similar to the various HBMs: large differences seen in the kinematic curves are not captured in the force responses, as best demonstrated by the kyphotic posture which never unloads, but shows a similar force output to the other postures investigated. For this reason it is again recommended to always include kinematic data for HBM validations

The differences between the various postures and the experiments make it difficult to draw conclusions. It could be that there is a critical level of lumbar lordosis, above which realistic kinematics cannot be modelled with the current state of the art. This level of lordosis must lie between the reclined posture and the lordotic posture. However making such a sweeping claim from the basis of three data points is likely premature. It would be better to do a design of experiments set of simulations to try to more deterministically find where the models diverge from the experiments and by how much. Using the framework established to describe the position of the lumbar spine as described in Section 5.2 makes this possible, but the large range of possible positions makes the task daunting. It would also be beneficial to have a larger pool of experiments with which to compare these simulations in order to ensure that error from interpolating results remains low.

Comparison Considering Boundary Conditions Considering the amount of variability between models as well as within the same model having different postures, the question could arise to how sensitive the model kinematics are to boundary conditions. By changing the location of the caudal cylinder ± 2mm anteriorly and posteriorly, the robustness of the THUMS v5 kinematics was investigated, with the results shown in Figure 5.22. Percent differences to the experimental kinematics as measured by their peak bending angles varied from -93% to 66%, this compares with peak percentage differences ranging from -271% to 71.6% for the different HBMs and range of -318% to 218% for the various THUMS v5 postures [1]. This means that the external boundary conditions can account for a portion of the kinematic behavior. This might also mean that the kinematic difference seen between the models and postures has more to do with their geometry and how this geometry influences the loading behavior. More investigations should be undertaken to better understand the spinal kinematics, including measuring how far each vertebral center is from the point of applied loading. Once loading begins however, a more complex analysis should be developed in order to follow the detailed flow of forces, which might bifurcate into separate load paths through the discs and posterior elements. A similar analysis has been applied to head impact experiments and is discussed in Fuchs [46]. The deformation of the discs themselves will also have an influence on the distributions of forces and how they are spread. Looking at the 2 mm posterior loading boundary condition, kinematic similarities can be seen to the lordosis THUMS v5 posture. Both of these show higher amplitude oscillations and similar T12-L1 kinematics. The 2 mm posterior condition loads the spine more in compression and less in flexion than the basis position, which leads to a mostly compressive loading. The lordodic posture has a similar tendency, but in this case because the spine has very little curvature with which bending can be expressed. That these dissimilar configuration can have similar tendencies show how complex of a system multi-segment spines can be. More research is needed to fully understand all of the intricacies associated with spinal kinematics, as well as to understand how well the in silico models represent actual human responses.

[1] The maximum difference in the postures are observed for the more kyphotic case. Excluding the kyphosis case from the tally the peak angle difference range becomes -193% to 71.6%

Chapter 6

Use Case: Full Scale Low Speed Comparison

6.1 Introduction

One possibility for human body models is their applicability in new scenarios where traditional dummies are not considered valid. One such application field relates to non-standard seating configurations being considered in future highly automated driving scenarios. In a reclined seating position for example, the occupant will have different kinematics and likely a new type of restraint system or restraint system strategy. Having a different kinematic response means that current ATDs which were not designed with this type of response in mind are likely to perform differently to a human body model, with its more detailed anatomical geometry. The question of how well both ATDs and HBMs arises can predict real world performance, as well as questions of validity for both kinds of surrogates. In order to test validity, new physical experiments are required. What simulations with models of ATDs and HBMs allow, are a-priori estimates to what kind of validation experiments are required. For example: running a simulation of a HBM and and ATD in a new seating environment will likely give two distinct responses, and based on these responses, experimentalists can better estimate what specifically should be measured or expected in the test.

This approach works the best when there is already an established basis validity associated with a model. If a model has been validated for a certain loading scenario, then the same scenario with only slightly changed boundary conditions should have a similar response. This eventually becomes a question of limited resources: if every test requires the same amount of time and resources to run, instead of testing many small differences which may be insensitive and yield similar responses, it is better instead to validate with cases that vary widely from

one another, in order to see as broad a range of responses as possible.
In this use case the THUMS 5 HBM response is compared with a low speed volunteer test in a reclined seating position. The THUMS 5 model has the validity of its lumbar disc response evaluated in Chapter 3, as well as the FSU response Chapter 4, and the full lumbar spine response Chapter 5. As all of these loading scenarios generated responses in the physiological non-injurious range, they are considered well applicable to compare to volunteer tests which also have responses that remain in the non-injurious range.
The experiments from this experiment are based on experiments performed during the European Union funded project SENIORS [120]. The basic sled setup from the SENIORS project remains the same as was used for matched volunteer testing. A new pulse is used due to system constraints, and the goal is to incrementally rotate the seat, checking with HBM simulations in every new configuration in order to show that the loading configurations are acceptable for volunteer testing. The setup consists of a rigid seat pan, with an angles seat ramp and sides, as seen in Figure 6.1. The seat is mounted to a 6 DOF force and moment transducer. The setup also has a rigid foot box, and an adjustable b-pillar where the restraint systems are mounted.

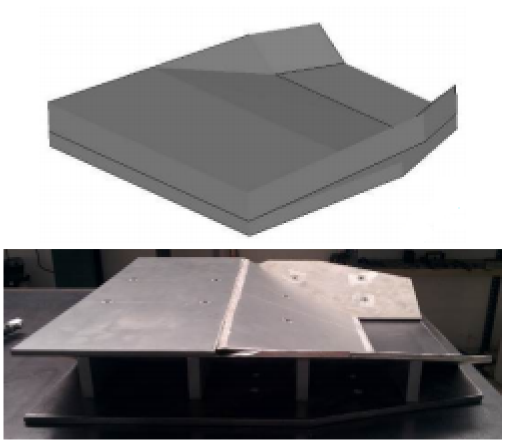

Figure 6.1: The seat used in the original SENIORS Project [40].

6.2 Method

The test was carried out using a single volunteer of approximate 50th percentile male anthropometry (1.75m tall, weighing 78kg). Two configurations were considered for these experiments. The first configuration was in an upright standard occupant posture, with a seat back composed of fabric bands. The seat used was a steel un-upholstered configuration, which can be seen in Figure 6.1. For this configuration the feet were resting upon an instrumented foot box. This configuration (albeit with a different pulse) is described in more detail in [69]. For the second configuration a more reclined seating position was investigated. Here the seat was rotated to have an angle of 40° to the horizontal. A rigid backrest was used which also had an angle of 40° to the horizontal. The footrest normally associated with the foot well for upright seating positions was replaced by a leg rest with nothing supporting the feet in the direction of the applied pulse. This leg rest was positioned to be parallel with the horizontal. For both configurations a three-point seat belt was used without any sort of retraction or load limiting, and was positioned to mimic a seat integrated seatbelt system. The belt path passed over the right clavicle and maintained a good fit with the Iliac crests. The pulse for the upright configuration had a peak value of 3g, and acted to brake the sled which was moving at a constant velocity of 2m/s. For the reclined setups this pulse was scaled down to 2g. A picture of the test setup in the second configuration can be found in Figure 6.2

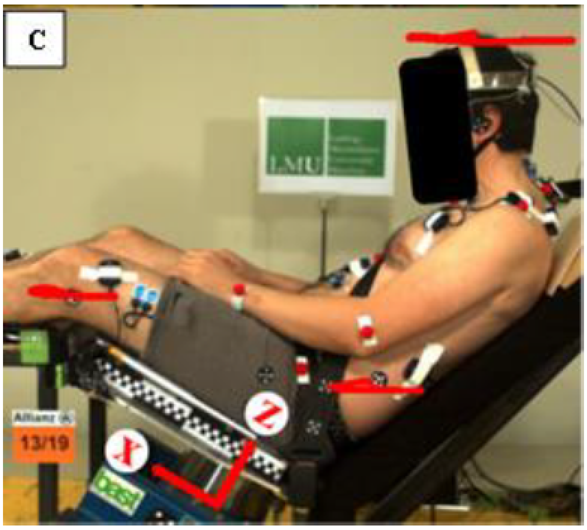

Figure 6.2: The experimental test setup for the reclined volunteer test, from [77]

The Human Body Model simulation was carried out using the THUMS v5.01, using a sled environment validated from the SENIORS project [40]. For the first configuration no modifications of the sled were required, only the pulse had to be adapted. For the second more reclined setup, first the environment model was adapted to the experimental protocol. This involved rotating the entire environment by 30°. The leg rest was modelled to be horizontal, as described in the experimental protocol [77]. The HBM was brought into the environment positioned using a spring damper system in order to bring the trunk and limbs

into agreement with an image taken of the initial position of the volunteer test as seen in Figure 6.2. Each positioning simulation consists of two distinct phases. The first phase is a settling phase which uses a gravitational body force to ensure contact between the HBM and the seat at all relevant positions, this phase lasts 300ms, which was found to be sufficient to bring the model into equilibrium. The second phase of the simulation is when the pulse is applied in the global x direction. The model was defined to have section force definitions at the same locations as were measured in the experimental setup: underneath the seat (thus also rotated for both model and experiment) and on the seat belt in the standard locations.
With the proper amount of setting time, simulations were run in order to match the reclined volunteer tests as described in Muehlbauer [77]. The simulations were carried out looking at an initial occupant posture (the THUMS v5 as delivered) positioned as described above and with gravity settling into the seat, for both the upright and the reclined seating positions. The three spinal postures described in Chapter 5 were also investigated in the reclined seating setup, also with gravity settling into the seat.
After the simulation was run, the simulation results were compared with the experimental results by focusing on a kinematic comparison of the head, iliac crest, and knee movements. Additionally, the lumbar forces and kinematics were evaluated and compared with the validations already presented in the previous chapters.

6.3 Results

From the global kinematics as seen in Figure 6.3, one can see that the deformation mode of the lumbar spine is one of flexion bending rather than one of compression. Looking at the angular kinematics of this simulation as seen in Figure 6.4, a confirmation of the global kinematics is reflected in the local bending at the disc level. In the figure postive angles correspond with flexion, and when the pulse starts at t=300ms all of the discs excluding the T12-L1 and L4-L5 are already in flexion. With the onset of the pulse acting on the spine at t=400ms the T12-L1 disc also goes into flexion.

Results for the Upright Position

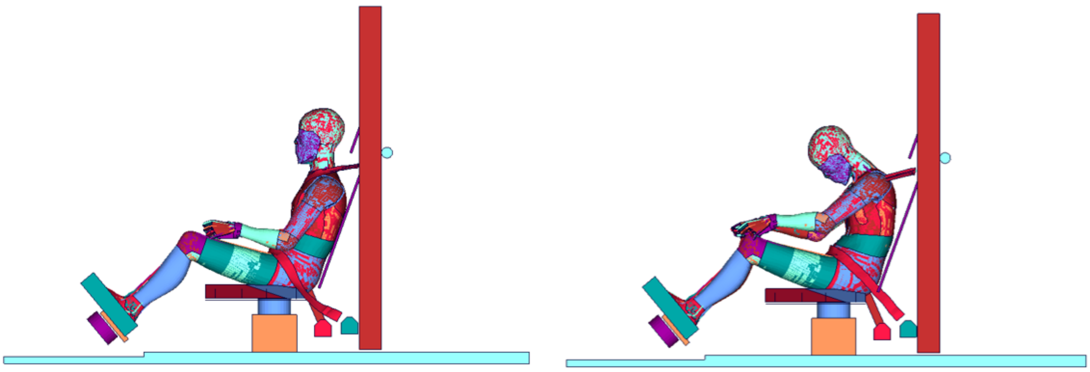

Figure 6.3: Kinematic results of a simulation of the upright position with the THUMS v5 model.

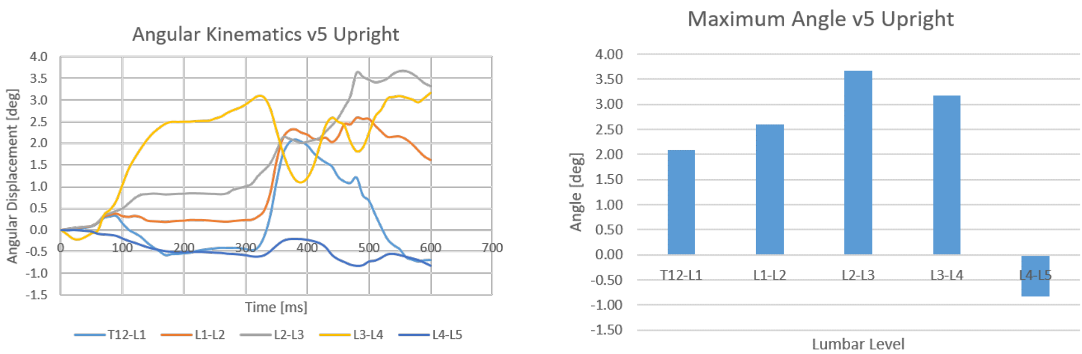

Figure 6.4: Angular kinematic results of the THUMS v5 upright posture as measured at the lumbar spine. Positive angles represent flexion, negative angle represent extension.

The upright THUMS v5 force response as seen in Figure 6.5 tells largely the same story as the disc angular kinematics. Before 300ms the discs are all loaded into compression, with the most caudal vertebrae experiencing the greatest compressive loads. And then after the onset of the pulse some lumbar levels experience more axial force, followed by a period of unloading, where less axial force is transmitted, and then the peak axial forces are experienced for the L4 and L5 levels, whereas the T12 - L3 levels all experience drop offs in force, with the most cranial vertebrae having the largest drop offs.

The THUMS v5 upright posture disc compression also has many features which are the results of bending, as seen in Figure 6.6. The L3.L4 disc for example experiences most of its axial compressive displacement due to the effects of the gravity settling and not due to the applied pulse.

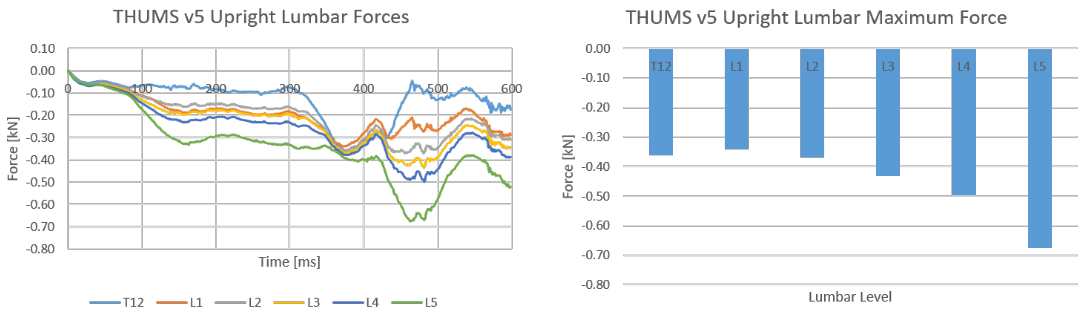

Figure 6.5: Force results measured at the lumbar spine for the upright position. Positive values represent tension, negative values represent compression.

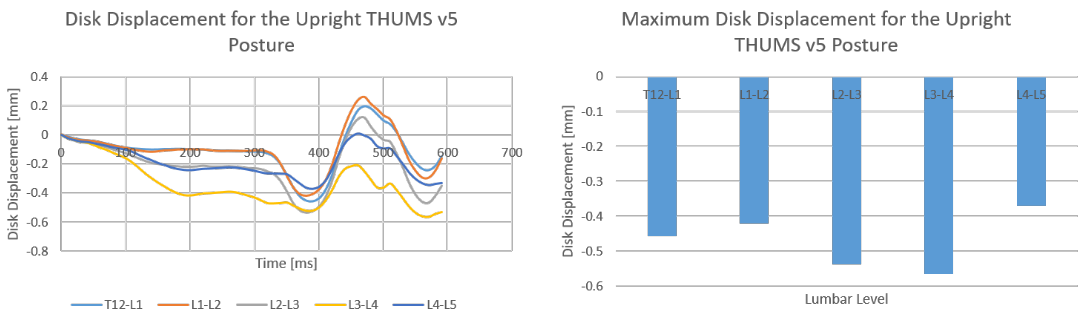

Figure 6.6: disc displacement results measured at the lumbar spine for the upright position. Positive values represent tension, negative values represent compression.

Results for the Nominal Reclined Posture

Figure 6.7 shows simulation set up in the initial and most deformed positions. The most visible global movements are those of the head, which experiences a forward movement causing flexion in the cervical spine, and the extension of the knees. Both of these movements are inertial in nature.

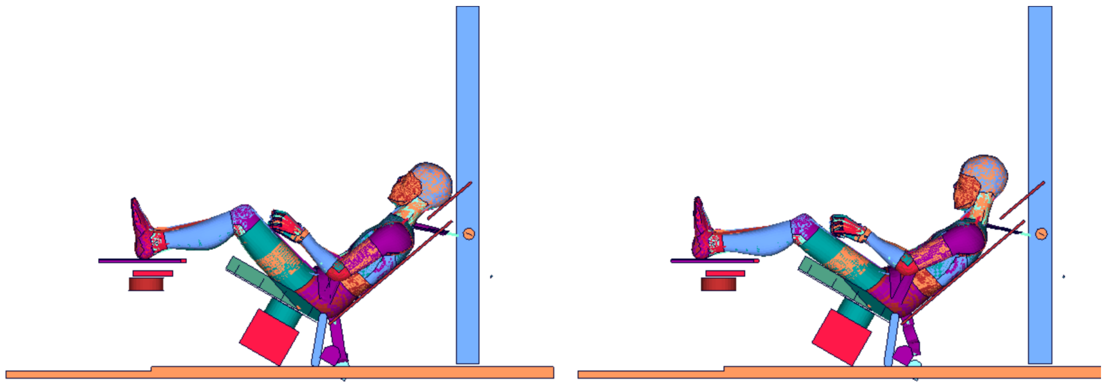

Figure 6.7: Kinematic results of the reclined position.

Figure 6.8 shows the final positions and the movement trajectories of the subject in the reference experiment compared with the positioned THUMS v5 used in the validation simulation. The trajectories are visualized as red lines, and follow markers set at the head, knee joint center, and iliac crest.

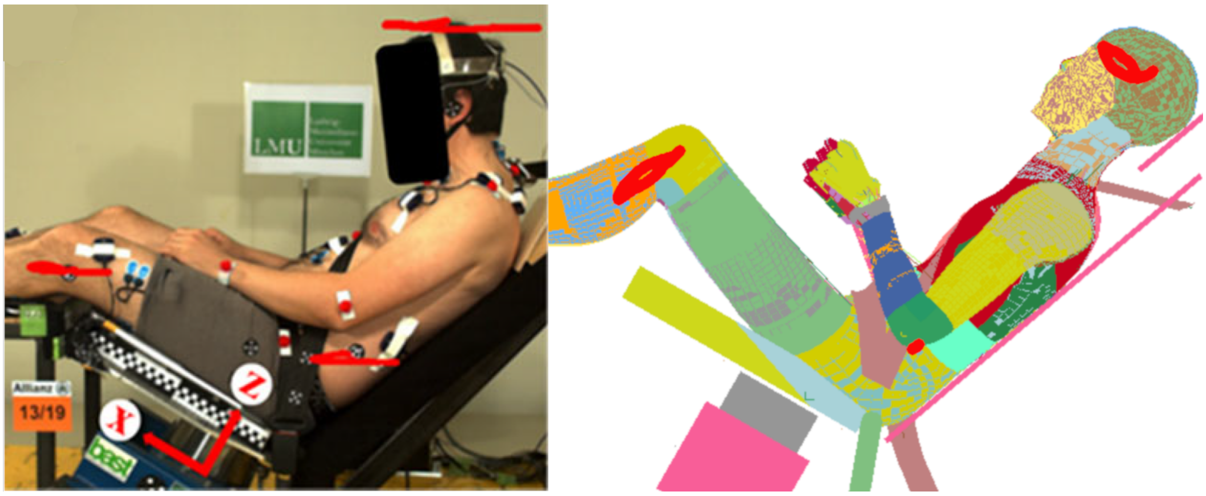

Figure 6.8: Kinematic comparison of the volunteer tests performed by Muehlbauer et al. [77] (left) with the simulation results from THUMS v5 model angled at an incline of 30°(right)

Figure 6.9 shows the displacement streamlines for markers at the head, ASIS, and knee plotted in red, using the seat base as the coordinate system origin. For the volunteer test, all of the displacements show a horizontal trend, in line with the action of the pulse.

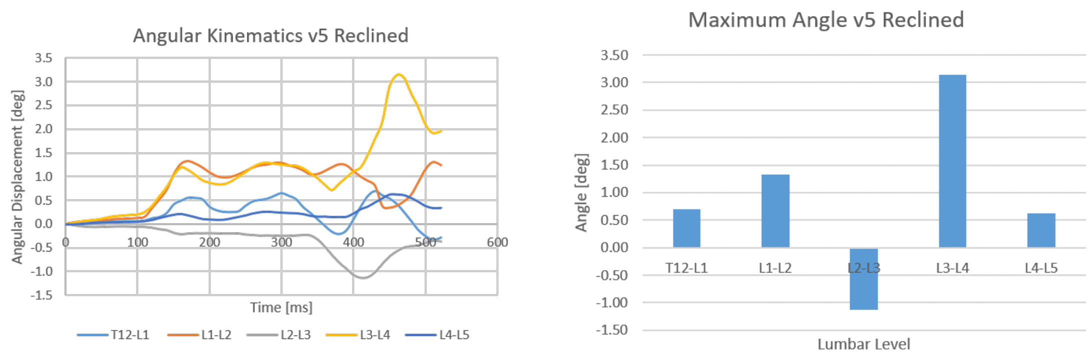

Figure 6.9: Angular kinematic results measured at the lumbar spine for the reclined THUMS v5 angled at an incline of 30°. Positive angles represent flexion, negative angle represent extension.

A summary of the lumbar spine forces as measured in the 30 degree reclined position simulation can be seen in Figure 6.10. Nearly all of the maximum force experienced is due to the pulse loading phase, and not a result of the gravity settling phase.

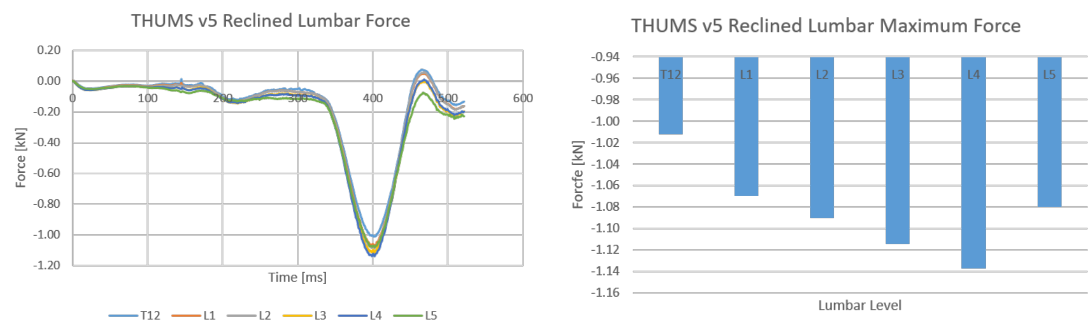

Figure 6.10: Force results measured at the lumbar spine for the reclined THUMS v5 angled at an incline of 30°. Positive values represent tension, negative values represent compression.

Figure 6.11 shows the simulation results of how the lumbar discs behave during the reclined position simulation. The discs are compressed to a comparable level of physiological loading as reported by Newell et al. [83].

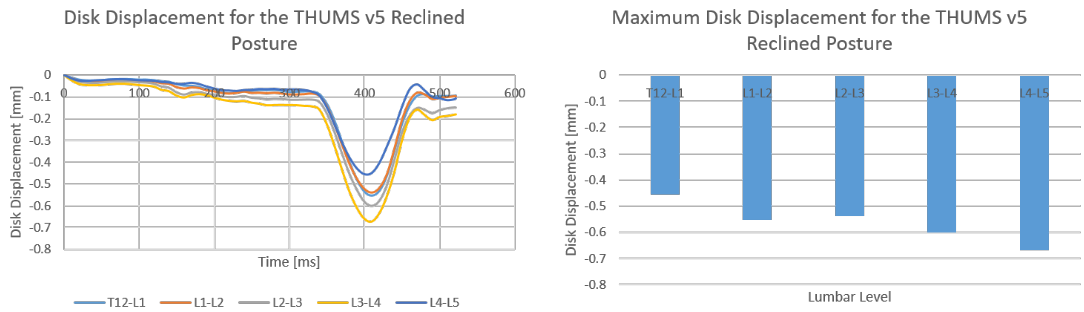

Figure 6.11: disc displacement results measured at the lumbar spine for the reclined position. Positive values represent tension, negative values represent compression.

Results for the more Lordotic Reclined Posture

By comparing Figures 6.7 and 6.12, the effects of lordosis on the kinematic response can be observed. For the nominal posture, L1-L2 and L3-L4 show the most flexion, and with L2-L3 going into extension. For the more lordotic posture, L1-L2 goes into extension whereas L4-L5 shows the maximum flexion deformation angle.

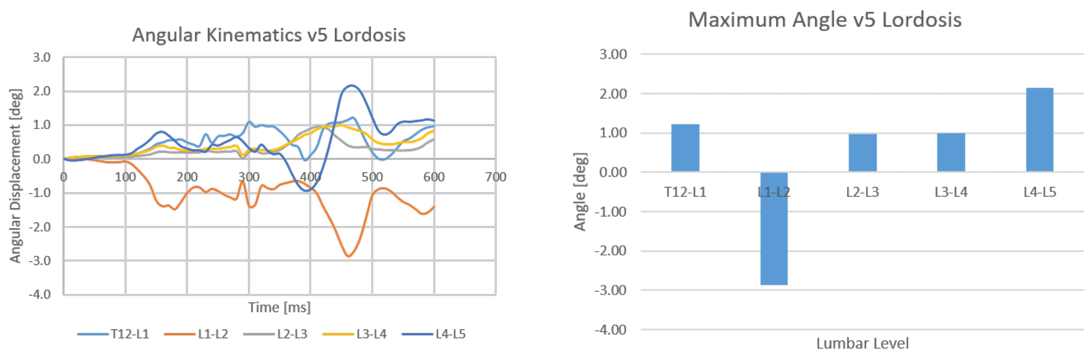

Figure 6.12: Angular kinematic results measured at the lumbar spine for the more lordotic reclined THUMS v5 angled at an incline of 30°. Positive angles represent flexion, negative angle represent extension.

Figure 6.13 shows the force curves have more spread than for the nominal posture at the onset of the pulse at t=300ms, with the T12 force even going slightly into tension.

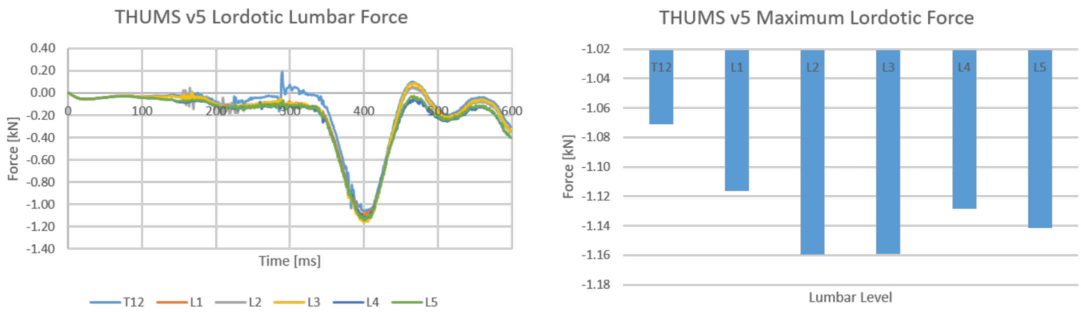

Figure 6.13: Force results measured at the lumbar spine for the more lordotic reclined THUMS v5 angled at an incline of 30°.Positive values represent tension, negative values represent compression.

Figure 6.14 shows the same general pattern seen in the nominal reclined position, with very little deformation due to the gravity loading phase followed by smooth consistent compressive deformation after the onset of the pulse. Where the nominal case showed the highest deformations caudally, and the smallest deformations cranially, the lordotic posture has no clear trend, with both T12-L1 and L3-L4 having large displacements.

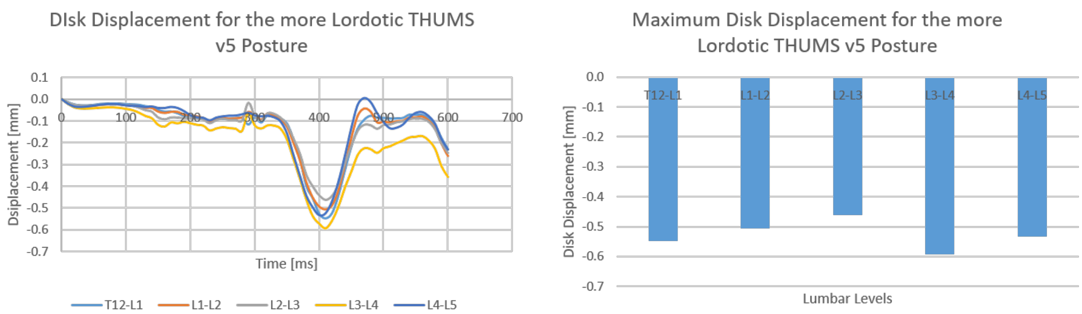

Figure 6.14: disc displacement results measured at the lumbar spine for the more lordotic reclined position. Positive values represent tension, negative values represent compression.

Results for the more Kyphotic Reclined Posture

By comparing Figures 6.7 and 6.15 the kinematics differences resulting from a more kyphotic posture can be seen. The kyphotic posture sees the angular kinematics of L2-L3 and L3-L4 have a relatively constant increase in flexion until they reach their peak values.

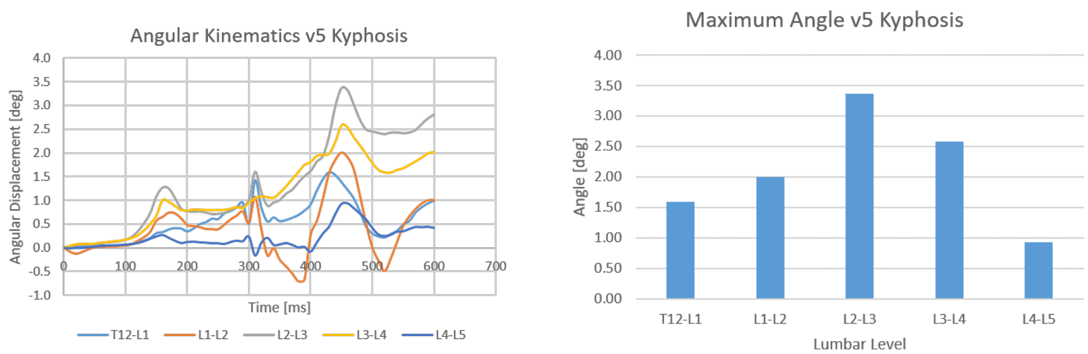

Figure 6.15: Angular kinematic results measured at the lumbar spine for the more kyphotic reclined THUMS v5 angled at an incline of 30°. Positive angles represent flexion, negative angle represent extension.

From the force response for the more kyphotic posture in Figure 6.16, a delta of 114N is observed between the maximum at T12 and the minimum at L5. Whereas the nominal posture and the have relatively normal distributions of the peak force spread across the lumbar levels, the kyphotic posture has a double peak, with the second highest force occurring at L4.

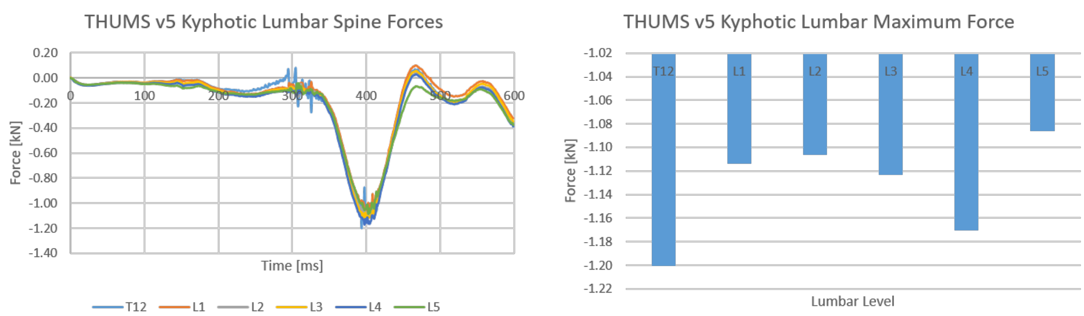

Figure 6.16: Force results measured at the lumbar spine for the more kyphotic reclined THUMS v5 angled at an incline of 30°.

Figure 6.17 show maximum displacements in line with what was observed for the nominal reclined posture with a similar pulse dominant response to what was observed for the two other reclined postures.

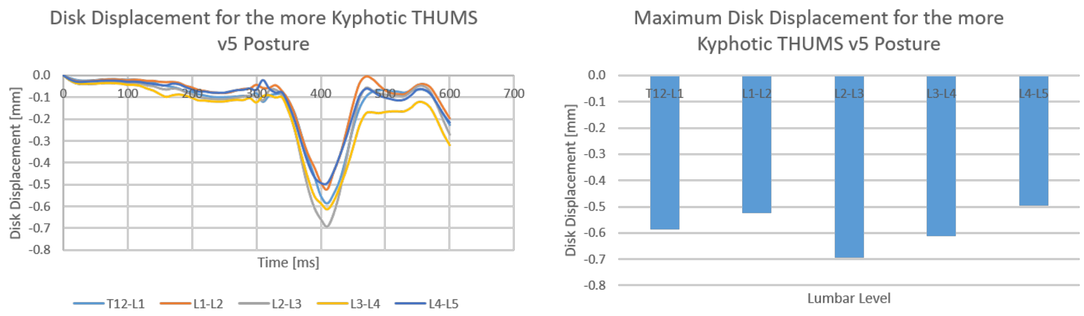

Figure 6.17: disc displacement results measured at the lumbar spine for the more kyphotic reclined position

A comparison of the global kinematics between the reclined posture, the more lordotic posture and the more kyphotic posture can be seen in 6.18. Between the three postures only very minimal differences can be seen in the head and lower leg kinematics responses.

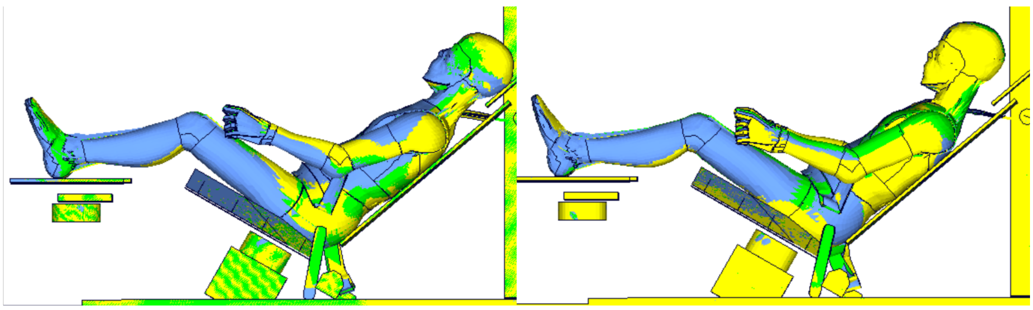

Figure 6.18: Kinematic results of the three various postures angled at an incline of 30°. Blue is the MRI based reclined posture, green is the more lordotic posture, and yellow in the more kyphotic posture.

6.4 Discussion

The objective of this case study is to establish baseline measurements for use in future volunteer testing, where kinematics and boundary conditions are no longer consistent with what has been proven to be safe. In general this baseline can be described as experiencing 1kN of compressive force, and up to 1mm of disc compression, which was derived from the disc force seen in the IVD experiments of Newell et al. [84]. Here it can be said that the THUMS v5 which is being used does have some validation load cases in the lumbar spine region which are based on low speed or quasi-static experiments. What remains unknown is how well these component level validations fit in with a full scale low speed experiment, like the ones which are being investigated in this chapter. The lumbar spine experiments of Demetropoulos et al. [33] and Stemper et al. [109] offer some meaningful stepping stones, showing non-injurious behaviour at a total lumbar spine compression of 5mm with forces ranging from 0.75 kN to 2.5 kN for the experiments of Demetropoulos, and peak forces of 1.7 kN in the case of Stemper. That the full lumbar spines were reported to have higher forces than the component disc tests goes against the common conception that a single FSU will fail at higher forces than a multi-level segment, is only because all of the Authors reported what they observed as non-injurious, none were trying to establish what the threshold for injury would have been[1] Full scale and volunteer testing concerning spinal data remains an area of research with few points of data; this is an issue that comes up often, as the spine is located quite centrally in the body tracking its kinematics or measuring its force response is very difficult in full-scale experiments. Intrusive techniques can be used with PMHSs, but these may influence the outcome of experiments (i.e. mounting tracking brackets on the vertebral bodies may weaken them leading to a fracture which would otherwise not have occurred).

Some experiments have been performed intrusively on volunteers [36], [68], but these also have biases. For the case of Dreischarf et al. [37], all of the subjects had preexisting conditions. For the case of Ledet et al. [68] Baboons were investigated, which have limited aplicability towards human subjects.

Most volunteer studies do not allow for intrusive measurements, and the current state of the art Open-MRIs which can allow for non-intrusive measurements of spinal kinematics are not able to produce videos of motion, and even less capable of being mounted on moving sleds, as would be required to investigate this kind of behavior. What studies like current paired volunteer tests and simulation investigations provide, are data which can be used to calibrate HBMs. Similar to the baseline which was established here, at the end of this set of experiments there will be real world data with which one can compare the HBM response in order to have a map of what levels of force in displacement in the HBM correspond to a non-injurious response in a volunteer. This of course does not mean that the volunteer is experiencing these forces or displacements (which as of yet cannot be readily measured). Nor does it mean that the response of a single volunteer is representative for the entire population.

[1]For the case of Stemper et al. [109], injury risk curve derivation was the goal of the experiments, but the individual test which is referenced here was a preliminary purely non-injurious study.

Upright Position

From the global kinematics as seen in Figure 6.3, one can see that the deformation mode of the lumbar spine is one of flexion bending rather than one of compression. Looking at the angular kinematics of this simulation as seen in Figure 6.4, a confirmation of the global kinematics is reflected in the local bending at the disc level. In the figure postive angles correspond with flexion, and when the pulse starts at t=300ms all of the discs excluding the T12-L1 and L4-L5 are already in flexion. With the onset of the pulse acting on the spine at t=400ms the T12-L1 disc also goes into flexion. What is interesting is that the flexion seen here has not returned to equilibrium even after and additional 300ms of simulation. This is because this bending is global in nature and is dominated by the weight of the head and torso combined with a primarily pelvis based restraint system. This is in contrast to the simulations and experiments of Stemper et al. as seen for example in Figure 5.24, where the discs return to equilibrium after 300ms. The experiments of Stemper et al. are primarily in compression and experience bending only as a results of the natural instability of the lumbar spine. Another notable feature of the volunteer upright sled test simulations is that there is disc extension seen in the L3-L4 and T12-L1 levels due to the first 300ms of gravity settling. The peak angular deflection in L3-L4 is due to gravity settling rather than due to the onset of the pulse, which under flexion corrects the angle back towards equilibrium. This points to a model deficiency when dealing with the lumbar spines of full-scale human body models: defining the point of reference. Humans in the physical world are always under the influence of gravity, so no settling times, or gravitational corrections are required, but for explicit finite element models applying gravity is a known load which must be applied correctly. For the case of an upright volunteer the amount of angular disc deflection due to gravity is comparable to the amount of angular disc deflection seen from a non-injurious pulse. For any future references, gravity must be taken into account and any descriptions of the angular kinematics must be described with references to the steady state angles or positions.

The upright THUMS v5 force response as seen in Figure 6.5 tells largely the same story as the disc angular kinematics. Before 300ms the discs are all loaded into compression, with the most caudal vertebrae experiencing the greatest compressive loads. And then after the onset of the pulse some lumbar levels experience more axial force, followed by a period of unloading, where less axial force is transmitted, and then the peak axial forces are experienced for the L4 and L5 levels, whereas the T12 - L3 levels all experience drop offs in force, with the most cranial vertebrae having the largest drop offs. This is as expected because the more cranial vertebrae experience more bending and therefore less purely compressive forces . Because the upright posture is bending dominant,

axial forces are a poor choice for quantifying the lumbar loading, however as the reclined postures are loaded more axially, and for component and specimen level tests much data exists on the compressive loading of the lumbar spine, axial compression for the lumbar spine was also evaluated.
The THUMS v5 upright posture disc compression also has many features which are the results of bending, as seen in Figure 6.6. The L3.L4 disc for example experiences most of its axial compressive displacement due to the effects of the gravity settling and not due to the applied pulse. T12-L1 and L1-L2 show very little compression due to the gravity preload, but a large compressive peak immediately after the onset of the pulse, followed by an even larger peak where both discs enter the tensile regime as the torso momentum pulls forward.

Reclined Position

The reclined posture has a seat pan which is reclined, in addition to the reclined backrest. The test setup has a leg rest supporting the calves and thighs instead of a footrest. These changes allow different kinematics than in the upright position as the feet can now travel forward freely instead of coming into contact with the footrest. This also means that with no footrest, the loadpath from the footrest through the feet and into the trunk no longer exists. Instead the primary load is transferred from the seat through the buttocks into the trunk, and of course via the belt, but due to the reclined backrest, the angle of attack between the torso (and thus the spine) has been reduced, increased the amount of load that is expected to travel through the torso and the spine. Figure 6.7 shows simulation set up in the initial and most deformed positions. A direct comparison to the experiments of Muehlbauer [77] concerning the kinematics evaluated at a pair of key markers can be seen in Figure 6.9. Here the displacement streamlines for markers at the head, ASIS, and knee have been plotted in red, using the seat base as the coordinate system origin. For the volunteer test, all of the displacements show a horizontal trend, in line with the action of the pulse. The THUMS v5 Model shows no movement at the ASIS, and a radial pattern of the knee and head, where they appear to be rotating about the ASIS in the sagittal plane. These differences are likely the result of the HBM modelling, the belt modelling, and the initial positioning. Human Body Models in general are mostly stiffer than humans [67] [91], which is due to the mathematics of finite elements and the economics of total vehicle crash simulations. This over-stiffness is accounted for by most of the validation load cases for any given HBM. However as most HBM validation load cases are based on the loading seen in a crash scenario, if the applied external loads are scaled down to the level of say a non-injurious volunteer test, then the model over-stiffness can be even further exaggerated. A similar phenomena is also likely occurring in the restraint system for this volunteer test: the safety belt in the volunteer test has some preload that is not quantifiable to the resolution which is needed to accurately define the Finite Element simulation. For example the volunteer always has contact with the belt, and the belt has some preload because of this contact. In LS-Dyna initial contacts and the prestresses therefrom are prohibited, so instead the belt is dynamically loaded during the simulation in order to generate the preload, but this then has dynamic effects. In Figure 6.7 the THUMS head can be seen to have forward motion. But instead of having pure forward motion like the volunteer, the over stiff HBM joints pivot about the over stiff belt causing a more radial motion, The legs can also be seen to be moving forward in the same Figure, but as there is space between the Gluteus Maximus and the seat pan in the initial position, first the legs rotate about the hip joint centers until they come into contact with the seat pan. The volunteer test has contact between the seat pan and the Gluteus Maximus throughout the experimental duration, making this kind of rotation impossible, and thus instead leading to a translational behavior.

Looking more locally at the lumbar spine kinematics, as seen in Figure 6.8 a much different response can be seen as compared with the upright lumbar kinematics, as seen in Figure 6.4. In the upright loadcase, L1-L2, L2-L3, and L3-L4 are all loaded into flexion during the gravity loading phase, with L3-L4 reaching its peak in flexion just after the onset of the pulse, and therefor more due to the gravitational load. The nominal reclined posture shows almost no angular displacements for the first 100ms of gravity loading followed by flexion across all lumbar levels except L2-L3. These differences during the gravity loading phase suggest that the initial reclined position is less stable than the initial upright position, and therefor undergoes a more complex settling process before is can reach equilibrium. The reason behind this instability is most likely the reclined seating configuration itself: for the upright case the HBM as delivered fits nicely into the seat, whereas the HBM must first be positioned into a reclined posture, and even then the fit isn't perfect. Addition gravity settling is needed to smooth out and areas where the HBM is too far away from the seat, and any contacts in the torso will have the knock on effect of changing the angles in the spine.

During the pulse itself the reclined posture sees a slight extension deformations for the T12-L1, L2-L3, and L3-L4, followed by a flexion rebound immediately thereafter. This flexion rebound produces the maximum peak flexion, which occurs at L3-L4. This simulation failed due to instabilities after 500ms so it also appears to be in an equilibrium state. However; the reclined simulation has much less upper body inertia driven behavior than the upright simulation: the reclined simulation torso remains in contact with the backrest throughout the simulation.

The upright load case sees higher levels of flexion then the reclined load case for every lumbar level except for L4-L5, with T12-L1 showing 66.5% more flexion, L1-L2 48.7% more flexion and L3-L4 1.3% more flexion. For the reclined case L2-L3 in extension, and so percent differences provide little elucidation. The higher flexion values point to the global flexion nature of the upright case. The reclined case on the other hand has a much more axial response, which can be seen by comparing the forces responses as seen in Figures 6.10 and 6.5.
In general this shows even at the low rates of loading seen in volunteer test, there is little to be won by comparing reclined seating positions to upright seating positions. It also shows how bending dominates in the upright seating position while axial compression is the dominant load form for the reclined load case.
By comparing the disc deformation from the nominal reclined position as seen in Figure 6.11 with the disc deformations seen in the upright seating position in Figure 6.6, a similar pattern to the force response can be observed. For the upright position the maximum displacements are lower than the reclined position, and the development to the maximum displacement shows more deformation during the gravity loading phase. For the case of the upright position, uniaxial disc deformation poorly described the bending undergone by the discs. In forward flexion the anterior disc compression, while the posterior part of the disc simultaneously goes into tension; when summed these two deformation can nullify one another. For the reclined posture there is less deformation during the gravity loading, as the reclined spine's compressive axis is disaligned with the gravity field, but there are larger deformation due to the pulse, and the more compressive nature of the loading. For both load cases disc displacement were found to be well below 1mm in compression, meaning the discs are far away from the point of being damaged according to Newell et al. [82].

Reclined Position with Lordosis

A more lordotic THUMS v5 posture was also tested in the same reclined setup in order to investigate anthropomorphically specific effects on the lumbar loading. As was discussed in Chapter 5, an axially loaded lumbar spine is an unstable system, one where the initial boundary conditions (in this case the initial position) can have an effect on the kinematic and force response.
By comparing Figures 6.7 and 6.12, the effects of lordosis on the kinematic response can be observed. For the nominal posture, L1-L2 and L3-L4 show the most flexion, and with L2-L3 going into extension. For the more lordotic posture, L1-L2 goes into extension whereas L4-L5 shows the maximum flexion deformation angle. The general angular kinematic trajectories are also different between the nominal and more lordotic reclined models, with the lordotic model showing a movement in extension in T12-L1 and L4-L5 before their respective

peaks in flexion. This is because the higher lumbar lordosis is more stable than the nominal position: when compressed the lordotic configuration remains lordotic, having angular displacements along its boundaries. The nominal position however shows a tendency towards instability in the form of a buckling type movement about L2 in flexion. This is not full buckling, but it is also not as stable as the lordotic configuration
Look at the force response for the lordotic reclined posture as seen in Figure 6.13, one can see that the force curves show more of a spread than for the nominal posture at the onset of the pulse at t=300ms, with the T12 force even going slightly into tension. The peak forces for the lordotic posture however are more tightly aligned showing a delta of 88N between the max L2 and min T12, as compared with a delta of 125N for the nominal posture with the max being at L4 and the min at T12.
The disc displacements for the reclined posture with more lordosis as seen in Figure 6.14 show the same general pattern seen in the nominal reclined position, with very little deformation due to the gravity loading phase followed by smooth consistent compressive deformation after the onset of the pulse. Where the nominal case showed the highest deformations caudally, and the smallest deformations cranially, the lordotic posture has no clear trend, with both T12-L1 and L3-L4 having large displacements. The largest displacements for the lordotic load case are still 0.1mm smaller than the largest deformations observed in the nominal case. The reason for this different peak deformations across the lumbar level is due to the lumbar lordosis. For the relatively straight nominal spine, the more caudal discs are being compressed for a longer time than the more cranial discs, and must also support the weight above them. Both of these mechanisms still hold for the lordotic posture, but the spinal curvature deforms less, likely leveraging the posterior elements to transmit the force instead of needing the discs to act as the load path, and in the process deform themselves.

Reclined Position with Kyphosis

By comparing Figures 6.7 and 6.15 the kinematics differences resulting from a more kyphotic posture can be seen. The kyphotic posture sees the angular kinematics of L2-L3 and L3-L4 have a relatively constant increase in flexion until they reach their peak values. This is in contrast to the nominal and lordotic positions which have more plateau-like responses before reaching peak values in both flexion and extension. The kyphotic case has no lumbar levels which deform globally in extension. The kyphotic model shows the same unstable tendency as the nominal posture, but is exacerbated due to having even less lumbar lordosis.
From the force response for the more kyphotic posture in Figure 6.16, a delta of 114N is observed between the maximum at T12 and the minimum at L5.

Whereas the nominal posture and the have relatively normal distributions of the peak force spread across the lumbar levels, the kyphotic posture has a double peak, with the second highest force occurring at L4. The kyphotic posture also has the highest peak, at 1.2kN, whereas the lowest peak lumbar force can be seen in the nominal position, landing at 1.01 kN. All three positions show very similar bell-curve loading across all lumbar levels, and due to this similarity force data alone is not sufficient to differentiate individual kinematics. For the case of volunteer experiments it follows that load cell measurements at the seat pan and foot rest also cannot provide meaningful correlations to kinematic data.
The disc deformations for the more kyphotic posture, as seen in Figure 6.17 show maximum displacements in line with what was observed for the nominal reclined posture (i.e. noninjurious) with a similar pulse dominant response. The distribution of the maximum displacement across the lumbar discs shows a different pattern to both the nominal position as well as to the more lumbar posture. The kyphotic posture shows a maximum for the L2-L3 disc, which is also where the lowest forces were measured. This supports the theory that with the posterior elements as the primary load paths, higher forces in general are transmitted, while at the same time causing less disc deformation. This means that for injury prediction both force and displacement must be taken into account, as both quantities have an inverse relationship for certain spinal postures.

Chapter 7

Use Case: Effects of Initial Spinal Posture on Response

7.1 Introduction

With the advent of more and more autonomous functionality in production vehicles, studies have shown that customers expect to be able sit in seating positions that are very different to what is offered in today's vehicles [65][88]. In order to provide these kinds of seating configurations, first conceptual research and development must investigate their feasibility. A first investigation into these types of seating configurations at BMW was performed by Huf et al. [57]. An example of how these types of hardware tests differ from a traditional seating position can be seen in Figure 7.1. Hardware tests are performed using Athromopomorphic Test Devices (ATDs), which are more commonly known as crash test dummies. The two most prevalent ATDs for use in frontal crash scenarios are the Hybrid 3 50th Percentile male dummy (H350) [45], and the Test device for Human Occupant Restraint (THOR) [50].

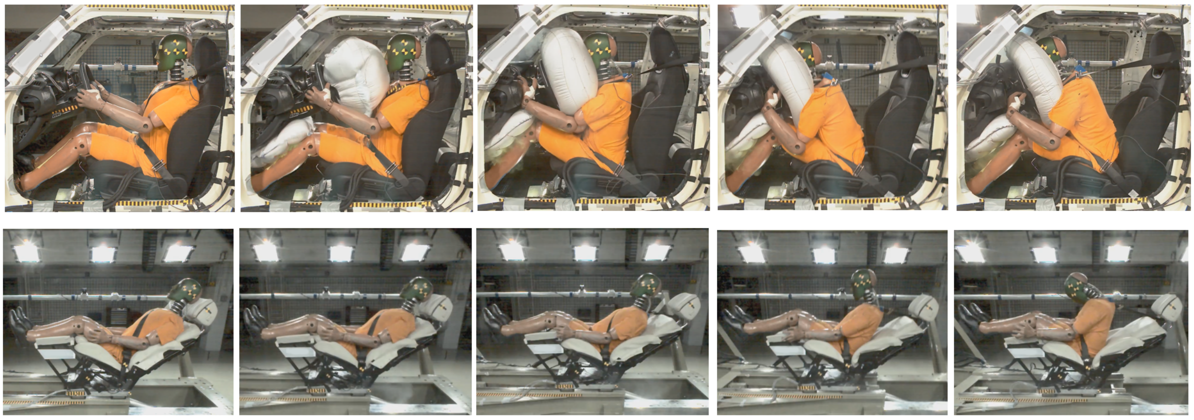

Figure 7.1: A comparison of a sled test performed for a standard seating position, top, and for a proposed reclined seating position, bottom [57].

In that study a prototype reclined seat was developed and then tested with various ATDs. A later study [35] then continued these investigations by comparing the ATD response to the response of a HBM, which found the HBM to be much more flexible than the ATD, as seen in Figure 7.2.

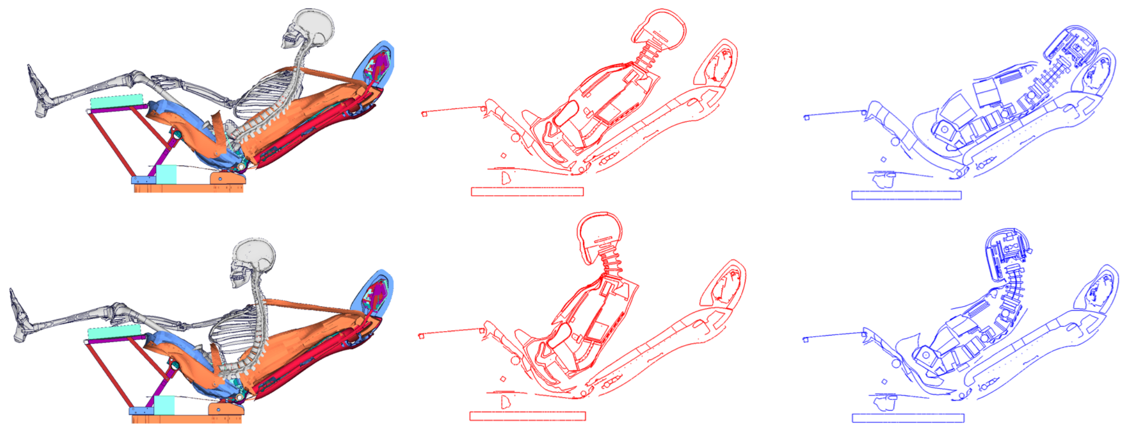

Figure 7.2: A comparison of HBM response vs. ATD response in a reclined seating environment under a frontal loading condition. The red ATD is a H350 dummy, and the blue is a THOR 50th percentile male dummy.

Part of this study looked at a HBM positioned similarly to an H350 dummy as compared to an HBM positioned like an actual occupant, as measured by scanning a volunteer, which can be seen in Figure 7.3 [35].

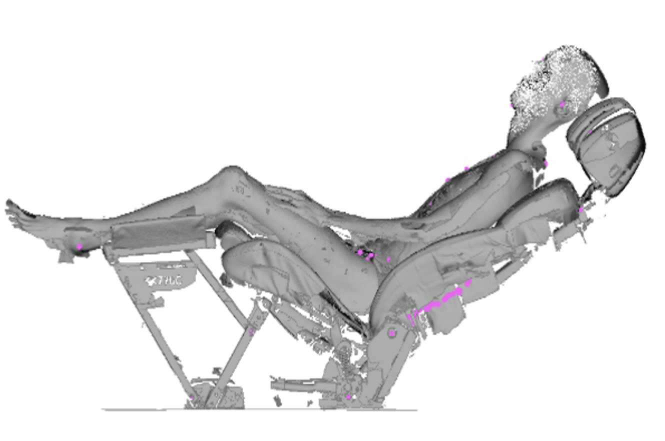

Figure 7.3: The scan of a volunteer with the same anthropometry as a H350 ATD was used to position the HBM into a more realistic seating position [35]

The position based on the H350 ATD and the position based on the volunteer had different global positions, the H350 head for example does not touch the headrest. From the volunteer scan however it is not clear how the spine is positioned, as only external markers can be measured and this was not enough to give an unambiguous spinal position. Because of this discrepancy, a third source of data was used to achieved an empirically measured lumbar spine position. This third source of data was in the form of open MRI scans of an individual in a reclined position. An image of the spinal cross section obtained from the MRI can be seen in Figure 7.4.

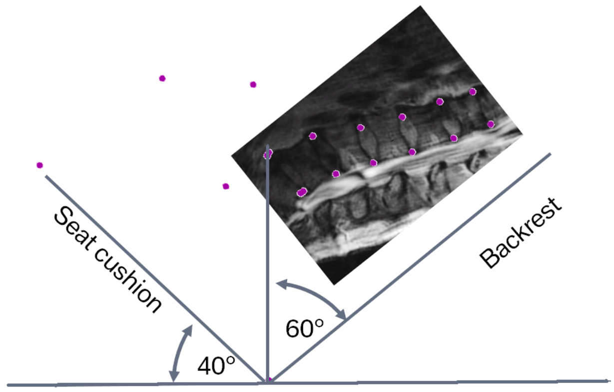

Figure 7.4: The MRI scan of a volunteer with the same anthropometry as a H350 ATD was used to position the HBM spine into a more realistic position.

The final volunteer and MRI based position as compared to the H350 based position can be seen in Figure 7.5.

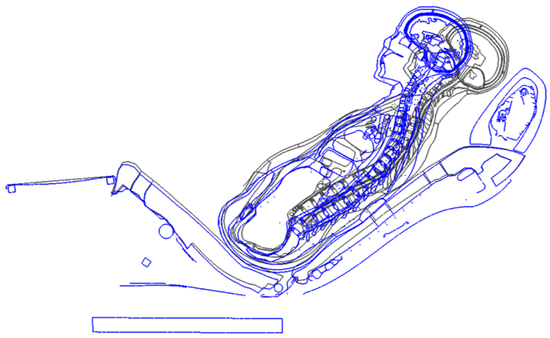

Figure 7.5: Geometry comparison of the positions investigated by the preliminary study. Each curve represents the axial force measured at a lumbar vertebra. The blue model has the H350-like position, and the gray model has the volunteer-like position.

After simulating these positions a difference was noted between their peak force responses. These force curves can be seen in Figure 7.6. These differences were the motivation to perform a sensitivity study to find if the influence of initial spinal posture on the spinal kinematics and spinal force response.

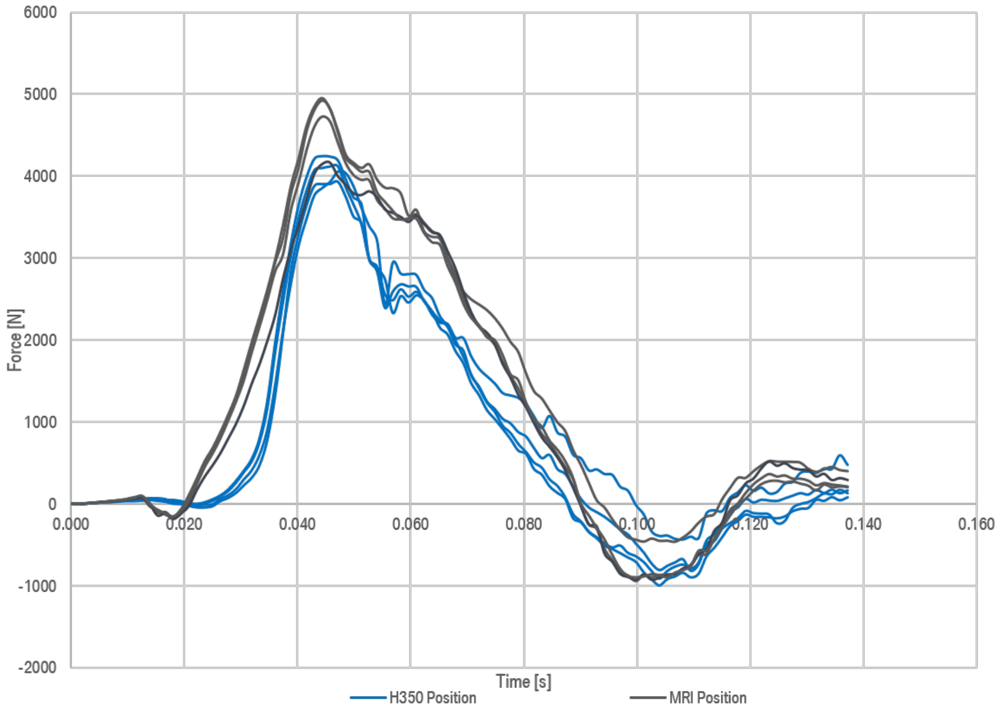

Figure 7.6: Axial force comparison of the positions investigated by the preliminary study. The blue curves are from the H350-like position, and the gray curves are from the volunteer-like position.

7.2 Methods

Positioning of the Lumbar Spine

A sensitivity study was constructed in order to investigate the influence of spinal posture on the kinematic and force response. As a baseline the THUMS v5 HBM positioned according to the volunteer studies was chosen. This was because the H350 position seemed quite unrealistic, especially in how its head was positioned away from the headrest. Also as the volunteer position had a spinal position which was derived from an MRI, it should also be seen as more accurate than the H350 position, whose spinal position came from reclining the spine from an initial occupant position. The positioning method to achieve the more lordotic and kyphotic postures is described in Chapter 5.2. How the various postures look in the context of the full scale HBM simulations, can be seen in Figure 7.7.

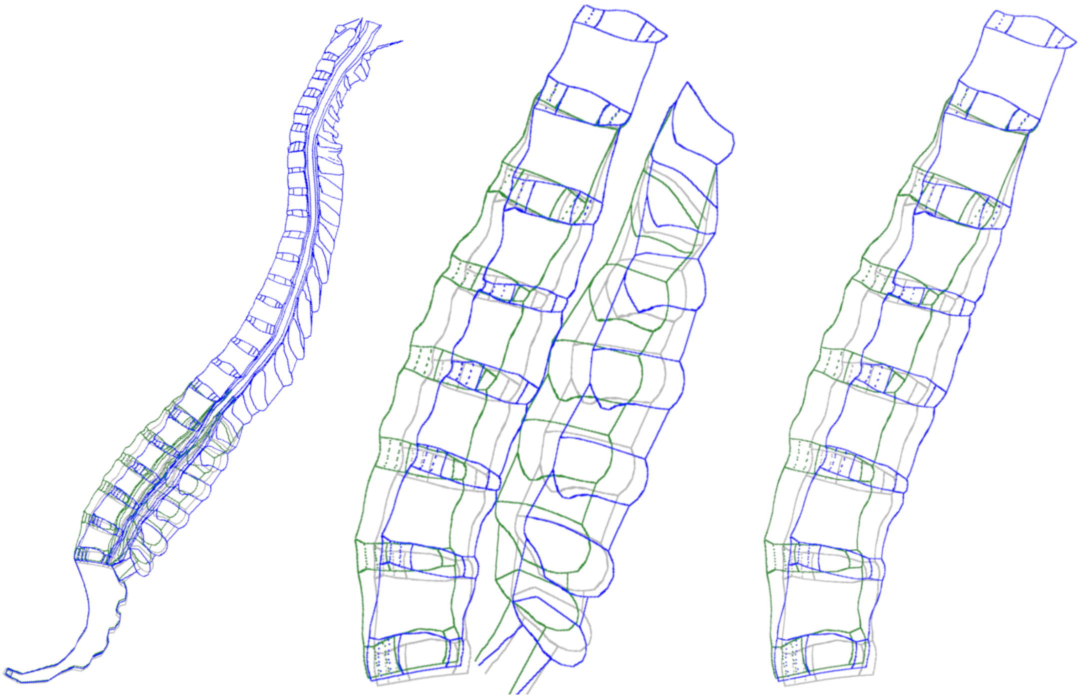

Figure 7.7: A comparison of the spinal position for the different postures for the full scale simulations; gray is the baseline, green with more lordosis, and blue with more kyphosis

Investigation into the global behavior of the positioned spines using a sled test setup

The full scale simulations were carried out in the form of sled test simulations. These sled tests were chosen as they match hardware sled tests were performed using ATDs, and also subsequently to validate the seat model [57]. The baseline model was seated and belted first. As both the lordotic and kyphotic models have the same outer geometry as the baseline model, they were able to be brought into the simulations directly without the need for further seating procedures. For the lordotic model a small change in the belt routing was needed, so a re-belting step was performed. The seated and belted occupant models were then all loaded with the same pulse, namely a USNCAP full frontal pulse. This pulse comes from a production vehicle undergoing an impact with a velocity of 56kph and impacting a rigid barrier. The simulations were also ran with a seat based load limiter, which allowed translation between the seat and the sled undergoing the pulse. A more detailed description of the system can be found in [57]. As this prototype reclined seating position is different to what is currently offered in production vehicles, a small summary of the reclined seat geometry is presented in Table 7.1

	Standard	Reclined
Seat Back Angle	52°	49°
Seat Pan Angle	11°	23°
Lower Leg Angle	34°	8°
Foot Position	Floor	Leg Rest
Integrated Seatbelt	No	Yes

Table 7.1: Differences between standard seat and reclined geometries. These angles can be seen in the hardware experiments shown in Figure 7.1

7.3 Results

Results for the Nominal Reclined Position

For the highspeed reclined seating pulse, in the nominal position as seen in Figure 7.8, the kinematics can be characterized by an initial extension between T12 and L1, followed by flexion across all lumbar levels.

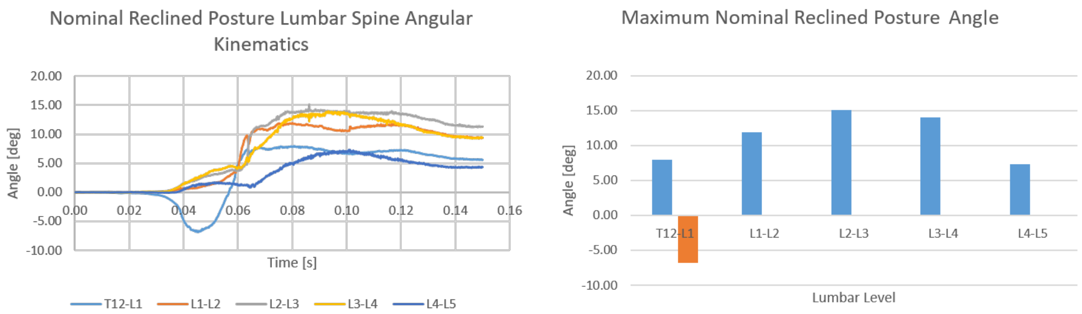

Figure 7.8: Lumbar kinematics results from the nominal reclined posture in the high speed test case. Positive angles represent flexion, negative angles represent extension.

The force response for the nominal posture can be seen in Figure 7.9. Here one can observe a very synchronized peak force in both the cranial extreme of T12 and the caudal extreme of L5.

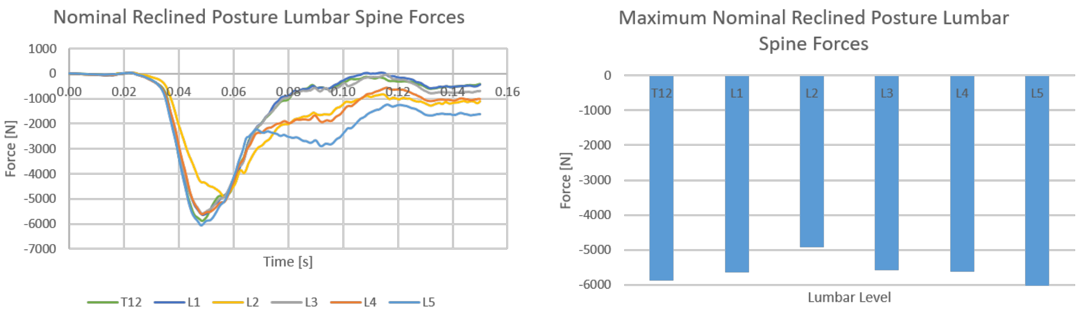

Figure 7.9: Lumbar force response results from the nominal reclined posture in the high speed test case. Positive force represent tension, negative forces represent compression.

The IVD axial displacements for the nominal reclined posture, as seen in Figure 7.10, shows the earliest peak compression of all three postures at 50ms.

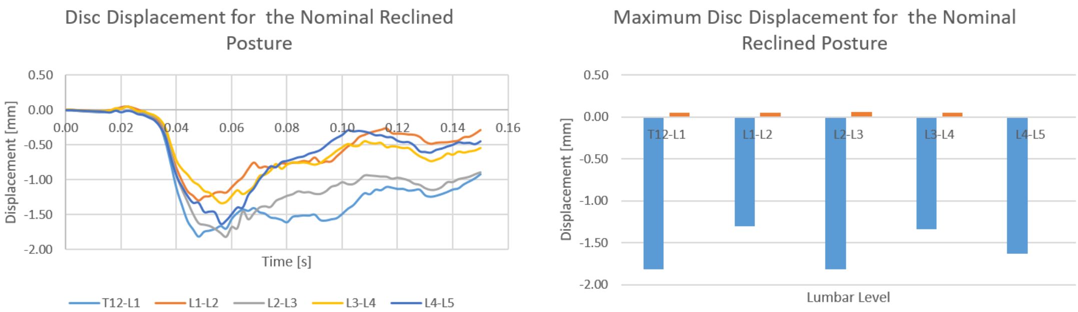

Figure 7.10: Lumbar disc displacement results from the nominal reclined posture in the high speed test case. Positive displacements represent tension, negative displacements represent compression.

Results for the more Lordotic Position

The lordodic posture kinematics, as seen in Figure 7.11, track a similar trajectory of an initial T12-L1 extension alignment followed by flexion across all lumbar levels.

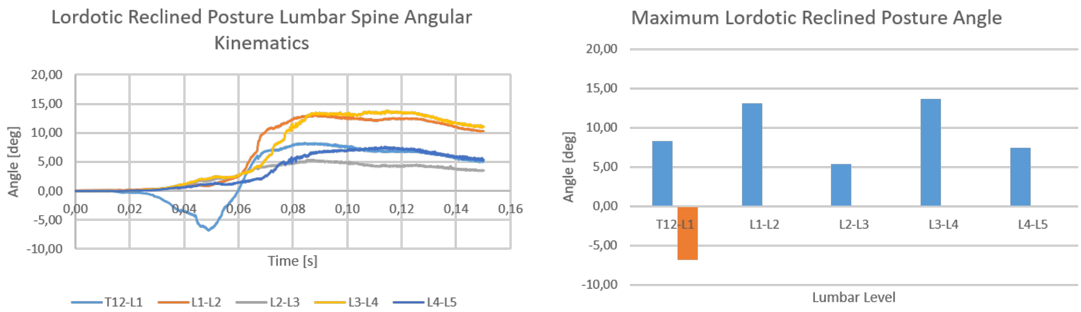

Figure 7.11: Lumbar kinematics results from the more lordotic reclined posture in the high speed test case. Positive angles represent flexion, negative angles represent extension

The force response for the nominal posture can be seen in Figure 7.12. Here one can observe a similar trend to the baseline reclined posture in the form of synchronized peak forces between T12 and L5, but at a lower magnitude when compared to the baseline posture.

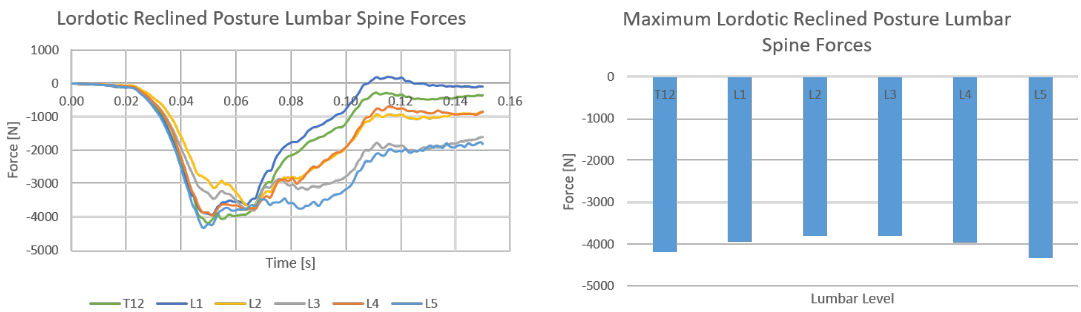

Figure 7.12: Lumbar force response results from the more lordotic reclined posture in the high speed test case. Positive force represent tension, negative forces represent compression.

The axial IVD displacements for the more lordotic posture reaches its peak IVD axial compression the slowest of all the posture at 90ms, but it sees the overall highest compression of 2.12mm at T12-L1, as seen Figure 7.13.

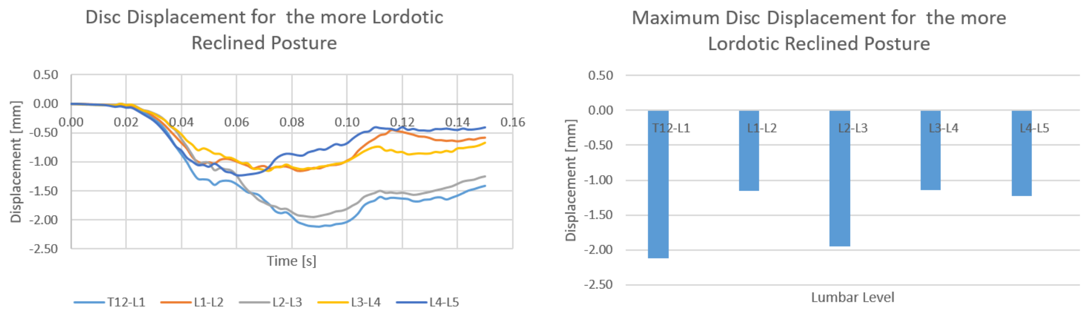

Figure 7.13: Lumbar disc displacement results from the more lordotic reclined posture in the high speed test case. Positive displacements represent tension, negative displacements represent compression.

Results for the more Kyphotic Position

The kinematics of the more kyphotic posture for the high speed pulse as seen in Figure 7.14, differ from the kinematics of the other two postures: in the initial extension set-up has lower peak bending of -3.32°as compared with -6.81°for the nominal posture and -6.78°for the more lordotic posture.

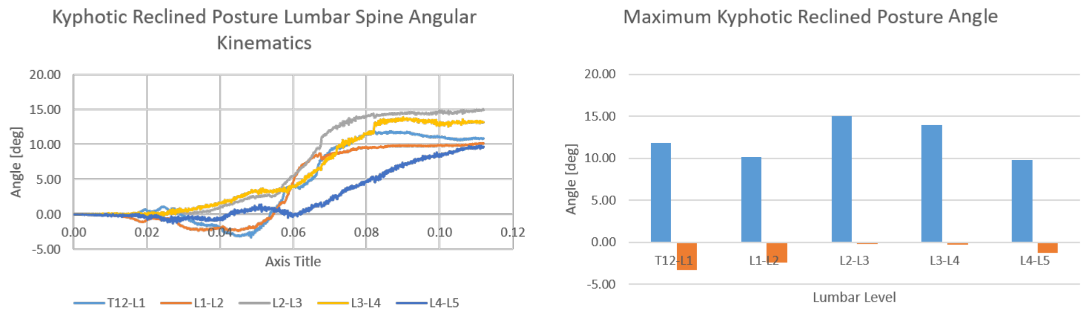

Figure 7.14: Lumbar kinematics results from the more kyphotic reclined posture in the high speed test case. Positive angles represent flexion, negative angles represent extension

The force response for the nominal posture can be seen in Figure 7.15. Here one can observe a synchronous first peak for all of the lumbar vertebrae, followed by a second peak some 15ms later in L2, L4, and L5. The second peak is much less pronounced for T12, L1 and L3. The force magnitudes of the kyphotic posture are greater than the lordotic posture, but less than those obtained in the baseline reclined posture.

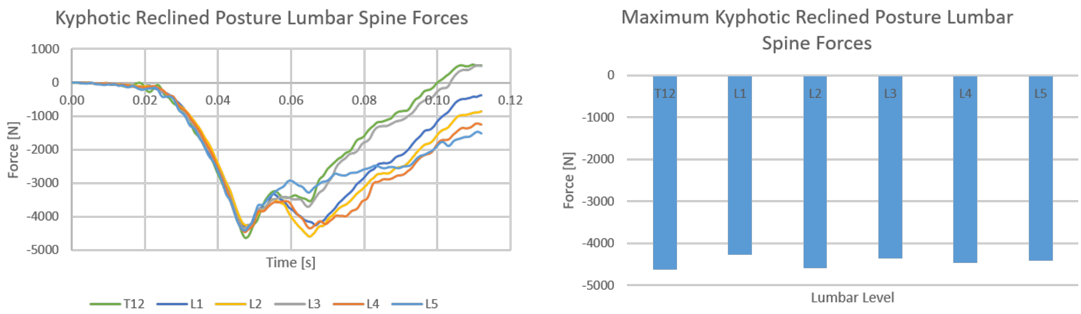

Figure 7.15: Lumbar force response results from the more kyphotic reclined posture in the high speed test case. Positive force represent tension, negative forces represent compression.

The axial IVD displacements of the more kyphotic posture as seen in Figure 7.16, experiences a double peak at some lumbar levels in a similar manner to how the force response for this posture developed, with the first peak occurring at 50ms, as in the nominal posture, and the second peak at 90ms, as in the more lordotic posture.

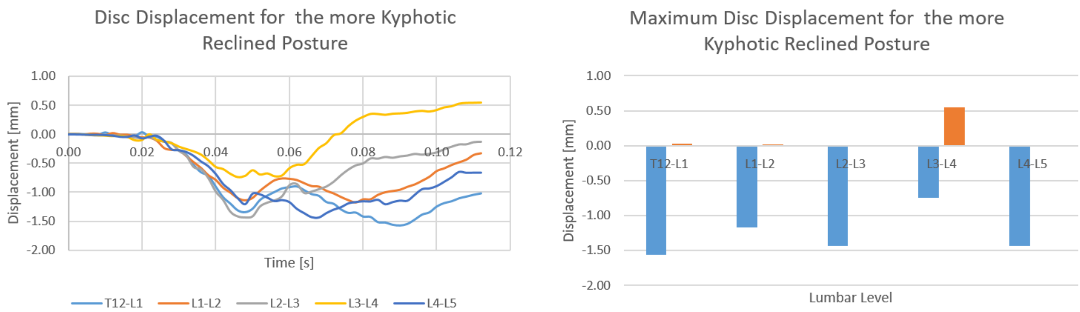

Figure 7.16: Lumbar disc displacement results from the more kyphotic reclined posture in the high speed test case. Positive displacements represent tension, negative displacements represent compression.

The global kinematics of all three postures can be seen in Figure 7.17. When all three posture are overlaid in this manner only small differences can be observed to the order of millimeters at the model extremities.

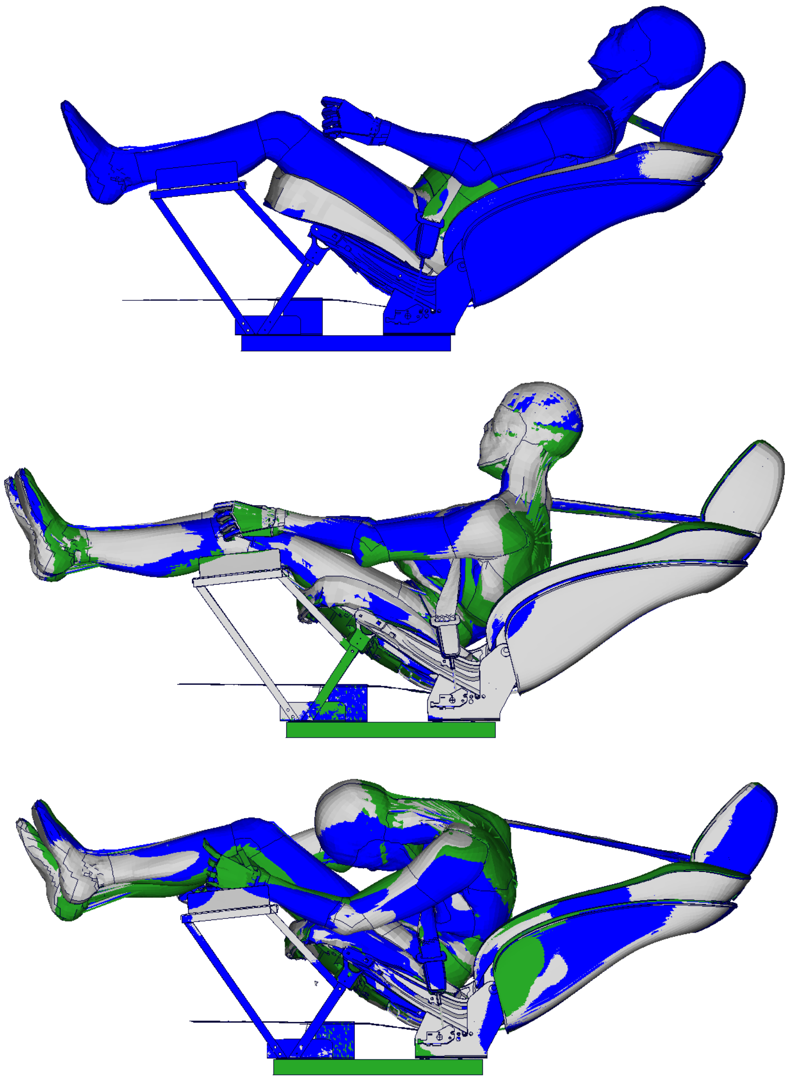

Figure 7.17: Kinematic sensitivities for the various lumbar spine postures which were investigated: gray is the baseline, green with more lordosis, and blue with more kyphosis

7.4 Discussion

7.4.1 High Speed Pulse Kinematic Comparison

Nominal Reclined Posture

For the highspeed reclined seating pulse, in the nominal position as seen in Figure 7.8, the kinematics can be characterized by an initial extension between T12 and L1, followed by flexion across all lumbar levels. The timing of the initial extension occurs just after 40ms, and the largest extension angular displacements are observed between L2 and L3, squarely in the middle of the lumbar column. The T12-L1 IVD is the only disc to go into extension in this posture, and observed extension peak is followed by a swift transition into flexion, where it then plateaus at an angle of 8°. The abruptness of the start of the plateau suggests that the intraspinous ligament and or the supraspinous ligament may be limiting the T12-L1 motion in flexion. The maximum angles in flexion follow a Gauss distribution in both the amount of bending and the lumbar level at which the bending occurs, centered about the maximum angle of 15.11° observed at L2-L3.

Lordotic Posture

The lordodic posture kinematics, as seen in Figure 7.11, track a similar trajectory of an initial T12-L1 extension alignment followed by flexion across all lumbar levels. The initial T12-L1 extension has a sharper peak for the lordotic posture, and it occurs 10ms later than that of the nominal posture. Looking at Figure 7.7, one can see that the lordotic posture has slightly more initial flexion at between T12 and L1, which means it has slightly further to travel in extension before it reaches the equivalent point of maximum extension as defined by the nominal posture. The plateau seen in the T12-L1 angle is also present in this posture configuration. The more lordotic posture also experiences the least amount of peak flexion in the L2-L3 IVD, as opposed to the maximum flexion in the nominal posture. Whereas the nominal posture pivots about L2-L3, cause large deformations, the Lordotic posture is more stable throughout the lumbar region and due to this stability experiences less angular deformation than the nominal case does. The maximum flexion angles for the case with more lordosis do not fit a Gauss distribution, but rather is two humped in nature. This is because the maximum flexion angle in the nominal posture occurred at L2-L3, whereas for the lordotic posture the least amount of flexion bending is observed at L2-L3 due to the increased stability of this posture.

Kyphotic Reclined Posture

The kinematics of the more kyphotic posture for the high speed pulse as seen in Figure 7.14, differ from the other two postures in the initial extension set-up has lower peak of -3.32° as compared with -6.81° for the nominal posture and -6.78° for the more lordotic posture. Additionally the kyphotic posture also sees an initial extension deformation in the L1-L2 disc, which was not observed for the other postures. The kyphotic posture has more initial extension at the T12-L1 level , and the L1-L2 is more posterior in the kyphotic posture, which means is also lower relative to the seat. The initial extension means the kyphotic posture does not have to deform so far in extension to reach the maximum extension deflection, which explains the lower relative angle of the the extension peak in T12-L1. Because L1-L2 is aligned with T12-L1, the extension is transferred across multiple levels. This maximum extension is not characterized by contact between the posterior elements but rather some sort of disc load sharing equilibrium. The extension is only present until sufficient compressive load can be developed to then transition the spine into the forward flexion, which in turn needs sufficient energy to deform the discs in flexion. The more kyphotic posture does not see the highest flexion angles, but it has the highest flexion across all lumbar levels, with each displaying a maximum flexion of over 10°. The T12-L1 plateau at 8° for the nominal and lordotic postures has now shifted to 12°. This can be explained by the increased level of initial extension in the kyphotic posture when compared with the nominal and more lordotic postures: the kyphotic posture can thus flex more for a given length of maximum ligament deformation before the range of motion is arrested. Because of these high flexion angles across all lumbar levels, the kyphotic posture does has a near constant maximum force distribution.

All three postures see maximum disc angles of 15° or more for this particular load case. Adams et al. [3] reported the limit of flexion as being 14.8° for their quasi-static experiments, so it is unclear if at the higher strain rates applied in this simulation study if comparable damage would be expected to the supraspinous and intraspinous ligaments as was observed by Adams et al. In addition to the plateaus seen at the T12-L1 level after the transition from extension to flexion for every posture, all of the other levels also experience plateau-like behavior after reaching their respective peaks in flexion. The angular magnitude at which each of these plateaus occurs differs according to the posture. The maximum range of motion in flexion as limited by the supraspinous and intraspinous ligaments is due to increasing reaction forces in the ligaments generated by increasing elongations. Eventually the force becomes large enough to prevent further flexion, even though the momentum of the upper body is still trying to flex the lumbar spine. The differences come from the initial state, or by giving a limit on how much the ligaments can than elongate. But because the elongation is linear and the movement is rotation, the point of rotation, as well as the length of the posterior elements forming the lever arm via which the movement functions both play a role. For these reasons it is important to model the discs as solids so that the center of rotation can wander as it does in vivo [28, 7].

7.4.2 High Speed Pulse Kinematic Comparison to Low Speed

For all of the low speed postures, the gravity settling has an effect on the initial posture (the posture not when the simulation begins, but when the pulse loading phase begins). In general when compared with the high speed load scenario, all of the low speed postures have more kyphotic pelvic tilt, which leads to a more horizontally oriented spine than the corresponding posture in the high speed case. The initial high speed postures, and the pre-gravity loading low speed postures were positioned based upon scans of a volunteer in a reclined seating position [35]. However these scans were performed using rigid foam blocks, and only approximate the posture of an occupant in a potential production seat with the option of reclining to this level. The influence for example of lumbar support bolsters has not been investigated, and may be an effective way of controlling the initial posture and therefor the lumbar kinematics, however this is an area for future research.

The high speed pulse decelerated from a velocity of 56kph whereas the volunteer pulse decelerated from a velocity of 7.2 kph. The deceleration distance for the high speed pulse is around 40g as opposed to 3g for the volunteer pulse; in short, the high speed load condition is much more energy intensive than the low speed test case. This can be seen in by comparing both the kinematics and the force responses between the low speed and the high speed cases. The maximum bending angle seen for the low speed cases was 3.4°, occurring at L2-L3 of the more Kyphotic posture, but for the high speed case, a maximum flexion of 15.1° was observed in the nominal reclined posture. This difference reflects the scale of how much more energy is in the high speed pulse. To the degree at which these energies may become injurious is also a wide open field where more research is required.

The development of the kinematic curves is also different: for the high speed cases all of the postures go into flexion bending, with the differences being in the timing and amount of flexion experienced. For the low speed cases however some lumbar levels go into extension, and each of the three postures exhibits its own distinguishable behavior, unique from the other two postures. This could be due

to robustness factor at low end of the scale. Because the applied forces are not large enough to consistently bring low speed postures into flexion as is seen in the high speed cases. Sometimes the spinal models compress fully axially, or even experience local extension. Another reason for the differences in kinematics could be due to noise in the model. For example: a difference of 0.5° of flexion for the low speed would be 15% of the maximum angular response, whereas for the highspeed cases the same change of angle would account for less than 3% of the maximum. In this way for the low speed cases the signal to noise ratio might be influencing the results.
Additionally the plateau behavior seen for the high speed cases is not present in the low speed cases, suggesting that the flexion seen in the low speed cases is more due to the unstable nature of the spine under axial load than due to the global flexion driven by upper body inertia as seen in the high speed cases.

7.4.3 High Speed Pulse Force Comparison

Nominal Reclined Posture

For the nominal posture all of the lumbar levels reach their peak force in a synchronized fashion, with a smooth up to the peak, followed by a trailing off which varies by lumbar level. The exception of the L2 level, which reaches its peak as all of the other levels are already trailing off. The L2 force ramp up also a small step before its peak, suggesting some kind of alignment or motion before the vertebra becomes able to bear force again. As the L2-L3 level showed the highest angle of flexion for the nominal load case, but the L1-L2 level had 3° less angle, this difference could mean that the L2 vertebral body is taking more shear and moment loading than axial loading, but this is not the case for L4, which has an even larger angular delta of 6°. The peak in force for the L2 level corresponds to a kink in the kinematic curve for L1-L2 reaching its plateau and L2-L3 increasing its flexion at an increasing rate. This difference in the rate of angular loading could also be the energy sink that causes the axial force to be lower. The general distribution of the force has the minimum force in the center of the lumbar spine at L2 with the maximum towards the extremities of T12 and L5. This distribution is roughly Gaussian but not so smooth.

Lordotic Reclined Posture

The lordotic force response shows a less synchronous initial increase in the axial forces then the nominal reclined posture: both the L2 and L3 vertebrae take longer to reach the peak, and both have the step before the peak seen in L2 for the nominal posture. For the more lordotic posture the L3 and L5 levels also show less tailing off, with more of a prolonged plateau before returning to lower force levels. This could be that the flexion causes the lordotic posture to become more axially aligned, and thus more suited to bearing axial loads, at a later time point than the nominal posture. And even though the plateaus seen for the lordotic posture means it has to bear peak forces over longer time spans, the peaks are themselves lower, with a peak of 4332N in compression for the lordotic case compared with a peak of 6052N in compression for the nominal posture.

Kyphotic Reclined Posture

The more kyphotic posture shows the most synchronous build up to the force peak with all levels reaching their peaks at the same time, while following the same increasing slope. The kyphotic posture is however the only posture to exhibit a double peak behavior, with a second peak showing starkly at the L1 L2 and L4 levels, and with a less pronounced peak in T12 and L3, and with a step or plateau for L5, all of which occur at the same time. This second peak could be due to a sort of snap through effect seen in the transition from extension into flexion as seen in the angular kinematics. The first peak occurs when the lumbar spine is in extension, and the peak diminishes while the spine flexes into the next stable position where it can again bear axial load, after which further flexion causes a consistent decrease in force. The more kyphotic posture is the most axial initially, as seen in Figure 7.7. As the most axial, it should also have the highest propensity to exhibit instabilities under axial load. For the case observed here the initial instability goes into extension at T12-L1 and L1-L2. The peak forces for the kyphotic load case are somewhere between those of the nominal and more lordotic case, with maximum forces in compression of 4629N.

7.4.4 High Speed Pulse Force Comparison to Low Speed

The lumbar spine being a multi-jointed system likely has a stable configuration in which it can bear loads the most efficiently. This position will of course depend on the individual anatomy and tissue properties of the lumbar spine but also on other factors such as posture preferences, muscle strength and attachment locations, and ligament elasticity. For both the low and the high speed cases, more stable configurations of the lumbar spine were reached, as can be seen as steady increases in the loading without associated kinematic movement, but these stable configurations were transiently passed through. As the models were run with no failure, it could be the case that the force kinematic relationships are not conservative enough, but not enough validation data is readily available to being to predict lumbar fracture in all of its various modes for the strain rates seen in automotive crash applications. For the low speed cases, no injuries were observed in the volunteers for the same setup and pulse, and therefore the levels of force seen in the HBM simulations can be assumed to be non-injurious. For the case of the highspeed simulations, no data exist with which to judge if these levels of loading are injurious or not. But seeing as how each posture under the same loading displays a unique force response, in both the peak force and the force development curve, the more interesting question is how can this type of loading be evaluated as injurious or non-injurious in the future.

7.4.5 High Speed Pulse Disc Displacement Comparison

For the high speed pulse load case the disc displacement can provide additional insights when combined with the kinematic and force data. The axial disc displacement should be related to the axial forces, higher forces generate larger axial displacements, but there is also a time needed for the force to be transferred into a displacement. The angular kinematics have a less straightforward relationship with the axial displacements. A compressed IVD should be harder to bend than an uncompressed disc, but energy used to compress the IVD might instead cause deformations in shear and bending, and thus not be available for axial deformations.

Nominal Reclined Posture

The IVD axial displacements for the nominal reclined posture, as seen in Figure 7.10, shows the earliest peak compression of all three postures at 50ms. This peak also has the steepest increase in compression, with a peak strain rate of 9.23s^{-1}. The first peak is not entirely consistent temporally across all lumbar levels with T12-L1 and L2-L3 compressing 10ms earlier than the more caudal levels. This goes contrary to what might have been expected as the more caudal levels are closer to the seat pan applying the loads; however the force response does not differ between more caudal and more cranial levels. After the peak T12-L1 remains compressed in a compression plateau while L2-L3 shows levels of relaxation at 60-70% of its peak values, with all other lumbar levels returning to under 0.8mm of compression.

Lordotic Reclined Posture

The axial IVD displacements for the more lordotic posture reaches its peak IVD axial compression the slowest of all the posture at 90ms, but it sees the overall highest compression of 2.12mm at T12-L1, see Figure 7.13. The longer time of loading might explain this behavior as the T12 vertebra experienced a force plateau in the lordotic posture, where the force was applied at a high level from

50-90ms. This high level reached more slowly than the other postures yields a strain rate of $3.65s^{-1}$.

Kyphotic Reclined Posture

The axial IVD displacements of the more kyphotic posture as seen in Figure 7.16, experiences a double peak at some lumbar levels in a similar manner to how the force response for this posture developed, with the first peak occurring at 50ms, as in the nominal posture, and the second peak at 90ms, as in the more lordotic posture. The L3-L4 disc goes into tensile displacement at 70ms and is the only lumbar to do so across all three postures. This may be due to how the axial displacements are measured. By only measure at the midpoints of the endplates, large amounts of being can be construed to look like tension. This is indeed the case at L3-L4, with the bending being caused by the buckling like instability about L3. The kyphotic case has the lowest peak axial compression displacements, with the highest being T12-L1 compressive displacement of 1.57mm. The peak strain rate of $6.35s^{-1}$ is seen in L2-L3 leading up to the first peak. All three postures show the highest axial displacements at T12-L1 and L2-L3, with L4-L5 following and L1-L2 and L3-L4 showing the lowest displacements. The T12-L1 peak displacement occurs as a result of the global transition from the axial loading of the lumbar spine to the forward pitching caused by the restrained pelvis. The torso coming forward rotates about T12, which already being compressed from the axial loading leads to even further compression. That L2-L3 experiences high levels of compression appears to be because it is the most stable joint in the middle of the lumbar spine for the longest. There is always flexion seen at the L2-L3 joint but it always occurs after or concurrently to the peak compression. The simplification of only using a single datum for the compression also means that this flexion could be contributing to the amount of compression observed in the plots.

7.4.6 High Speed Pulse Disc Displacement Comparison to Low Speed

The most striking difference to the disc displacements observed in the volunteer low speed loading as compared to the high speed loading is the increased amount of axial compression seen in the loading, with the high speed simulations showing more than 280% higher displacements than the low speed. Another noticeable difference is in the variation in the development of the displacement curves observed in the high speed simulation, absent in the low speed simulations. This parallels what was seen for the force response, with the low speed simulations being tightly clustered together whereas the high speed simulations show a wider spread in their response across the postures investigated. This suggests that the levels of loading seen in the high speed simulations have crossed a robustness threshold for lumbar spine stability which the low speed simulations are still below. It is unclear if this threshold is deformation based, force based, or perhaps rate based. Further studies will also have to be undertaken to see if what was observed in the simulations also occurs in human subjects. This could also mean that certain spinal postures are more stable than others. This would have an effect on injury outcomes, as the stability effects the kinematics, and in turn the force response. As their is currently very limited data available to evaluate spinal injury due to buckling, more research is needed, especially as it concerns to kinematic correlations and timing of lumbar injuries.

Conclusions

With the instability observed in the high energy full body simulation, as well as in the simulations of the experiments of Stemper et al., numerous questions arise for which there are currently no answers. What are the kinematic behaviors that lead to lumbar spine injury? Can kinematics be globally controlled, or are they subject specific? How prevalent will lumbar spine injuries be in the field, and how severe? The purpose of this thesis is to leverage human body modelling in order to help make alternative seating positions as safe as possible. The lack of experimental data with which to correlate the HBM simulations makes this task very challenging. Less force and lower accelerations correlate with lower incidence of injury, but there is currently no accepted way to measure injury in the lumbar spine, let alone a metric at which an acceptable level of safety can be defined. In the experiments of Richardson et al. [100] for example, the primary restraint mechanism in use was the lap belt, which led to pelvic fractures in some of the specimens. With lower hip belt forces, submarining may have occurred. If one were to grade a submarining event as compared with an event with a pelvic fracture on the AIS scale, the submarining would most likely be graded as more injurious, as there is a likelihood of internal organ injury and bleeding, plus associated rib fractures. But of course the AIS outcome always depends on the exact individual. The BMW restraint system investigated in this chapter uses the seat pan as the primary mechanism of restraint [57], which is conceptually very different to, and with a very different physiological loading from the experiments of Richardson et al. The differences make comparisons very difficult. Each type of system has its own advantages and disadvantages, but evaluating which is safer is outside the scope of this thesis, and impossible without further experiments, none of which are planned to the author's knowledge. Additionally the spinal kinematics will be influenced by the spinal musculature, as well as internal organ pressure and contact. These influences will be difficult to elucidate using PMHS experiments, and any comparative evaluations made using HBM simulation studies will currently have a limited validation basis.

Potential Injury Risk Assessment Two common models to map injury levels from force and force-related outputs are the Head Injury Criteria (HIC) [116], which predicts head injuries, and the Nij criteria which predicts cervical spine injuries [41]. Lumbar injury criteria analogous to both HIC and Nij could be developed to predict lumbar injury. Using something like the HIC considers not only the peak accelerations reached, but also the timing associated with the accelerations, with higher accelerations over longer times being more injurious. It may be that for the case of the lumbar spine the axial force could be used as the proxy measured input, and the time development of this input force could then provide a prediction of the likelihood of injury. The Nij predicts neck injuries based on peak forces in compression and tension combined with peak moments in flexion and extension (which in turn are calculated from anterio-posterior shear forces). The same approach could be calibrated for the lumbar spine which has a comparable structure as the cervical spine. The advantage to a HIC like approach would be the simplicity of measuring the proxy force in any number of seating configurations, with the major disadvantage being that it neglects the influence of the posture on the kinematics, as well as any bending or shear related injury mechanisms. An Nij-like approach would be able to directly applied to the lumbar spine, with the same weaknesses that the approach has in the cervical spine: the validation data used to develop it are not transient. Transient experimental data is needed to identify if the order of loading (say extension and then axial compression vs. axial compression and then extension) makes a difference to injury outcomes, which judging from the kinematic data in the HBM simulations, it should. For the Nij this ordering is less critical as until now the Nij has only been considered in frontal and rear crashed were the kinematics of the neck are consistent. For reclined seating concepts which restrain occupants using different strategies, this may not necessarily be the case for lumbar spine kinematics. For the HIC like approach the experiments of Stemper et al. [109] could provide a first basis, as they measure axial force and have both injurious and non-injurious outcomes. They would need to be complemented by additional experiments in which the time to peak force and the duration time of the peak force are also investigated for injury outcomes, which would likely make the experiments more difficult both to perform and to validate. The Nij like criteria would require a complete experimental matrix of the combinations of axial forces and flexion-extension bending moments in order to identify the mechanisms leading to injury. The confounding effects of the order of applied load would also have to be somehow investigated, possibly acting as a multiplier of the matrix size.

Chapter 8

Outlook and Conclusions

For the first step in the hierarchical validation process, a validation was done using experimental data from Newell et al. [84] to evaluate five Human Body Models (HBMs) for how well their respective intervertebral discs (IVDs) performed in compression. These experiments involved compressing IVDs axially using a material testing machine at a rate of $1s^{-1}$ Five models were used to investigate the IVD response. The model with the best CORA score was the THUMS v3 with a CORA of 0.74, followed by the THUMS v5 with a CORA score of 0.68. All of the models had a similar response due in axial loading, but currently aside from studies done by Adams et al. [1] bending and shear in IVDs has not been investigated in detail sufficient for HBM validation. More validation should be done on the IVD in flexion and extension bending to see how the IVD deforms and transmits bending forces, in the best case with shear, bending, and axial loading all investigated independently of one another. Additionally combined bending compression tests could be developed afterwards to be used for HBM validations, including to high levels of force, moment, and strain needed to investigate failure modes and injury criteria.

Functional spinal units (FSUs) were investigated as being one hierarchical level more complex than IVDs. The FSU consists of a single IVD as well as the two vertebral bodies (VBs) adjacent to the disc, and the intervertebral, supraspinous and intraspinous ligaments. This investigation was done using the same five HBMs seen in the IVD validation to simulate specimen based experiments performed by Christou [25] as a reference. These experiments consist of a drop tower to apply a pulse to the FSU, and then measuring the force transmitted to a transducer located below the specimen. The differences observed between the simulations with and without facet joint contact shows the importance of the facet joints in FSU loading. The FSUs also lack validation in shear and bending just as is the case for IVDs, and could greatly benefit from any improved non-axial validations of the IVDs. The FSU however, also has a facet joint and additional ligaments which must be taken into account for any validations. Another possibility would be to study the individual geometries of facet joints in individuals to develop better kinematic modelling. Current models use geometry and friction, but perhaps other modelling methods could capture these FSU movements more true to the physiology. The uncertainty which results from using drop tower testing should also be better quantified, perhaps by using twinned studies of the same specimens in drop towers as well as material testing machines. Such a study would allow for the transfer of the more suited for validation results from material testing machine experiments to the more easily performed drop tower experiments. The difficulty in modelling drop tower experiments comes mainly from the unknown boundary conditions in the form of potting materials, any foam cushions, and strain rate dependencies associated with the high rates of loading. If a method could be found which decreases the amount of uncertainty involved, allowing for simplified models where unknown boundary conditions need not be considered, then the pool of existing studies which could be used for HBM validations would also increase.

The next level of validation consist of the whole lumbar spine, and is based upon reference experiments from Demetropolous et al. [33] and Stemper et al. [109]. For the quasi-static material testing experiments of Demetropolous et al. [33], all of the HBMs bar THUMS v4 lie within the experimental force-displacement corridor under axial load, but for the quasi-static flexion bending load case, all five of the HBMs are too stiff, as defined by their applied moment-angular displacement profiles. This highlights the lack of validation in bending seen in both the FSUs and IVDs. For the dynamic drop tower tests described in Stemper et al. [109] the kinematic behavior as measured by the angular deformation of the IVDs is best matched by the THUMS v5 model. This is due more to the initial geometry of the the THUMS v5 than to other modelling parameters. That the geometry was found to be the best predictor, more studies focused on what the geometries of lumbar spines look like in real populations would be of large interest. The experiments of Stemper et al. were simulated using largely artificial postures derived from the idealized HBM. Specimen specific geometries could be generated from CT data and then simulated again under the same boundary conditions to gain a better understanding of which aspects of the geometry cause the larger changes in the response. The dynamic experiments investigated were only considered in the non-injurious regime, so it would also be very enlightening to see if subject specific models could match failure patterns and injury mechanisms, which would in turn allow for a more detailed validation of the failure models in the HBMs.

For the full body validation the validation step was broken down in two parts, the first part consisting of a volunteer test used for validation, followed by a second part in which a full scale model was analyzed in a proposed seating concept to see how posture might effect the response. The volunteer sled tests performed by Muehlbauer [77] were used as the validation basis. In these tests a single individual was tested in an upright seating position as well as varying angles of recline. The global kinematics of the HBM simulations differed from what was observed in the volunteer testing. These differences show the need for other hierarchical validation studies in general. The total HBM kinematics are not a function of the lumbar spinal physiology alone, but rather the sum of all of the other biomechanical systems constituting the human body. If the skin, leg muscles, and hip soft tissues do not transfer physically coherent forces to the lumbar spine, then the lumbar spine kinematics will not reflect the reality. This problem is compounded by the differences in energy levels between volunteer test and high speed crashes. For the same individual undergoing the load analogous to a full vehicle crash, the contributions of the skin, leg muscles, and hip soft tissues, might be so dominated by the crash pulse that they can be neglected and not have an effect on the occupant kinematics or injury outcomes. But to find where the transition lies to go from physiognomy dominance to crash pulse dominance, more research is needed.

Looking at multiple HBM postures in high speed reclined seating configuration, with a focus on how initial postures effect the peak forces and kinematics in the lumbar spine shows how much of an effect that posture has on peak force and moment. The three postures investigated have over 10% difference in their force peaks while at the same time having only minimal affect on the global external occupant kinematics. As currently no widely accepted limit exists for lumbar loading in vehicle occupants, research is needed to investigate and propose criteria. This criteria must be developed as to be applicable to potentially modular, likely uniquely differing seating concepts and countermeasures. At the same time not only are the seating positions modular but the amount of posture and physiology variation seen within a population can be large. More research should be done to quantify these population based differences to make sure that any countermeasures provide a level of safety for all occupants.

Bibliography

[1] M. A. Adams and P. Dolan. A technique for quantifying the bending moment acting on the lumbar spine in vivo. *Journal of Biomechanics*, 24(2):117–126, 1991.

[2] M. A. Adams, T. P. Green, and P. Dolan. The strength in anterior bending of lumbar intervertebral discs. *Spine*, 19(19):2197–2203, 1994.

[3] M. A. Adams and W. C. Hutton. The effect of posture on the strength of the lumbar spine. *Engineering in Medicine*, 10(4):199–202, 1981.

[4] M. A. Adams and W. C. Hutton. Gradual disc prolapse. *Spine*, 10(6):524–531, 1985.

[5] T. Adolph, M. Wisch, A. Eggers, H. Johannsen, R. Cuerden, J. Carroll, D. Hynd, and U. Sander. Analyses of Thoracic and Lumbar Spine Injuries in Frontal Impacts. In *IRCOBI Conference 2013*, pages 91–102, 2013.

[6] D. Adomeit and A. Heger. Motion Sequence Criteria and Design Proposals for Restraint Devices in Order to Avoid Unfavorable Biomechanic Conditions and Submarining. *SAE transactions*, 84, 1975.

[7] A. Aiyangar, L. Zheng, W. Anderst, and X. Zhang. Instantaneous centers of rotation for lumbar segmental extension in vivo. *Journal of Biomechanics*, 52:113–121, 2017.

[8] G. B. Andersson, R. W. Murphy, R. Örtengren, and A. L. Nachemson. The influence of backrest inclination and lumbar support on lumbar lordosis, 1979.

[9] D. Asaro. The Evolution of the Crash Test Dummy, 2017.

[10] Z. Asgharpour, P. Zioupos, M. Graw, and S. Peldschus. Development of a strain rate dependent material model of human cortical bone for computer-aided reconstruction of injury mechanisms. *Forensic Science International*, 236:109–116, 2014.

[11] S. Barbat, Y. Fu, Z. Zhan, and C. Gehre. Objective rating metric for dynamic systems. *Enhanced Safety of Vehicles*, pages 1–10, 2013.

[12] J. F. Behrsin and C. A. Briggs. Ligaments of the lumbar spine: a review. *Surgical and Radiologic Anatomy*, 10(3):211–219, 1988.

[13] P. Beillas, P. Petit, S. Kleiven, A. Chawla, E. Jolivet, F. Faure, N. Praxl, and A. Bhaskar. Specifications of a Software Framework to Position and Personalise Human Body Models P. In *IRCOBI Conference 2015*, pages 1–2, 2015.

[14] D. J. Benson. The History of LS-DYNA, 2007.

[15] J. G. Betts, P. Desaix, E. Johnson, J. E. Johnson, O. Koral, D. Kruse, B. Poe, J. A. Wise, M. Womble, and K. A. Young. *Anatomy & Physiology*. Openstax CTX, Houston, TX, 2013.

[16] J. E. Bischoff, E. M. Arruda, and K. Grosh. Finite element modeling of human skin using an isotropic, nonlinear elastic constitutive model. *Journal of Biomechanics*, 33(6):645–652, 2000.

[17] K.-U. Bletzinger. Theory of Plates, 2002.

[18] J. W. Brinkley and J. T. Shaffer. Dynamic Simulation Techniques for the Design of Escape Systems. Technical report, USAF, 1971.

[19] A. J. Brock. *Galen on the natural faculties*. W. Heinemann, 1916.

[20] K. Buchholz. Futurist Kurzweil discusses acceleration of intelligent technology, 2015.

[21] Bulger, Dissanaike, Kaufman, and Mack. The Effects of Seatback Reclined Positions of Occupants in Motor Vehicles Collisions. Technical report, Seattle CIREN Team, 2007.

[22] A. Cappozzo. Compressive loads in the lumbar vertebral column during normal level walking. *Journal of Orthopaedic Research*, 1(3):292–301, 1983.

[23] R. K. Chintapalli, S. Breton, A. K. Dastjerdi, and F. Barthelat. Strain rate hardening: A hidden but critical mechanism for biological composites? *Acta Biomaterialia*, 10(12):5064–5073, 2014.

[24] A. Christou. *Chapter 3 The response of a single segment under impact*. PhD thesis, Imperial College London, 2017.

[25] A. Christou, G. Grigoriadis, D. Carpanen, N. Newell, and S. D. Masouros. Biomechanics of a lumbar functional unit using the finite element method. In *IRCOBI Conference 2017*, pages 668–669, 2017.

[26] J. Cobb. Outline for the Study of Scoliosis. *Instr Course Lect AAOS*, 5:261–275, 1948.

[27] J. S. Coogan, W. L. Francis, T. D. Eliason, T. L. Bredbenner, B. D. Stemper, N. Yoganandan, F. A. Pintar, and D. P. Nicolella. Finite Element Study of a Lumbar Intervertebral Disc Nucleus Replacement Device. *Frontiers in Bioengineering and Biotechnology*, 4(December):1–11, 2016.

[28] J. W. Cossette, H. F. Farfan, G. H. Robertson, and R. V. Wells. The instantaneous center of rotation of the third lumbar intervertebral joint. *Journal of Biomechanics*, 4(2):149–153, 1971.

[29] L. Cristofolini, N. Brandolini, V. Danesi, M. M. Juszczyk, P. Erani, and M. Viceconti. Strain distribution in the lumbar vertebrae under different loading configurations. *Spine Journal*, 13(10):1281–1292, 2013.

[30] C. Darwin. *Origin of Species*. J. Frances, 1869.

[31] D. E. De Carvalho and J. P. Callaghan. Influence of automobile seat lumbar support prominence on spine and pelvic postures: A radiological investigation. *Applied Ergonomics*, 43(5):876–882, 2012.

[32] H. de Visser, C. Adam, and M. Pearcy. The neutral zone in lumbar joint movements and how it is affected by preload. *Journal of Biomechanics*, 39:56, 2006.

[33] C. K. Demetropoulos, K. Yang, M. J. Grimm, K. K. Artham, and A. I. King. Mechanical Properties of the Hybrid III and Cadaveric Lumbar Spines. *SAE Technical Paper*, 983160(724), 1999.

[34] S. P. Desjardins. Establishing Lumbar Injury Tolerance for Energy Absorbing Seats Criteria and Testing Limitations. *American Helicopter Society 64th Annual Forum*, (April 2008), 2008.

[35] D. Draper, A. Huf, P. Wernicke, and S. Peldschus. The Influence Of Reclined Seating Positions On Lumbar Spine Kinematics And Loading In Frontal Impact Scenarios. In *Enhanced Safety of Vehicles*, pages 1–10, Eindhoven, 2019.

[36] M. Dreischarf, A. Rohlmann, F. Graichen, G. Bergmann, and H. Schmidt. In vivo loads on a vertebral body replacement during different lifting techniques. *Journal of Biomechanics*, 49(6):890–895, 2016.

[37] M. Dreischarf, T. Zander, A. Shirazi-Adl, C. M. Puttlitz, C. Adam, C. S. Chen, V. K. Goel, A. Kiapour, Y. H. Kim, K. M. Labus, J. P. Little, W. M. Park, Y. H. Wang, H. J. Wilke, A. Rohlmann, and H. Schmidt. Comparison of eight published static finite element models of the intact lumbar spine: Predictive power of models improves when combined together. *Journal of Biomechanics*, 47(8):1757–1766, 2014.

[38] Dummies4you. Hybrid III Lumbar Spine, 2013.

[39] S. Ebara, J. C. Iatridis, L. a. Setton, R. J. Foster, V. C. Mow, and M. Weidenbaum. Tensile Properties of Nondegenerate Human Lumbar Anulus Fibrosus. *Spine*, 21(4):452–461, 1996.

[40] A. Eggers, J. Ott, B. Pipkorn, D. Bråse, K. Mroz, F. L. Valdez, D. Hynd, and S. Peldschus. A New Generic Frontal Occupant Sled Test Set-up Developed Within The Eu-project SENIORS. In *25th International Technical Conference on the Enhanced Safety of Vehicles (ESV)*, 2017.

[41] R. Eppinger, E. Sun, F. Bandak, M. Haffner, N. Khaewpong, M. R. Maltese, S. Kuppa, T. Nguyen, E. Takhounts, R. Tannous, A. Zhang, and R. Saul. Development of Improved Injury Criteria for the Assessment of Advanced Automotive Restraint Systems - II By. Technical Report November, National Highway Traffic Safety Administration, 1999.

[42] Euro NCAP. Euro NCAP 2025 Roadmap: In pursuit of Vision Zero. Technical report, EuroNCAP, 2017.

[43] L. Evans. The effectiveness of safety belts in preventing fatalities. *Accident Analysis and Prevention*, 18(3):229–241, 1986.

[44] A. Farquharson. Movement of animals. *The Complete Works of Aristotle*, 1:1087–1096, 1984.

[45] J. Foster, J. O. Kortge, and M. Wolanin. Hybrid III-a biomechanically-based crash test dummy. *SAE transactions*, 86(4):3268–3283, 1977.

[46] T. Fuchs. *Objektivierung der Modellbildung von verletzungsmechanischen Experimenten für die Validierung von Finite-Elemente Menschmodellen.* PhD thesis, Ludwig-Maximilians-Universität München, 2017.

[47] F. S. Gayzik, D. P. Moreno, N. A. Vavalle, A. C. Rhyne, and J. D. Stitzel. Development of the Global Human Body Models Consortium mid-sized male full body model. *Injury Biomechanics Research*, pages 39–12, 2011.

[48] C. Gehre, H. Gades, and P. Wernicke. Objective Rating of Signals Using Test and Simulation Responses. *International Technical Conference on the Enhanced Safety of Vehicles (ESV)*, pages 1–8, 2009.

[49] S. Gertzbein, R. Holtby, A. Kapasouri, K. Chan, and B. Cruickshank. Determinination of a Locus of Instantaneous Centers of Rotation of the Lumbar Disc by Moire Fringes, 1984.

[50] GESAC. THOR-NT User's Manual. Technical Report March, National Highway Traffic Safety Administration, 2005.

[51] J. P. Grant. *Mapping the Structural Properties of the Lumbosacral Vertebral Endplates*. PhD thesis, University of British Columbia, 2000.

[52] R. C. Haut and R. W. Little. A constitutive equation for collagen fibers. *Journal of Biomechanics*, 5(5):423–430, 1972.

[53] T. Hedman, J. Kostuik, G. Fernie, and W. Hellier. Design of an Intervertebral Disc Prosthesis. *Spine*, 16(6 Suppl):256–60, 1991.

[54] H. B. Henninger, S. P. Reese, A. E. Anderson, and J. A. Weiss. Validation of Computational Models in Biomechanics. *Proc Inst Mech Eng H*, 224(7):801–812, 2010.

[55] T. Hines. Anatomy of the Human Spine. Technical report, Mayfield Clinic, 2013.

[56] D. C. Hoaglin and B. Iglewicz. Rules for Some Resistant Outlier Labeling. *Journal of the American Statistical Association*, 82(400):1147–1149, 1987.

[57] A. Huf and S. Sengottu Velavan. Development Of Occupant Restraint Systems For Future seating Positions In Fully Or Semi Autonomous Vehicles. In *Airbag*, 2018.

[58] J. C. Iatridis, M. Weidenbaum, L. a. Setton, and V. C. Mow. Is the nucleus pulposus a solid or a fluid? Mechanical behaviors of the nucleus pulposus of the human intervertebral disc, 1996.

[59] I. Isaksson-Hellman and H. Norin. How thirty years of focused safety development has influenced injury outcome in volvo cars. *Annu Proc Assoc Adv Automot Med*, 49:63–77, 2005.

[60] M. Iwamoto, Y. Kisanuki, I. Watanabe, K. Furusu, K. Miki, and J. Hasegawa. Development of a finite element model of the total human model for safety (THUMS) and application to injury reconstruction. *Proceedings of the International Research Council on the Biomechanics of Injury conference*, 30:12 p., 2002.

[61] M. Iwamoto, Y. Nakahira, and H. Kimpara. Development and Validation of the Total HUman Model for Safety (THUMS) Toward Further Understanding of Occupant Injury Mechanisms in Precrash and During Crash. *Traffic Injury Prevention*, 16(June):36–48, 2015.

[62] T. Izumiyama, N. Nishida, H. Iwanaga, X. Chen, J. Ohgi, K. Mori, T. Hayashi, I. Sakuramoto, R. Asahi, S. Sugimoto, and M. Ueno. The Analysis of an Individual Difference in Human Skeletal Alignment in in Seated Posture and Occupant Behavior Using HBMs. In *IRCOBI 2018*, pages 549–560, 2018.

[63] L. Jakobsson, T. Bergman, and L. Johansson. Identifying Thoracic And Lumbar Spinal Injuries In Car Accidents. In *IRCOBI Conference 2006*, number September, pages 61–71, 2006.

[64] L. Jakobsson, M. Bjorklund, and A. Westerlund. Thoracolumbar Spine Injuries in Car Crashes. In *Proceedings of IRCOBI Conference*, pages 16–22, 2016.

[65] S. Jorlov, K. Bohman, and A. Larsson. Seating Positions and Activities in Highly Automated CarsA Qualitative Study of Future Automated Driving Scenarios. In *IRCOBI Conference 2017*, pages 749–750, 2017.

[66] A. Kemper, C. McNally, and S. Duma. The influence of strain rate on the compressive stiffness properties of human lumbar intervertebral discs. *Biomedical Sciences Instrumentation*, 2007.

[67] T. Kitagawa, Y.; Yasuki. Development and Application of THUMS Version 4. In *CAHRS Human Modeling and Simulation in Automotive Engineering*, pages 1–138, 2014.

[68] E. H. Ledet, M. P. Tymeson, D. J. Dirisio, B. Cohen, and R. L. Uhl. Direct real-time measurement of in vivo forces in the lumbar spine. *Spine Journal*, 5(2005):85–94, 2005.

[69] F. J. Lopez-Valdes, K. Mroz, A. Eggers, B. Pipkorn, J. Muehlbauer, S. Schick, and S. Peldschus. Chest injuries of elderly Post Mortem Human Surrogates (PMHS) under seat belt and airbag loading in frontal sled

impacts. Comparison to matching THOR tests. In *Annals of advances in automotive medicine*, 2017.

[70] LSTC. LS-DYNA Keyword user's manual R7.1, 2014.

[71] R. B. Martin. A Genealogy of Biomechanics. *American Society of Biomechanics*, pages 1–8, 1999.

[72] S. F. Mason. *A History of the Sciences*. Macmillan General Reference, 1962.

[73] S. M. McKenna-Lawlor. The Hon. Mrs Mary Ward (1827–1869) Astronomer, Microscopist, Artist and Entrepreneur. In *Whatever Shines Should be Observed*, pages 19–51. Springer, 2003.

[74] G. Miyasaki. *Automobile Crash Test Facility and Preliminary Analysis of Low Speed Crush Characteristics*. PhD thesis, University of British Columbia, 1987.

[75] D. Mohr, H.-W. Kaas, P. Gao, D. Wee, and T. Möller. Automotive Revolution Perspective Towards 2030, 2016.

[76] J. Motavelli. Automakers Rethink Seats for Self-Driving Cars. *The New York Times*, pages 1–2, 2015.

[77] J. Muehlbauer, S. Schick, D. Draper, F. J. Lopez-valdes, I. Symeonidis, and S. Peldschus. Feasibility study of a safe sled environment for reclined frontal deceleration tests with human volunteers. *Traffic Injury Prevention*, 0(0):1–3, 2019.

[78] C. W. Müller, D. Otte, S. Decker, T. Stübig, M. Panzica, C. Krettek, and S. Brand. Vertebral fractures in motor vehicle accidents-a medical and technical analysis of 33,015 injured front-seat occupants. *Accident Analysis and Prevention*, 66:15–19, 2014.

[79] A. L. Nachemson and G. Elfstrom. Intravital dynamic pressure measurements in lumbar discs, 1970.

[80] National Highway Traffic Safety Administration. Traffic Safety Facts: 2015. *U.S. Department of Transportation*, (August):1–9, 2015.

[81] National Highway Traffic Safety Administration. Automated Driving Systems 2.0 A Vision for Safety. Technical report, NHTSA, 2017.

[82] N. Newell. 1-s2, 2017.

[83] N. Newell, D. Carpanen, A. Christou, G. Grigoriadis, J. P. Little, and S. D. Masouros. Strain Rate Dependence of Internal Pressure and External Bulge in Human Intervertebral Discs during Axial Compression. In *IRCOBI Conference 2017*, volume 44, pages 670–671, 2017.

[84] N. Newell, J. P. Little, A. Christou, M. A. Adams, C. Adam, and S. D. Masouros. Biomechanics of the human intervertebral disc: A review of testing techniques and results. *Journal of the Mechanical Behavior of Biomedical Materials*, 69(January):420–434, 2017.

[85] G. L. Niebur, M. J. Feldstein, J. C. Yuen, T. J. Chen, and T. M. Keaveny. High-resolution finite element models with tissue strength asymmetry accurately predict failure of trabecular bone. *Journal of Biomechanics*, 33(12):1575–1583, 2000.

[86] W. L. Oberkampf, T. G. Trucano, and C. Hirsch. Verification, validation, and predictive capability in computational engineering and physics. *Applied Mechanics Reviews*, 57(5):345, 2004.

[87] J. Östh, M. M. Vazquez, M. Y. Svensson, A. Linder, and K. Brolin. Development of a 50th percentile female human body model. *2016 IRCOBI Conference Proceedings - International Research Council on the Biomechanics of Injury*, pages 573–575, 2016.

[88] M. Östling, A. Larsson, H. Wu, and C. Sunnevång. Driver Behaviour in Automated Vehicles and Effects on Safety A Swedish and Chinese perspective How do we save more lives in the future ? In *VDI Safety Systems 2018*, 2018.

[89] A. L. Osvalder, P. Neumann, P. Lövsund, and A. Nordwall. A method for studying the biomechanical load response of the (in vitro) lumbar spine under dynamic flexion-shear loads. *Journal of Biomechanics*, 26(10):1227–1236, 1993.

[90] M. M. Panjabi, J. J. Crisco, A. Vasavada, T. Oda, J. Cholewicki, K. Nibu, and E. Shin. Mechanical properties of the human cervical spine as shown by three-dimensional load-displacement curves. *Spine*, 26(24):2692–2700, 2001.

[91] M. Panzer. Body region modeling and validation. In *IRCOBI 2018 HBM Workshop*, pages 41–61, 2018.

[92] G. Park, T. Kim, J. R. Crandall, C. Arregui-Dalmases, and B. J. Luzón Narro. Comparison of kinematics of GHBMC to PMHS on the side

impact condition. *Proceedings of IRCOBI Conference 2013*, 1(434):368–379, 2013.

[93] F. A. Pintar, N. Yoganandan, D. Maiman, M. Scarboro, and R. W. Rudd. Thoracolumbar spine fractures in frontal impact crashes. *Annals of advances in automotive medicine*, 56:277–83, 2012.

[94] F. A. Pintar, N. Yoganandan, T. Myers, A. Elhagediab, and A. Sances. Biomechanical properties of human lumbar spine ligaments. *Journal of Biomechanics*, 25(11):1351–1356, 1992.

[95] B. Pipkorn and J. Wass. PRE-CRASH TRIGGERED PRETENSIONING OF THE SEAT BELT FOR IMPROVED SAFETY. In *25th International Technical Conference on the Enhanced Safety of Vehicles (ESV)*, 2011.

[96] M. Prot, T. J. Cloete, D. Saletti, and S. Laporte. The behavior of cancellous bone from quasi-static to dynamic strain rates with emphasis on the intermediate regime. *Journal of Biomechanics*, 49(7):1050–1057, 2016.

[97] A. Race, N. D. Broom, and P. Robertson. Effect of loading rate and hydration on the mechanical properties of the disc. *Spine*, 25(6):662–669, 2000.

[98] P. P. Raj. Intervertebral disc: Anatomy-physiology-pathophysiology-treatment. *Pain Practice*, 8(1):18–44, 2008.

[99] M. H. Ray. REPEATABILITY OF FULL-SCALE CRASH TESTS AND A CRITERIA FOR VALIDATING SIMULATION RESULTS. *Transportation Research Record: Journal of the Transportation Research Board*, pages 155–160, 1996.

[100] R. Richardson, J. P. Donlon, K. Chastain, G. Shaw, J. Forman, S. Sochor, M. Jayathirtha, K. Kopp, B. Overby, B. Gepner, J. Kerrigan, M. Ostling, K. Mroz, and B. Pipkorn. Test Methodology for Evaluating the Reclined Seating Environment With Human Surrogates. *26th ESV Conference*, pages 19–0243, 2019.

[101] S. Roberts, H. Evans, J. Trivedi, and J. Menage. Histology and pathology of the human intervertebral disc. *The Journal of bone and joint surgery. American volume*, 88 Suppl 2(suppl 2):10–4, 2006.

[102] H. Schmidt, F. Galbusera, A. Rohlmann, and A. Shirazi-Adl. What have we learned from finite element model studies of lumbar intervertebral discs

in the past four decades? *Journal of Biomechanics*, 46(14):2342–2355, 2013.

[103] S. Sengottu Velavan and A. Huf. DEVELOPMENT OF OCCUPANT RESTRAINT SYSTEMS FOR FUTURE SEATING POSITIONS IN FULLY OR SEMI AUTONOMOUS VEHICLES. In *FISITA 2018*, 2018.

[104] J. S. Shah, W. G. J. Hampson, and M. I. V. Jayson. THE DISTRIBUTION OF SURFACE SURFACE STRAIN IN THE CADAVERIC LUMBAR STRAIN SPINE. *Journal of Bone and Joint Surgery*, 60(2):246–251, 1978.

[105] C. F. Silva, K. Foerner, and W. Polifke. Computational Thermo-Fluid Dynamics, 2016.

[106] I. O. f. Standardization. ISO/TS 18571: Objective Rating Metric for Non-ambiguous Signals, 2014.

[107] J. P. Stapp. Problems of Human Engineering in Regard to Sudden Decelerative Forces on Man. *The Military Surgeon (United States)*, 103(2):99–102, 1948.

[108] B. D. Stemper, S. Chirvi, N. Doan, J. L. Baisden, D. Maiman, W. H. Curry, N. Yoganandan, F. A. Pintar, G. Paskoff, and B. S. Shender. Biomechanical tolerance of whole lumbar spines in straightened posture subjected to axial acceleration. *Journal of Orthopaedic Research*, pages 1–10, 2017.

[109] B. D. Stemper, S. G. Storvik, N. Yoganandan, J. L. Baisden, R. J. Fijalkowski, F. A. Pintar, B. S. Shender, and G. R. Paskoff. A New PMHS Model for Lumbar Spine Injuries During Vertical Acceleration. *Journal of Biomechanical Engineering*, 133(8):081002, 2011.

[110] J. Sun, K. Lee, and H. Lee. Comparison of implicit and explicit finite element methods for dynamic problems. *Journal of Materials Processing Technology*, 105(1-2):110–118, 2000.

[111] S. H. Thomke. Simulation, learning and R&D performance: Evidence from automotive development. *Research Policy*, 27(1):55–74, 1998.

[112] C. Thunert. CORAplus Release 4.0.4 User ' s Manual, 2017.

[113] Toyota Motor Corporation. Documentation THUMS Version 5.02.1_201, 2018.

[114] M. Troke, A. P. Moore, F. J. Maillardet, and E. Cheek. A normative database of lumbar spine ranges of motion. *Manual Therapy*, 10(3):198–206, 2005.

[115] B. van Rietbergen, H. Weinans, R. Huiskes, and A. Odgaard. A new method to determine trabecular bone elastic properties and loading using micromechanical finite-element models. *Journal of Biomechanics*, 28(1):69–81, 1995.

[116] J. Versace. A Review of the Severity Index. Technical report, SAE, 1971.

[117] R. J. Wallace, P. Pankaj, and A. H. R. W. Simpson. The effect of strain rate on the failure stress and toughness of bone of different mineral densities. *Journal of Biomechanics*, 46(13):2283–2287, 2013.

[118] S. Wang, Q. Xia, P. Passias, K. Wood, and G. Li. Measurement of geometric deformation of lumbar intervertebral discs under in-vivo weightbearing condition. *Journal of Biomechanics*, 42(6):705–711, 2009.

[119] H. J. Wilke, P. Neef, M. Caimi, T. Hoogland, and L. Claes. New in vivo measurements of pressures in the intervertebral disc in daily life. *Spine*, 24(8):755–762, 1999.

[120] M. Wisch, M. Lerner, E. Vukovic, D. Hynd, A. Fiorentino, and A. Fornells. Injury Patterns of Older Car Occupants, Older Pedestrians or Cyclists in Road Traffic Crashes with Passenger Cars in Europe Results from SENIORS. In *IRCOBI Conference 2017*, pages 613–622, 2017.

[121] World Health Organisation. The top 10 causes of death:The 10 leading causes of death by income group (2011). Technical Report May, WHO, 2011.

[122] B. R.-j. Yang, A. Akkerman, D. F. Anderson, O. M. Faruque, and L. Gu. ROBUSTNESS OPTIMIZATION FOR VEHICULAR CRASH SIMULATIONS. *Computing in Science & Engineering*, pages 8–13, 2000.

[123] N. Yoganandan, M. W. J. Arun, B. D. Stemper, F. A. Pintar, and D. Maiman. Biomechanics of human thoracolumbar spinal column trauma from vertical impact loading. *Annals of advances in automotive medicine / Annual Scientific Conference ... Association for the Advancement of Automotive Medicine. Association for the Advancement of Automotive Medicine. Scientific Conference*, 57:155–66, 2013.

[124] N. Yoganandan, J. Moore, M. W. J. Arun, and F. A. Pintar. Dynamic Responses of Intact Post Mortem Human Surrogates from Inferior-to-Superior Loading at the Pelvis. *Stapp car crash journalpp*, 58(January 2014):123–143, 2014.

[125] A. Zaouk and N. Bedewi. Validation of a non-linear finite element vehicle model using multiple impact data. *Asme Applied ...*, pages 1–15, 1996.

[126] J. Z. Zhao and G. Narwani. Development of a Human Body Finite Element Model for Restraint System R & D Applications. *The 19th ESV Conference Proceedings*, 05(0399):1–13, 2005.